

Carborane-Based Design of Active Ligands of Nuclear Receptors for BNCT

Beatriz Brito

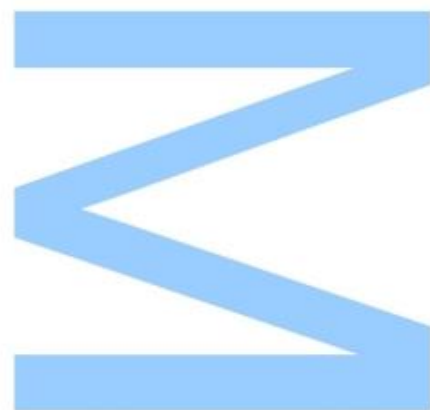
Mestrado em Bioquímica
Departamento de Química e Bioquímica
2018

Orientadores

Antonio Mouriño Mosquera, Facultad de Química, USC
Jose Enrique Rodriguez Borges, FCUP

Coorientadora

Rita Sigüeiro Ponte, Facultad de Química, USC

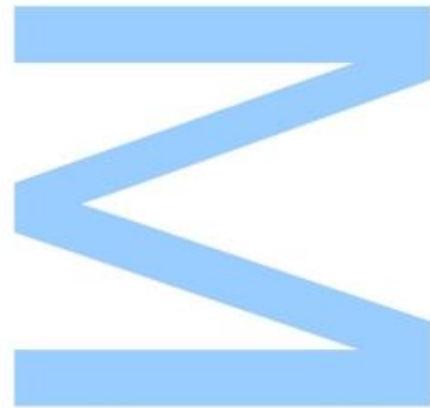




Todas as correções determinadas pelo júri, e só essas, foram efetuadas.

O Presidente do júri,

Porto, ____/____/____



Acknowledgments

Foremost, I would like to express my sincere gratitude to my advisors Professor Dr. Antonio Mouriño and Professor Dr. Enrique Borges for introducing me to the field of Organic Chemistry research and for giving me the opportunity to integrate this research group. Their guidance and teachings were invaluable.

I would like to thank Dr. Rita Sigüeiro for guiding me, often with big doses of patience, through this journey. For all her teachings and suggestions.

I am grateful to Professor Dr. Miguel Maestro and all my laboratory colleagues for the support, teachings and good environment provided. Special thanks to Patri and Xiao for their tireless support, infinite encouraging words and for the immeasurable fun times we had together.

I want to thank the University of Porto for giving me the opportunity to broaden my horizons through the Erasmus+ program. I also want to gratefully acknowledge the University of Santiago de Compostela for hosting me during this year.

Special thanks to my friends, Alfredo, Ana Beatriz, Bárbara, Gabriel, Gabriela, João, Rita, Ricardo and Tiago, for always keeping things lighthearted, if a little strange. And to Hélio, for always pushing me forward and never letting me drift astray.

Finally, I would like to express my deepest appreciation to my family, specially my mother, sister and grandmother, for supporting me unconditionally by means that words cannot explain.

Abstract

Icosahedral carboranes are highly stable boron-carbon clusters that have been used as unique pharmacophores in biological active compounds. Carboranes have promising applications in Boron Neutron Capture Therapy (BNCT), a technique based on the nuclear capture of neutrons by ^{10}B to produce high energy particles that selectively destroy tumors without affecting healthy tissues. The application of BNCT depends on the availability and selectivity of boron compounds which bind receptors in the tumors. The vitamin D nuclear receptor (VDR) is a potential target for cancer therapy, because it is expressed in many tumors and its ligand, $1\alpha,25\text{-dihydroxyvitamin D}_3$ (1,25D or calcitriol), can induce anticancer actions. To combine these properties with BNCT application, new VDR agonists based on the skeleton of the hormone 1,25D that contained *ortho*, *meta* and *para*-carboranes at the end of its side chain were designed. Docking studies revealed several promising carborane-containing calcitriol analogs. Three analogs were chosen as synthetic targets. The synthetic approach features a Pd-catalyzed construction of the triene system and an $\text{S}_{\text{N}}2$ displacement of a tosylate group by a carboranyl lithium reagent to afford three carborane-containing vitamin D analogs.

Key words: Carboranes, vitamin D, 1,25D, BNCT, analogs, docking, organic synthesis, Suzuki-Miyaura cross-coupling.

Resumo

Carboranos icosaédricos são complexos de boro-carbono altamente estáveis que têm sido usados como farmacóforos únicos em compostos biologicamente ativos. Os carboranos têm aplicações promissoras na Terapia de Captura de Neutrões pelo Boro (BNCT), uma técnica baseada na captura nuclear de neutrões pelo ^{10}B para produção de partículas de alta energia que destroem selectivamente tumores sem afetar tecidos saudáveis. A aplicação da BNCT depende da disponibilidade e selectividade dos compostos de boro que ligam a recetores tumorais. O recetor nuclear da vitamina D (VDR) é um potencial alvo para a terapia cancerígena, porque é expresso em vários tumores e o seu ligando, $1\alpha,25$ -dihidroxitamina D_3 (1,25D ou calcitriol), é capaz de induzir ações anticancerígenas. De modo a combinar estas propriedades com a aplicação da BNCT, foram desenhados novos agonistas do VDR cuja estrutura se baseia no esqueleto da hormona 1,25D que contivessem *ortho*, *meta* e *para*-carboranos no final da cadeia lateral. Estudos de docking revelaram promissores análogos do calcitriol com carboranos na cadeia lateral. Três compostos foram escolhidos como objetivo sintético. A abordagem sintética engloba a construção do sistema triénico catalisada por paládio e a substituição de um grupo tosilato por um reagente carboranilítio para se obter três análogos da vitamina D com unidades carborânicas diferentes.

Palavras-chave: Carboranos, vitamina D, 1,25D, BNCT, análogos, docking, síntese, cross-coupling de Suzuki-Miyaura

Index

ACKNOWLEDGMENTS	iii
ABSTRACT	v
RESUMO	vi
INDEX	vii
SCHEME INDEX	ix
FIGURE INDEX	xi
ABBREVIATIONS	xiii
INTRODUCTION	1
1. Vitamin D₃	3
1.1. <i>Structure and nomenclature of vitamin D</i>	3
1.2. <i>Biotransformation of vitamin D</i>	5
2. Mechanism of action of calcitriol	6
2.1. <i>Genomic actions of calcitriol</i>	6
2.2. <i>Non-genomic actions of calcitriol</i>	10
3. Biological activity of calcitriol	11
3.1. <i>Calcium and Phosphate Homeostasis</i>	11
3.2. <i>Cellular Differentiation and Proliferation</i>	12
3.3. <i>Immune System Regulation</i>	13
3.4. <i>Transcaltachia</i>	13
3.5. <i>Pharmacological Endeavours</i>	13
4. Carboranes	14
4.1. <i>Structure of carboranes</i>	15
4.2. <i>Electronic Properties</i>	16
4.3. <i>Hidrophobicity</i>	16
4.4. <i>Acidity</i>	17
4.5. <i>Molecular interactions</i>	17
4.6. <i>Chemistry</i>	18
4.7. <i>Boron Neutron Capture Therapy (BNCT)</i>	18
5. Background	20
OBJECTIVES	23
RESULTS AND DISCUSSION	27
1. Design and Docking of carborane-containing vitamin D analogs	29

1.1. Design of carborane-containing vitamin D analogs.....	29
1.2. Building of the proposed carborane-containing vitamin D analogs.....	30
1.3. Docking of the proposed carborane-containing vitamin D analogs.....	30
1.4. Docking Results	30
1.5. Choice of target analogs for synthesis.....	36
2. Synthesis of Carborane Analogs A1, A17 and A33.....	39
2.1. Retrosynthesis	39
2.2. Synthesis of benzoate 6	40
2.3. Synthesis of boronic ester 2	41
2.4. Synthesis of enol-triflate 3	43
2.5. Synthesis of tosylate 1	44
2.6. Synthesis of analogs A1, A17 and A33	46
CONCLUSIONS	53
EXPERIMENTAL SECTION	56
1. Docking calculations	57
2. General procedures	59
REFERENCES	71
APPENDIX	77
1. DOCKING RESULTS.....	79
1.1. Ortho series	81
1.2. Meta series	87
1.3. Para series.....	93
2. NMR Spectra.....	99
3. IR Spectra	115
4. Structure Index.....	121

Scheme Index

Scheme 1. Biosynthesis of vitamin D ₃ in the skin	5
Scheme 2. Biological activation of vitamin D ₃	5
Scheme 3. Catabolism of calcitriol.....	6
Scheme 4. Mechanism of genomic actions of calcitriol.....	9
Scheme 5. Mechanism for the non-genomic actions of calcitriol.....	10
Scheme 6. Schematic illustration of the effects of calcitriol on the calcium and phosphate homeostasis	12
Scheme 7. Synthesis of <i>ortho</i> , <i>meta</i> and <i>para</i> -carboranes	18
Scheme 8. Synthesis of target carborane RO . Reagents and conditions.....	21
Scheme 9. Retrosynthetic analysis planned for the synthesis of compounds A1 , A17 and A33 . P = protecting group	39
Scheme 10. Synthesis of benzoate 6 by metalation of diol 4	40
Scheme 11. Selective synthesis of benzoate 6	40
Scheme 12. Synthesis of boronic ester 2	41
Scheme 13. Proposed mechanism for the Miyaura borylation reaction in the synthesis of boronic ester 2	42
Scheme 14. Synthesis of enol triflate 3	43
Scheme 15. Synthesis of benzoate 13 <i>via</i> carbocyclization and Suzuki-Miyaura cross-coupling of 2 and 3	44
Scheme 16. Proposed mechanism of action of the Suzuki Miyaura cross-coupling to afford 13	44
Scheme 17. Synthesis of tosylate 1	45
Scheme 18. Synthesis of analog A1	46
Scheme 19. Synthesis of analog A17	48
Scheme 20. Synthesis of analog A33	49

Figure Index

Fig. 1. Structure of vitamin D ₃ and calcitriol	3
Fig. 2. Structure of calcitriol and other steroid hormones	3
Fig. 3. Conformational flexibility of the triene system, side chain and the A ring of calcitriol.....	4
Fig. 4. Schematic representation of the structure of human VDR	7
Fig. 5. A) Crystal structure of the 1,25D-LBD-VDR complex; B) Representation of polar interaction in the ligand pocket of VDR (PDB code: 1DB1).....	8
Fig. 6. Representation of non-polar interaction between the residues of LBD-VDR and calcitriol (PDB code:1DB1)	8
Fig. 7. Commercially available calcitriol analogs.....	14
Fig. 8. Commercially available boron-containing drug Velcade.....	15
Fig. 9. Representation of the three <i>closo</i> -carborane isomers.....	15
Fig. 10. Representation of an <i>o</i> -carborane, adamantane and benzene	16
Fig. 11. Two-dimensional representation of intermolecular interactions of <i>o</i> -carborane	17
Fig. 12. Selective neutron capture of neutrons by ¹⁰ B in a tissue ⁴⁷	19
Fig. 13. A) Representation of analog RO. B) Structure of the binding pocket of zVDR LBD bound to analog RO.....	20
Fig. 14. Target compounds.....	25
Fig. 15. Representation of carborane-containing analogs to analyze by docking in human VDR	29
Fig. 16. Conformation of the most promising docked analogs.....	31
Fig. 17. ¹ H-NMR and ¹³ C-NMR main signals for compound 6	40
Fig. 18. Main ¹ H-NMR and ¹³ C-NMR signals for boronic ester 2	42
Fig. 19. ¹ H-NMR and ¹³ C-NMR signals of enol-triflate 3	43
Fig. 20. Main ¹ H-NMR and ¹³ C-NMR signals of tosylate 1	45
Fig. 21. ¹ H-NMR spectrum of analog A1	47
Fig. 22. ¹¹ B-NMR spectrum of analog A1	47
Fig. 23. ¹ H-NMR spectrum of analog A17	48
Fig. 24. ¹¹ B-NMR spectrum of analog A17	49
Fig. 25. ¹ H-NMR spectrum of analog A33	50
Fig. 26. ¹¹ B-NMR spectrum of analog A33	50

Abbreviations

1,25D	1 α ,25-Dihydroxyvitamin D ₃ or calcitriol
1,25D-MARRS	1,25D membrane associated rapid response steroid binding
¹¹ B-NMRac	Coupled Boron-11 Nuclear Magnetic Resonance
¹¹ B-NMRdec	Decoupled Boron-11 Nuclear Magnetic Resonance
¹³ C-NMR	Carbon-13 Nuclear Magnetic Resonance
¹ H-NMR	Proton Nuclear Magnetic Resonance
25(OH)D ₃	25-Hydroxyvitamin D ₃
7-DHC	7-Dehydrocholesterol
AF-2	Activation function 2
APCI	Atmospheric-pressure chemical ionization
APCs	Antigen presenting cells
aq	aqueous
Arg	Arginine
B ₂ pin ₂	Bis(pinacolato)diboron
BNCT	Boron Neutron Capture Therapy
Cav-1	Caveolin-1
CDKIs	Cyclin-dependent kinase inhibitors
CoA	Coactivators
c-Src	Non-receptor tyrosine kinase
CYP24A1	Cytochrome P450 family 24 subfamily A member 1
CYP27B1	Cytochrome P450 family 27 subfamily B member 1
CYP2R1	Cytochrome P450 Family 2 Subfamily R Member 1
d	doublet
DBD	DNA binding domain
DBP	Vitamin D binding protein

DCs	Dendritic cells
dd	Doublet of doublet
ddd	Doublet of doublet of doublets
ddt	Doublet of Doublet of Triplets
DEPT	Distortionless Enhancement by Polarization Transfer
DIBAL-H	Diisobutylaluminium hydride
DMAP	4-Dimethylaminopyridine
DMP	Dess-Martin periodinane
DNA	Deoxyribonucleic acid
dt	Doublet of triplets
EtOAc	Ethyl acetate
ESI	Electrospray ionization
FGF23	Fibroblast growth factor 23
GA	Genetic algorithm
GMB	Glioblastoma multiform
H12	Helix 12
Hex	Hexane
His	Histidine
HPLC	High-performance liquid chromatography
HPT	Hyperparathyroidism
HRMS	High-Resolution Mass Spectrometry
Hz	Hertz
<i>J</i>	Coupling constant
LDA	Lithium diisopropylamide
LET	Linear energy transfer
Leu	Leucine
m	multiplet
M ⁺	Molecular ion

MHz	Mega Hertz
mRNA	Messenger Ribonucleic acid
MS	Mass Spectrometry
MTBE	Methyl <i>tert</i> -butyl ether
ⁿ BuLi	<i>n</i> -Butyllithium
nm	Nanometers
PCy ₃	Tricyclohexylphosphine
Pdia3	Protein Disulfide Isomerase Family A Member 3
Ph	Phenyl
Phe	Phenylalanine
ppm	Parts per million
PTH	Parathyroid hormone
Py	Pyridine
q	quartet
R _f	Retention Factor
rt	Room temperature
RXR	Retinoid X receptor
s	singlet
Ser	Serine
S _N 2	Bimolecular nucleophilic substitution
t	triplet
td	Triplet of doublets
THF	Tetrahydrofuran
TLC	Thin-Layer Chromatography
TOF	Time-of-flight
Trp	Tryptophan
UVB	Ultraviolet light B
Val	Valine

VDR Vitamin D receptor

VDREs Vitamin D receptor response elements

INTRODUCTION

Introduction

1. VITAMIN D₃

Vitamin D₃, through its hormonal form, the 1 α ,25-dihydroxyvitamin D₃ (calcitriol, 1,25D, Fig. 1) is essential for the maintenance of health. Indeed, calcitriol influences a large range of physiological processes, including calcium and phosphate metabolism, bone maintenance, cellular proliferation, differentiation, apoptosis and immune regulation.¹

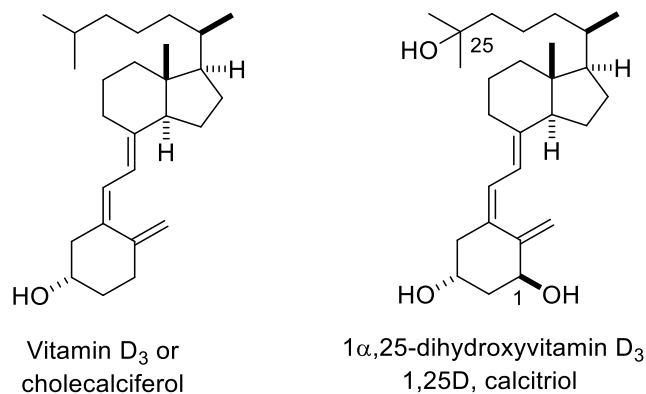


Fig. 1. Structure of vitamin D₃ and calcitriol

Calcitriol plays an important role in several pathologies, like psoriasis, multiple sclerosis, rheumatoid arthritis, diabetes and cancer, which has increased the interest in the development of vitamin-D based therapies.²

1.1. Structure and nomenclature of vitamin D

The structure and mode of action of calcitriol are closely related to that of classical steroid hormones, like cortisol, testosterone and progesterone (Fig. 2).

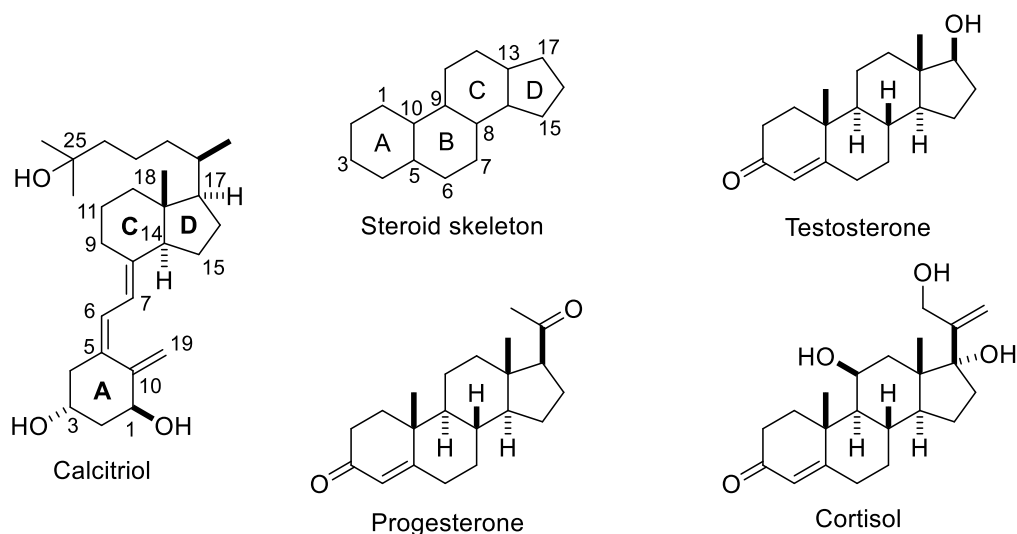


Fig. 2. Structure of calcitriol and other steroid hormones

The structure of steroids has a common cyclopentanephenanthrene skeleton composed of four rings (**A**, **B**, **C** and **D**). The cleavage of one of these rings is designed by the term “seco”. The vitamin D is classified as a secosteroid because its skeleton derives from the photochemical cleavage of the C9-C10 bond of the **B** ring of a steroid precursor.

The vitamin D and its metabolites are named and numbered according to their steroid precursor. They have more conformational flexibility than other steroid hormones, due to the presence of:

- 1) a triene system that can rotate around the C6-C7 bond, to afford two planar conformations: 6-*s-cis* and 6-*s-trans* (Fig. 3B);
- 2) a rotatable side chain with 5 single C-C bonds, that can freely rotate 360 ° (Fig. 3C);
- 3) an **A**-ring that can undergo a chair-chair interconversion, which changes the orientation of the 1 α and 3 β hydroxyl groups between the equatorial and axial orientation (Fig. 3D).³

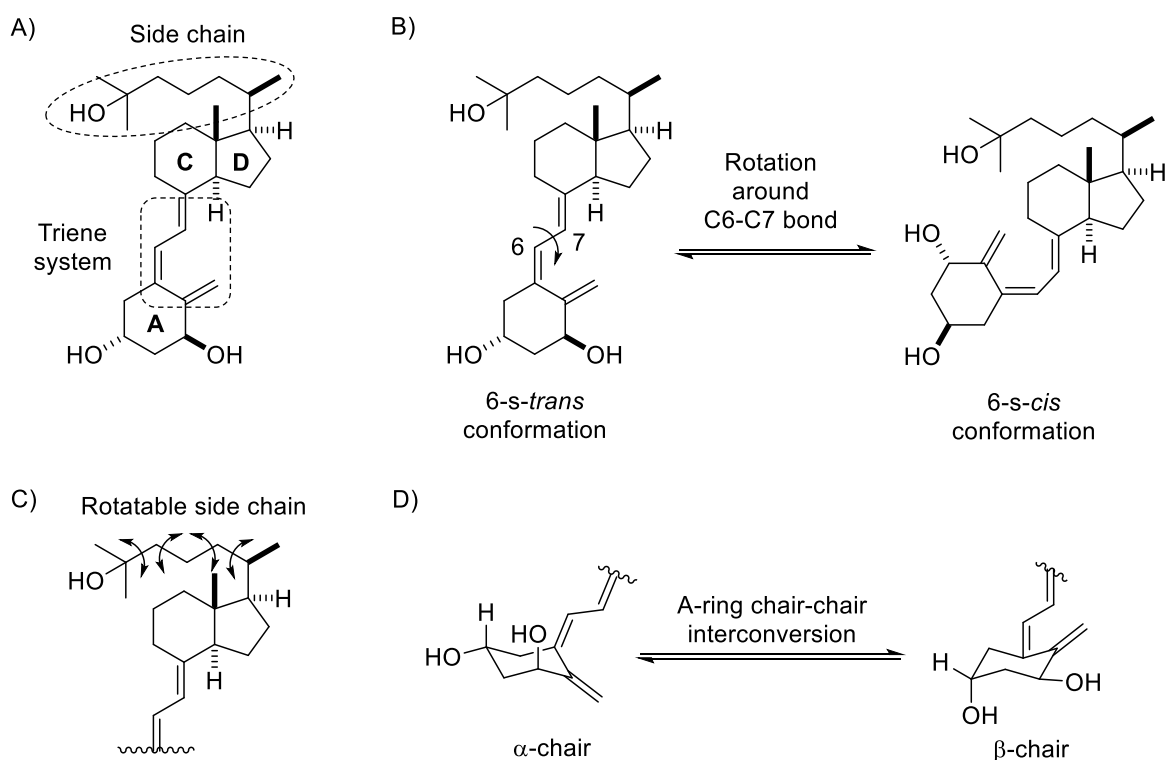


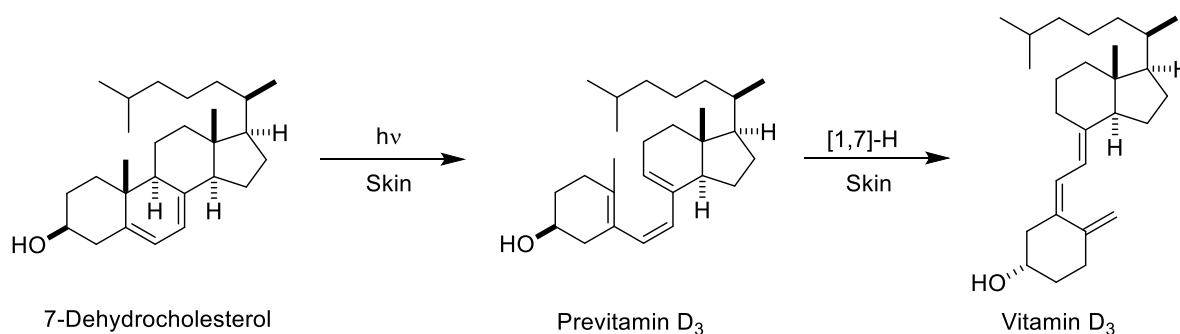
Fig. 3. Conformational flexibility of the triene system, side chain and the A ring of calcitriol

These highly mobile parts are linked to a rigid **CD**-ring system.

1.2. Biotransformation of vitamin D

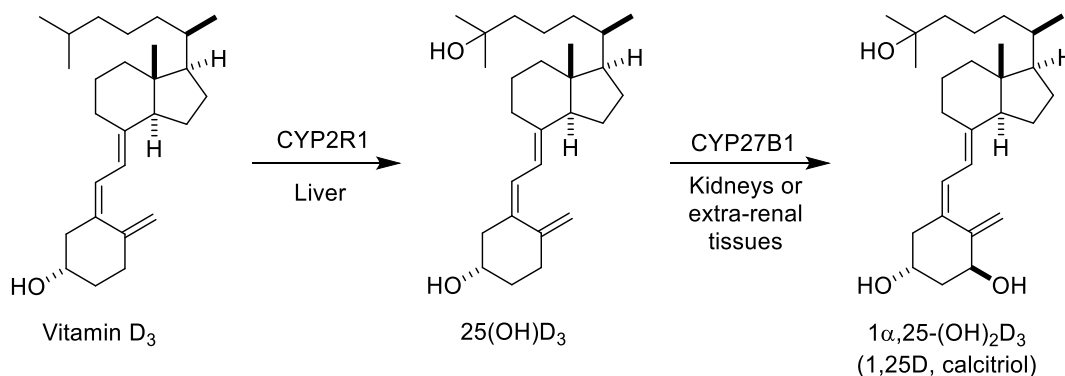
The predominant form of vitamin D in humans is vitamin D₃, which can be obtained through diet, dietary supplements or by endogenous production from 7-dehydrocholesterol (7-DHC, Scheme 1).⁴

The biosynthesis of vitamin D₃ is initiated in the skin by the photochemical ring opening of 7-DHC under UVB radiation (Scheme 1). The resulting previtamin D₃ undergoes a sigmatropic rearrangement [1,7]-H to afford the vitamin D₃.⁴⁻⁵



Scheme 1. Biosynthesis of vitamin D₃ in the skin

Vitamin D₃ goes through two enzymatic transformations to give the active form, calcitriol. These two hydroxylations occur first in the liver and then in the kidneys or extra-renal sites (Scheme 2).



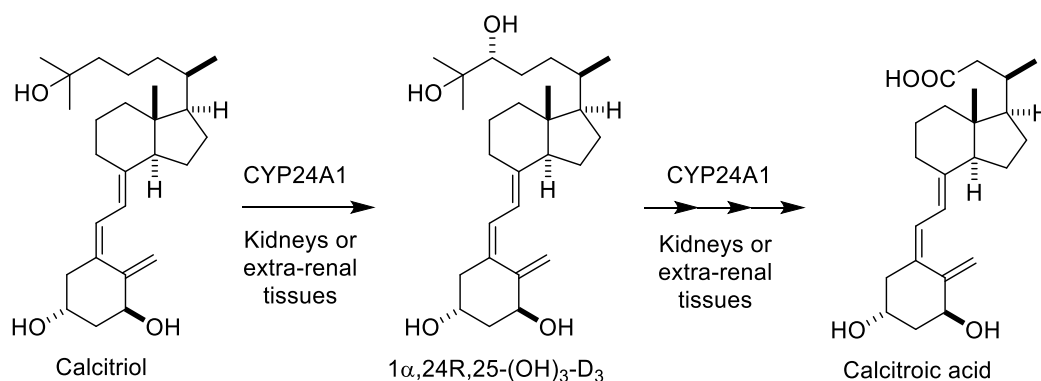
Scheme 2. Biological activation of vitamin D₃

The first hydroxylation is predominantly catalyzed by vitamin D-25-hydroxylase CYP2R1.² The resulting 25-hydroxyvitamin D₃, 25(OH)D₃ is the main circulating form of the vitamin in the serum. The generated 25(OH)D₃ associates with vitamin D binding protein (DBP),⁶ to reach the kidneys or extra-renal sites.²

A cytochrome P450 enzyme, CYP27B1, is responsible for the second hydroxylation, in the 1 α position, to produce the hormonal form of vitamin D, calcitriol.⁷

In extra-renal tissues, locally synthesized 1,25D works in an autocrine or paracrine manner, while calcitriol synthesized in the kidneys performs its functions in an endocrine manner, *via* association with DBP in the serum.

Calcitriol also undergoes metabolic degradation, mainly through an inactivating 24-hydroxylation, which is catalyzed by another cytochrome P450 enzyme, CYP24A1 (Scheme 3).²



Scheme 3. Catabolism of calcitriol

This enzyme catalyzes three consecutive oxidations of calcitriol at C-24 and C-23, leading to the formation of more water-soluble and less active metabolites. This ends with the production of the inactive calcitroic acid, which can easily be eliminated through urine.⁵

2. MECHANISM OF ACTION OF CALCITRIOL

Vitamin D, in consonance with other nuclear steroids, induces both genomic and non-genomic actions. The slow classical genomic functions of vitamin D occur *via* transcription activation triggered by nuclear vitamin D receptor (VDR). The fast non-genomic actions of the hormone involve second messengers generated by membrane-initiated signaling pathways.

2.1. Genomic actions of calcitriol

The genomic actions of calcitriol mediate hormone secretion, calcium and phosphate homeostasis and even regulate cellular proliferation, differentiation and apoptosis. These actions involve binding of calcitriol to the vitamin D receptor (VDR). Since the discovery of this nuclear receptor, in 1974,⁸ a lot of explorative studies were undertaken to collect information on the VDR's distribution, structure and mechanism of action.

The VDR (427 amino acids, 48 kDa) is a member of the superfamily of ligand-activated nuclear receptors that include receptors for steroid, retinoid and thyroid hormones. VDR is expressed in a multitude of tissues, including malign cells from breast, prostate and colon cancer, as well as acute myeloid leukaemia.⁹ This receptor modulates gene expression by association with its ligand, calcitriol, and its heterodimer partner, retinoid X receptor (RXR).

Structurally, it is composed of six regions (A to F), numbered from the *N*-terminal extension. Additionally, VDR is also divided in two distinct domains, based on functional aspects: a DNA binding domain (DBD) and a ligand binding domain (LBD) (Fig. 4). These domains are bound together by an unstructured linker.

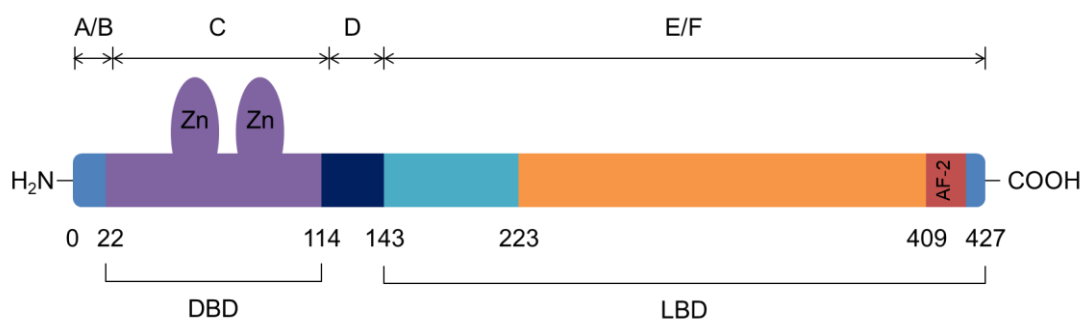


Fig. 4. Schematic representation of the structure of human VDR

The crystal structure of the entire VDR is not yet available. However, the crystal structures of the individual domains (DBD and LBD) have been published and are useful in the study of the function of calcitriol and VDR.¹⁰⁻¹¹

The DBD is a highly conserved domain that contains two zinc fingers. Structurally, this domain corresponds to the C region of the protein. This domain anchors VDR to specific DNA sequences, the vitamin D response elements (VDREs), through the zinc fingers.¹⁰ These VDREs are usually repeats of hexanucleotides with a spacing of 3 nucleotides between half sites, called DR3 VDR motifs.

The LBD is a highly variable *C*-terminal domain that corresponds to the E and F regions of the receptor. This domain confers the VDR high specificity and affinity towards its ligand, calcitriol. The three dimensional structures of the modified human, rat and zebrafish VDR(LBD) have been established, with the receptor bound to calcitriol and other ligands.¹¹⁻¹³ These structures show that the VDR(LBD) structure is comprised of 13 α helices sandwiched in 3 layers and 3 stranded β sheets that, together, form a highly hydrophobic ligand binding pocket (Fig. 5A).¹¹ This ligand

binding cavity is large (697 Å) and calcitriol only occupies 56% of the total volume. Indeed, there is additional space around the aliphatic chain and near position C2 of the A-ring.¹⁴

The 1,25D is anchored to this binding pocket by six hydrogen bonding interactions (Fig. 5B).¹¹ In the human VDR(LBD), the C1 α -OH of calcitriol interacts with Ser237 and Arg274, while the C3 β -OH binds to Tyr143 and Ser278. The C25-OH group at the side chain of calcitriol interacts with His305 and His397.

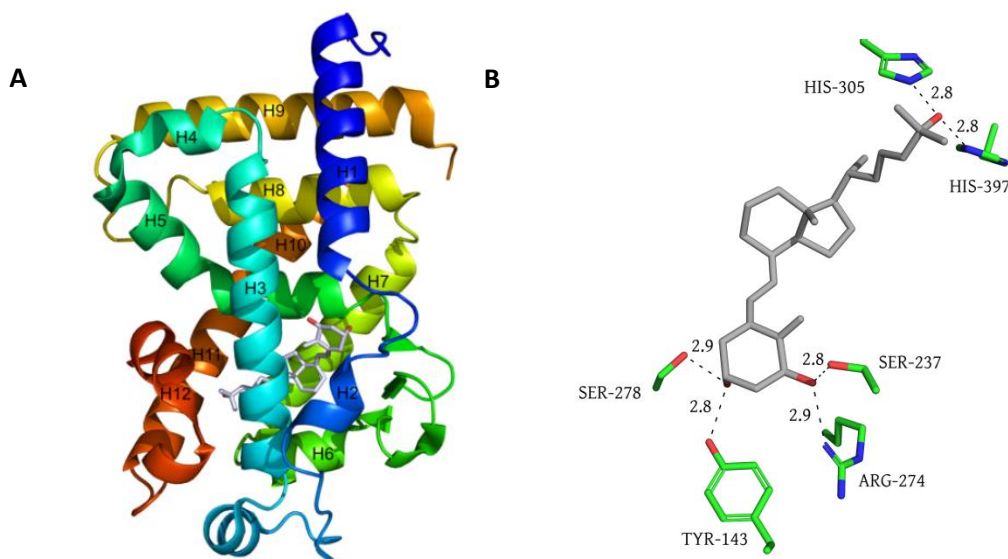


Fig. 5. A) Crystal structure of the 1,25D-LBD-VDR complex; B) Representation of polar interaction in the ligand pocket of VDR (PDB code: 1DB1)

Calcitriol is also anchored to the LBD by non-polar interactions, which greatly influence the conformation adopted by this hormone inside the binding pocket (Fig. 6). The conjugated triene system of the ligand accommodates a *trans* conformation tightly fitted in a hydrophobic channel made of Ser275 and Trp286 on one side and Leu233 on the other.

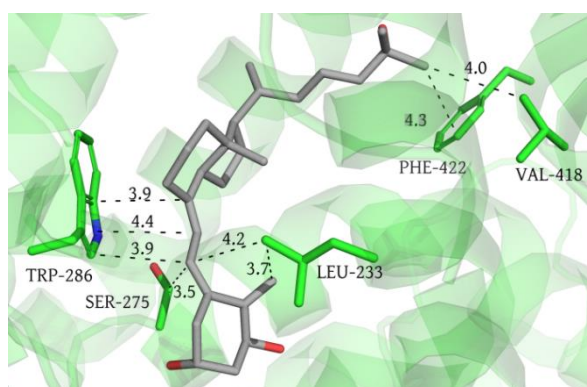
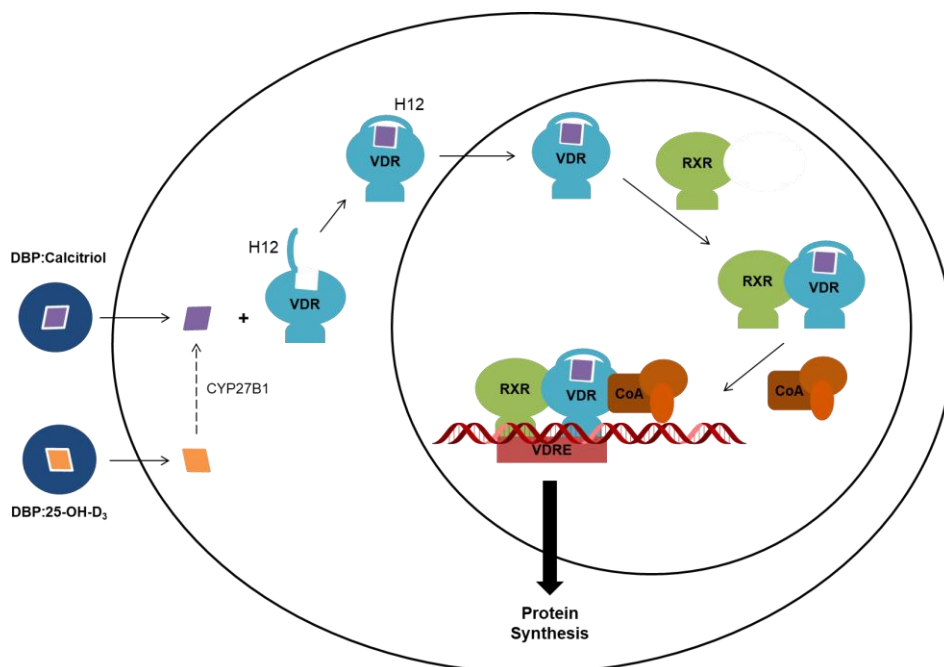


Fig. 6. Representation of non-polar interaction between the residues of LBD-VDR and calcitriol (PDB code:1DB1)

The aliphatic side chain of calcitriol is surrounded by hydrophobic residues and adopts an extended conformation parallel to the C13-C18 bond. The methyl group of the side chain of calcitriol makes two important van der Waals contacts with residues from the helix 12 (H12), Val418 and Phe422 (Fig. 6).

This interaction of calcitriol with the residues of the C-terminal H12 is particularly important for interaction of VDR with transcriptional machinery proteins. This helix contains a seven amino acid region called the ligand dependent activation function (AF-2) that acts as a molecular switch in a ligand-dependent manner.

Regarding the mechanism of action of VDR, it is known that this receptor induces gene expression *via* association with calcitriol, RXR and co-activators (Scheme 4).



Scheme 4. Mechanism of genomic actions of calcitriol

Calcitriol or 25(OH)D₃ are transported in the blood stream by DBP and enter target cells by passive diffusion. Inside the cell, 25(OH)D₃ is locally hydroxylated to calcitriol by CYP27B1. Calcitriol interacts with cytoplasmic VDR, inducing the conformational shift of helix 12. This molecular switch closes over the hormone in a mouse-trap mechanism that anchors calcitriol to VDR and facilitates the formation of protein interaction interfaces.

Upon calcitriol binding, VDR is rapidly translocated to the nucleus, where it forms a heterodimer with another nuclear receptor, RXR, to become transcriptionally active. Once the VDR-RXR heterodimer is formed, it associates with VDREs and recruits

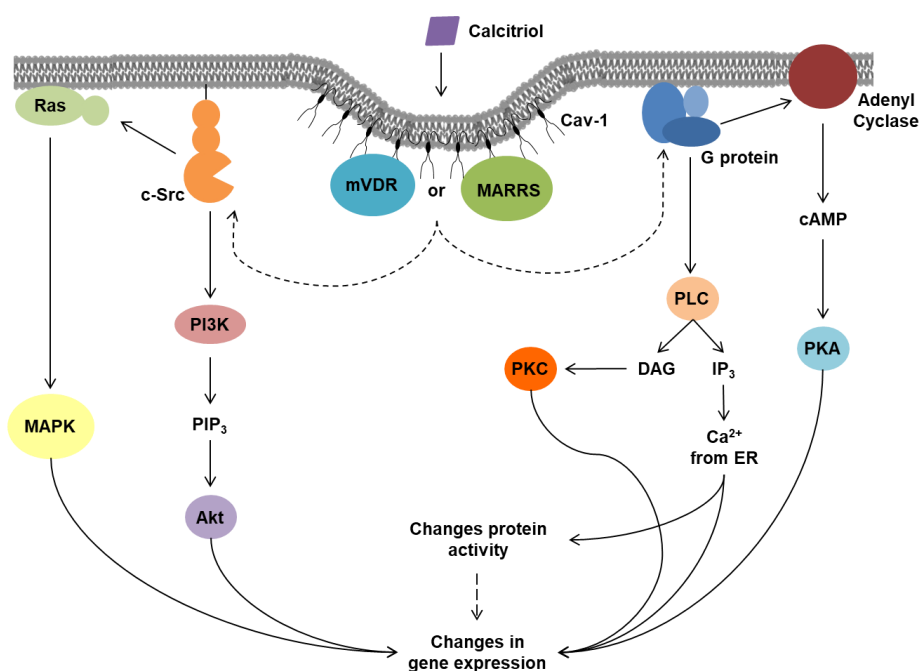
various coregulatory complexes to target gene promoters,¹⁵⁻¹⁶ resulting in activation of target gene expression.¹⁷

These highly specific changes in gene expression combine to orchestrate complex and tissue-specific responses. Indeed, using transcriptome-wide analysis, calcitriol was found to modulate the expression of 229 genes.¹⁸

2.2. Non-genomic actions of calcitriol

Besides the classical genomic actions, it is presently recognized that calcitriol also exerts fast, non-genomic actions. These actions work in a nuclear VDR independent manner, as they involve membrane-triggered processes. The mechanism of non-genomic action is gradually being unraveled and is thought to impact a wide range of cellular processes,¹⁹ such as transcalcitria, insulin secretion and phospholipid metabolism.¹⁵

These rapid responses involve two distinct membrane-bound receptors: the membrane associated rapid response steroid (MARRS), also known as Pdia3,²⁰ and membrane-bound VDR (Scheme 5). Although VDR is typically a nuclear receptor, it has been co-localized in caveolae-enriched plasma membranes, through association with a scaffolding protein, caveolin-1 (Cav-1).²¹⁻²³ MARRS also binds to Cav-1 in these caveolae. The presence of Cav-1 is then essential for the non-genomic actions of 1,25D.



Scheme 5. Mechanism for the non-genomic actions of calcitriol

Once VDR or MARRS are associated with Cav-1, calcitriol is able to bind to either one of these receptors. The interaction between calcitriol and the VDR/Cav-1 complex or the MARRS/Cav-1 complex triggers the initiation of different signaling pathways, through a not fully understood mechanism. Presumably, the binding of calcitriol to either of these complexes leads to the activation of G proteins or non-receptor tyrosine kinases, like Src kinase (c-Src),²⁴ which leads to the initiation of different signaling cascades. These signaling pathways are summarized in Scheme 5 and are responsible for the induction of changes in protein activity and even changes in gene expression, in a cell-type, cell-stage and gene specific manner.^{19, 25}

3. BIOLOGICAL ACTIVITY OF CALCITRIOL

Calcitriol, through both genomic and non-genomic mechanisms, is responsible for a multitude of biological functions that are divided in classic and non-classic actions. The role of calcitriol in the maintenance of calcium levels in extracellular fluids is a classic function of this hormone. On the other hand, the non-classic biological functions of calcitriol include the regulation of cellular proliferation and differentiation and modulation of the immune response.

3.1. Calcium and Phosphate Homeostasis

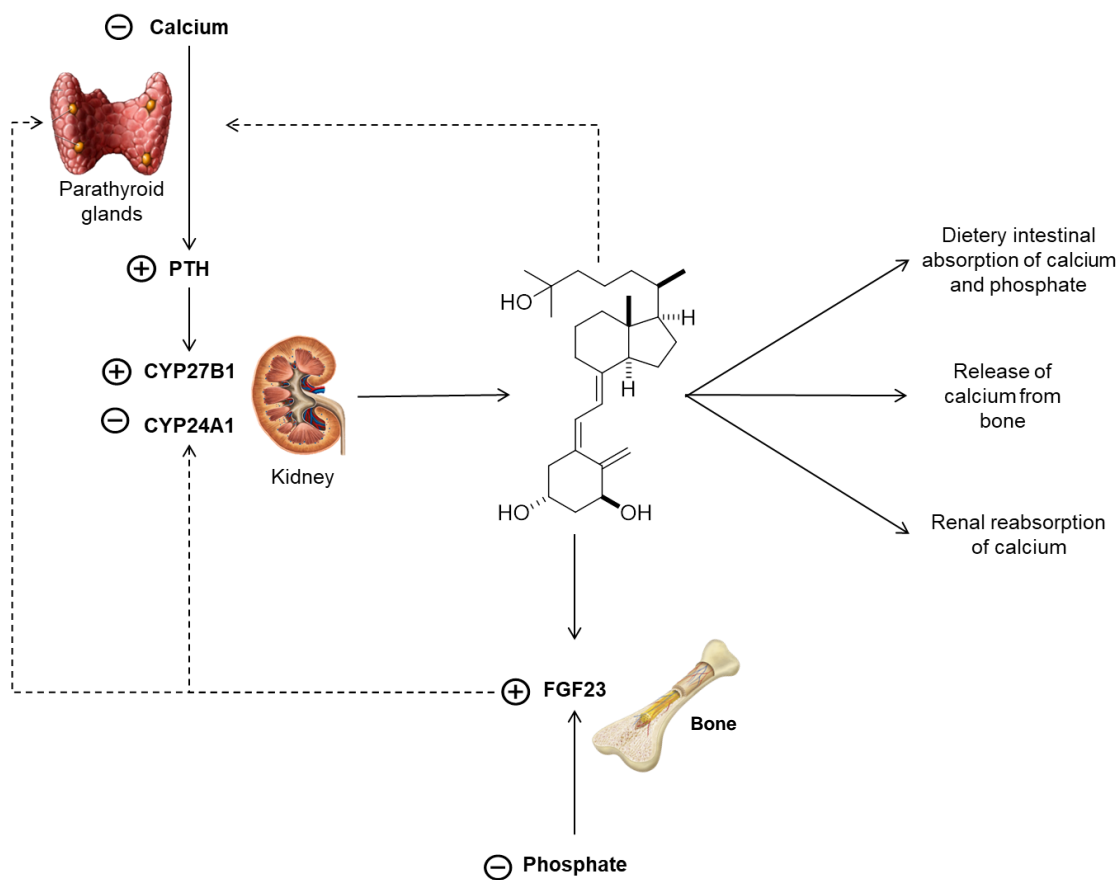
The maintenance of physiologic levels of extra and intracellular levels of calcium and phosphate is a highly complex and regulated process. This homeostasis is dependent on different enzymes and hormones, and involves a coordinated action of the parathyroid glands, kidneys, intestine and bone.

Calcitriol is responsible for the absorption of dietary calcium and phosphate from the gastrointestinal tract, the renal calcium reabsorption and the calcium release from bone (Scheme 6). These effects are regulated by a negative feedback mechanism, in which calcitriol inhibits the synthesis and secretion of the parathyroid hormone (PTH).

The parathyroid glands are responsible for the synthesis of the PTH. In response to low calcium levels (hypocalcemia), the glands secrete PTH, which stimulates the activation of renal CYP27B1 and renal degradation of CYP24A1 mRNA, leading to an increase of calcitriol production (Scheme 6).²⁶⁻²⁸

The calcium and phosphate homeostasis is also regulated by fibroblast growth factor 23 (FGF23).²⁶ The production of FGF23 by osteoblasts and osteocytes in the bone is stimulated by an increase of calcitriol levels. FGF23 participates in the

regulation of calcium and phosphate homeostasis, as it inhibits the synthesis and secretion of PTH and decreases renal CYP27B1 in response to elevated calcitriol and phosphate levels.²⁹



Scheme 6. Schematic illustration of the effects of calcitriol on the calcium and phosphate homeostasis

These classic actions of calcitriol can be applied clinically, through the use of calcitriol and its analogs in the control of secondary hyperthyroidism in renal failure and osteoporosis.

3.2. Cellular Differentiation and Proliferation

Calcitriol is known to have anti-proliferation and pro-differentiation effects in several cell types mainly through a genomic mechanism.⁹

Regarding its anti-proliferative function, calcitriol is known to increase the expression of cyclin-dependent kinase inhibitors (CDKIs) p21 and p27. These CDKIs are responsible for regulating the transition from the G1 phase (responsible for cell growth) to the S phase (responsible for DNA replication) of the cell cycle. Calcitriol increases the expression of these inhibitors, which prevents the progression of the cell cycle to the S phase, thus inhibiting cell proliferation.³⁰

Calcitriol has also been found to induce differentiation in several cells, from keratinocytes to breast and prostate cancer cells.³¹⁻³³

Given these functions, it was postulated that calcitriol and its analogs could have applications in cancer therapy. Additionally, taking into account that calcitriol induces differentiation and inhibits proliferation in keratinocytes, several calcitriol analogs are commercially available for the treatment of moderate forms of psoriasis.³²

3.3. Immune System Regulation

Calcitriol plays a role in immune regulation because it can be synthesized in and have effect on T cells,³⁴⁻³⁵ B cells³⁶ and antigen presenting cells (APCs).³⁷⁻³⁸ Therefore, calcitriol has immunomodulatory effects that could be used in the treatment of autoimmune diseases. Indeed, vitamin D-based therapies have been applied in the control of autoimmune disorders like systemic lupus erythematosus, rheumatoid arthritis, multiple sclerosis and type I diabetes.

3.4. Transcaltachia

Transcaltachia refers to the non-genomic rapid (2-10 minutes) stimulation of intestinal calcium transport. Although this process can have a useful role in calcium homeostasis, it greatly hinders the application of vitamin D-based therapies. Calcitriol and some of its analogs have poor clinical application due to side effects like hypercalcemia, mainly caused by transcaltachia. As such, there has been a major effort to synthesize non-calcemic calcitriol analogs.³⁹⁻⁴¹

3.5. Pharmacological Endeavors

The elucidation of the crystallographic structure of the LBD of VDR¹¹ has facilitated the rational design of new analogs.

Although more than 3500 analogs have been synthesized, only a few, are currently commercially available and are clinically applied (Fig. 7).⁴² Some of these drugs are used in the treatment of psoriasis, osteoporosis, multiple sclerosis, and bone and pancreatic cancer.

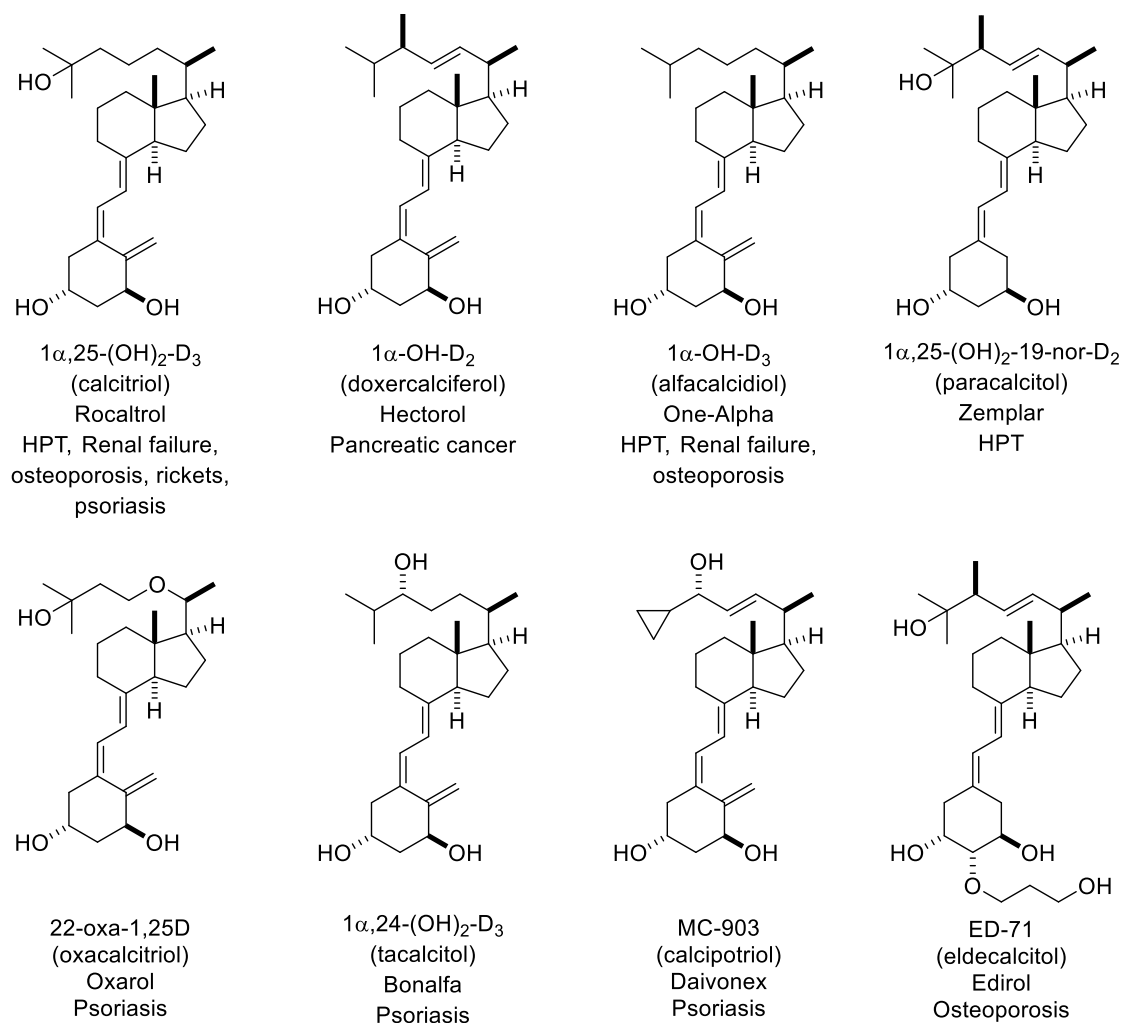
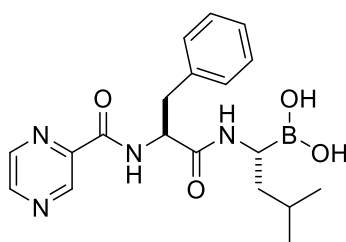


Fig. 7. Commercially available calcitriol analogs

The design of innovative VDR ligands with unique functional groups was propelled. This search for interesting novel leads has unveiled the great promise of a previously unexplored element in drug design: boron.

4. CARBORANES

Recently, the pharmaceutical industry and an increasing number of medicinal chemistry researchers are using boron as a substitute for carbon in different classes of drug molecules. Molecules with boron atoms are expected to be less complex than their carbon counterparts, reducing costs in drug research and manufacturing. Also, the possibility of new interactions of these molecules with biological targets unaffected by classical ligands makes the use of these boron moieties very alluring. A boron-containing drug, Velcade® is commercialized (Fig. 8) and several others have entered human clinical trials.⁴³⁻⁴⁵



Velcade
Multiple myeloma

Fig. 8. Commercially available boron-containing drug Velcade

Boron tends to form compounds with covalent B-H and B-B bonds called boranes. These boranes exist preferentially in polyhedral clusters with globular architectures.⁴⁶ One important class of polyhedral borane clusters are carboranes, in which two BH units of the *closo*-B₁₂H₁₂²⁻ cluster are replaced by 2 CH vertices.

The recent interest in applying carboranes to medicinal chemistry has arisen due to their particular electronic properties, geometry and versatility, together with the newest development in carborane chemistry.

4.1. Structure of carboranes

Carboranes, or carbaboranes, are polyhedral carbon-containing boron clusters. Among these, the dicarba-*closo*-dodecaboranes (C₂B₁₀H₁₂) are the most extensively studied and are usually referred to as simply carboranes. They are rigid molecules with an icosahedral structure, containing 10 BH vertices and 2 CH vertices. The carbon and boron atoms are hexacoordinated to compensate the low electron density, forming 20 triangular faces.

Carboranes exist in three isomeric forms, depending on the positioning of their 2 CH vertices: *ortho*- (or 1,2-), *meta*- (or 1,7-) and *para*- (or 1,12-) carborane (Fig. 9).

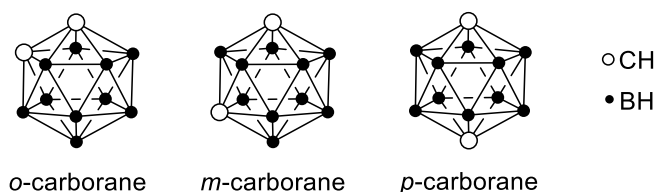


Fig. 9. Representation of the three *closo*-carborane isomers

The *ortho*- and *meta*-carboranes have C_{2v} symmetry, while the *p*-isomers have a D_{5d} symmetry. The overall size and the core volume of carboranes slightly decrease from *ortho*- to *para*-carboranes, though these differences are not significant. Generally, the

size and volume of carboranes is similar to that of adamantane and almost twice the spherical volume occupied by a phenyl ring (Fig. 10).

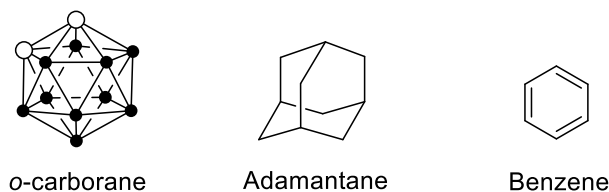


Fig. 10. Representation of an *o*-carborane, adamantane and benzene

4.2. Electronic Properties

Carboranes have non-classical bonding interactions, resulting in a very complex overall electronic structure. They have 26 electrons ($2n+2$ skeletal e^-) divided between the 12 vertices, which are three-dimensionally delocalized, meaning that carboranes are characterized as three-dimensional aromatic compounds. As such, these compounds are not easily defined by usual organic bond diagrams and the bonds between atoms represent only geometry.

In terms of electronegativity, the carbon and hydrogen atoms are more electronegative than the boron atoms, which explain some of the carborane properties. Additionally, boron-carbon bonds are stronger than carbon-carbon bonds, meaning that the more stable isomer has carbon atoms in nonadjacent positions.

4.3. Hydrophobicity

In terms of hydrophobicity, carboranes are usually more hydrophobic than their carbon counterparts. The hydrogens atoms of the BH vertices have partial negative charges, making them similar to hydrides, which explain the high hydrophobicity of carboranes.

The different carboranes isomers show differences in hydrophobicity, as the hydrophobicity increases in the order *ortho*, *meta* to *para* isomers.

The hydrophobicity of carboranes and carborane-containing drugs can be fine-tuned by choosing to substitute the different vertex positions. Free CH groups of carboranes, which are acidic, decrease the hydrophobicity of the carborane. On the contrary, C-substituted carboranes are more hydrophobic. B-substituted carboranes are less hydrophobic than their counterparts.

4.4. Acidity

The protons of the C atoms are relatively acidic, depending on the cluster isomer. The acidity of the carborane protons decreases in the order *ortho*-, *meta*- to *para*-carborane. Organometallic bases, such as ^tBuLi can remove a proton from C-H, generally creating a carboranyl nucleophile. B or C substituents influence both the acidity of the carborane protons and the acidity of the cluster protons.

4.5. Molecular interactions

The outer sphere of carboranes is composed of hydrogens, meaning that these hydrogen atoms are the main mediators of intermolecular interactions in unsubstituted carboranes.

Carboranes have two different types of hydrogen atoms: acidic hydrogens from CH groups and hydride hydrogens from BH groups.

These two types of hydrogen atoms are involved in distinct intermolecular interactions (Fig. 11). The CH moieties form classic hydrogen bonds (C-H • • •X) with electronegative atoms (O, N, S or F).

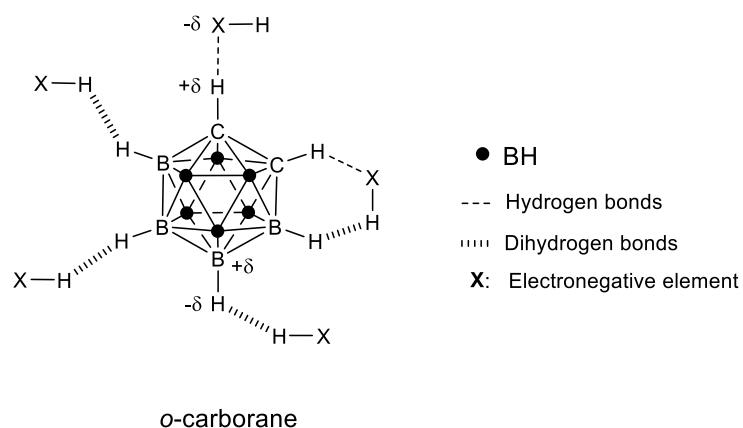


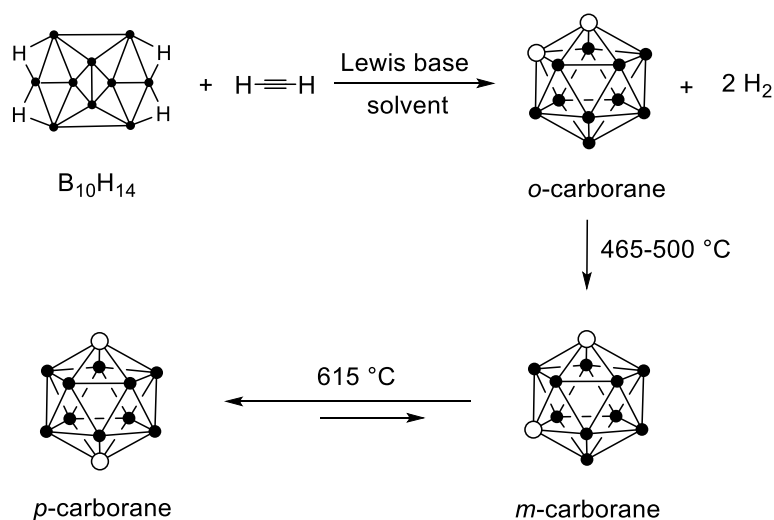
Fig. 11. Two-dimensional representation of intermolecular interactions of *o*-carborane

On the other hand, the hydride BH units can form dihydrogen bonds (B-H • • •H-X) with protons bound to electronegative atoms. These interactions occur with small molecules, as well as in the active site of proteins and enzymes, which makes carboranes very interesting pharmacophores.

4.6. Chemistry

The *ortho*-carborane can be obtained by reaction of decaborane ($B_{10}H_{14}$) with acetylenes in the presence of a Lewis base (Scheme 7). Thermal isomerization of *ortho*-carboranes, in an autoclave, leads first to the *meta* isomer (465-500 °C) and finally to the *para* isomer (615-700 °C).

These carboranes are chemically stable and are inert to water and atmospheric oxygen.



Scheme 7. Synthesis of *ortho*, *meta* and *para*-carboranes

They can be derivatized on the boron vertices, by electrophilic substitution; and on the carbon vertices, by removal of acidic CH protons with strong bases.

Carboranes can undergo metalation with nBuLi to afford the carboranyl lithium derivative, which can react with an electrophile to form a C-substituted carborane.

Thus, from a synthetic point of view, carboranes are interestingly versatile and can be used to create wide libraries of pharmacophores for distinct purposes.

4.7. Boron Neutron Capture Therapy (BNCT)

As most of their properties are prone to be fine-tuned, carboranes may prove to be superior bioactive molecules than their organic counterparts. Also, these *closo*-carboranes are great candidates for boron neutron capture therapy (BNCT).

This experimental cancer treatment uses boron compounds in the treatment of several cancers, mainly glioblastoma multiform (GBM). In this case, clinical studies have

demonstrated that BNCT is not only safe but at least as efficient as conventional radiotherapy.

This technique is based on the nuclear capture of neutrons by ^{10}B to produce high energy particles that selectively destroy tumors without affecting healthy tissues. It works as a two-component, or binary, therapy, since it uses two independent key components: the boron clusters and low energy thermal neutrons.

When irradiated, the non-radioactive ^{10}B isotopes present in boron clusters capture the low-energy neutrons and then fissure into kinetic energy and into high linear energy transfer (LET) particles: alpha particles (two protons and two neutrons) and lithium ions.⁴⁷ These high LET particles have path-lengths of about $10\ \mu\text{m}$, roughly the diameter of a single cell, which makes the cytotoxic effect largely confined to cells that accumulated the boron compound (Fig. 12).

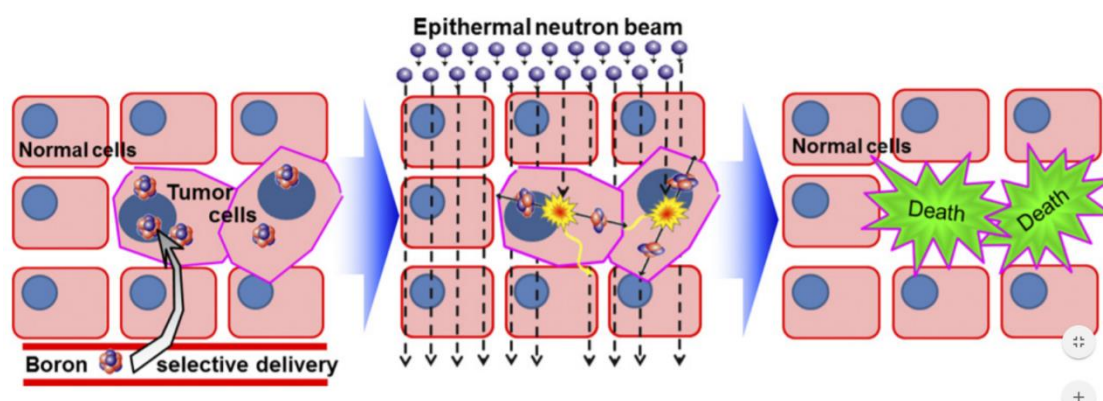


Fig. 12. Selective neutron capture of neutrons by ^{10}B in a tissue⁴⁸

The application of BNCT depends on:

- 1) the selectivity of the compounds for a target highly expressed in tumors, as that would mean that surrounding healthy tissue would be less affected;
- 2) the number of boron atoms accumulated in tumor cells, as a high number accumulated of boron atoms in tumor cells would increase the probability of neutron capture events.

As such, highly selective compounds that contain boron clusters like carboranes (1 moiety = 10 B) should be very efficient BNCT agents. Indeed, carboranes are currently being studied for that purpose, as they are being used in the synthesis of novel DNA metallointercalators that could bind to tumor cell DNA and of hypoxia-selective agents that could enter low-oxygen regions in tumors.⁴⁵

Another tumor-selective target that should be considered for BNCT therapy is the VDR. The VDR is a good target for selective application of BNCT because its expression is increased in some tumors, such as breast cancer. The next obvious step is, then, the design of VDR agonists that contain *ortho*-carboranes, an endeavor explored in this work.

5. BACKGROUND

Recently, a unique secosteroid vitamin D analog with an *ortho*-carborane moiety at the side chain (Fig. 13A) has been designed, synthesized and biologically tested.⁴⁹ This compound (**RO**) binds efficiently to VDR and induces similar biological activities with reduced calcemic effects, in comparison to 1,25D.

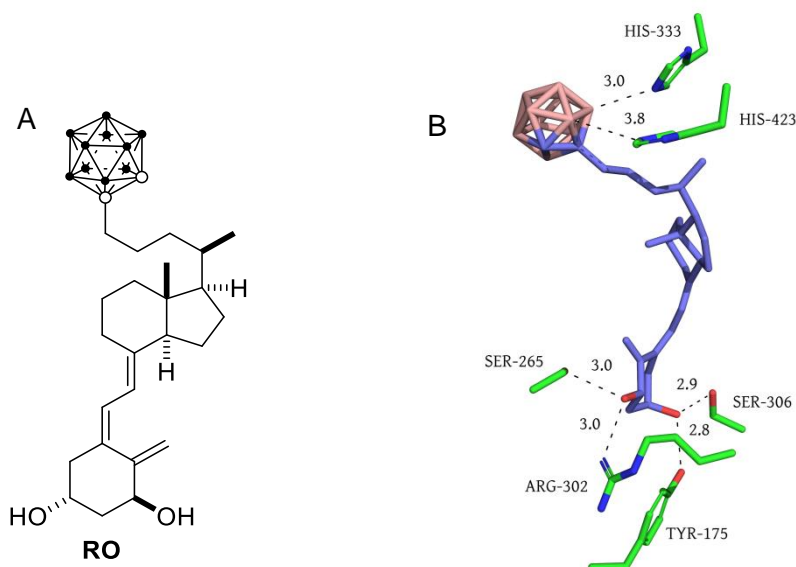


Fig. 13. A) Representation of analog **RO**. B) Structure of the binding pocket of zVDR LBD bound to analog **RO**.

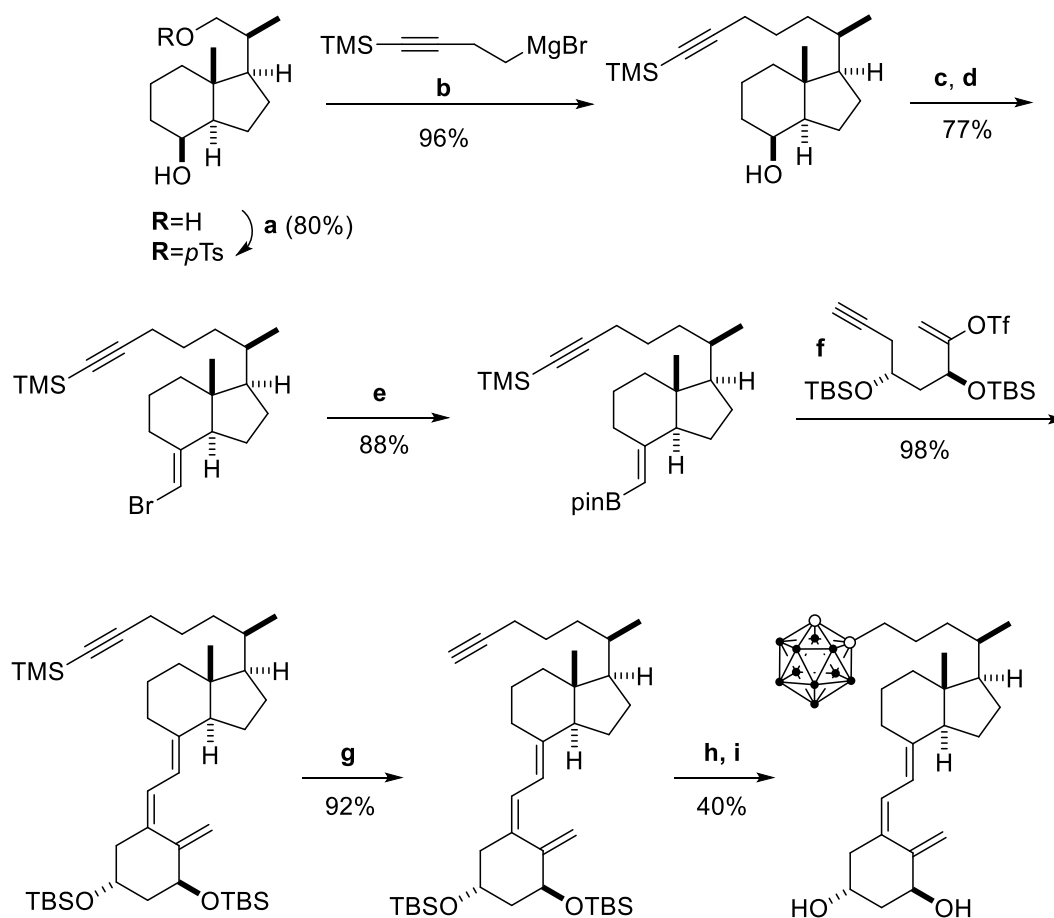
Analog **RO** was crystallized in the zebra-fish wild-type VDR LBD at a 2.4 Å resolution (Fig. 13B). This compound adopts the canonical active conformation of the calcitriol-VDR complex. The carborane unit mimics the interaction of the C25-OH in the binding pocket of VDR. It is even postulated that the carborane cage interacts with His333 and His423 (His305 and His397 in human VDR, respectively) through non-conventional dihydrogen bonds (BH...HN).

The synthesis of analog **RO** was accomplished in 9 steps and is illustrated in Scheme 8.

The *ortho*-carborane moiety of analog **RO** was formed late in the synthesis, to avoid complications regarding carborane chemistry and characterization. The carborane was

introduced in the side chain by reaction of an alkyne with decaborane ($B_{10}H_{14}$), in the presence of *N,N*-dimethylaniline.

These results proved that carborane-containing vitamin D analogs can be biologically active and have less calcemic effects than calcitriol itself. As such, the synthesis of analog **RO** paved the way for the rational design of new carborane-containing vitamin D analogs that could have medical and pharmaceutical application.



Scheme 8. Synthesis of target carborane **RO**. Reagents and conditions: a) *p*TsCl, py, 0 °C, 12 h; b) Et₂O/THF, Li₂CuCl₄, THF, -78 °C / rt, 12 h; c) PDC, CH₂Cl₂, rt, 5 h; d) (Ph₃PCH₂Br)Br, KO^tBu in THF, toluene, -15 °C / rt, 3 h; e) ^tBuLi, B(OⁱPr)₃, pinacol, toluene/THF, -78 °C / rt, 4 h; K₃PO₄ (2 M), PdCl₂(PPh₃)₂, THF, 2 h; (g) K₂CO₃, MeOH, rt, 14 h; (h) PhNMe₂, toluene, decaborane (B₁₀H₁₄), 110 °C, 1 h; (i) HF (48%), CH₂Cl₂/CH₃CN (2 : 1), rt, 12 h.

OBJECTIVES

Objectives

This work was developed to improve the properties of analog **RO** and explore potential application of other carborane-containing calcitriol analogs in BNCT. As such, the design and synthesis of new carborane analogs was planned. The objectives of this work were:

- 1) Docking of new carborane-containing vitamin D analogs into the 1,25D-VDR(LBD) complex to study their *in silico* affinity for the VDR.
- 2) Synthesis of the target analogs **A1**, **A17** and **A33** (Fig. 14).

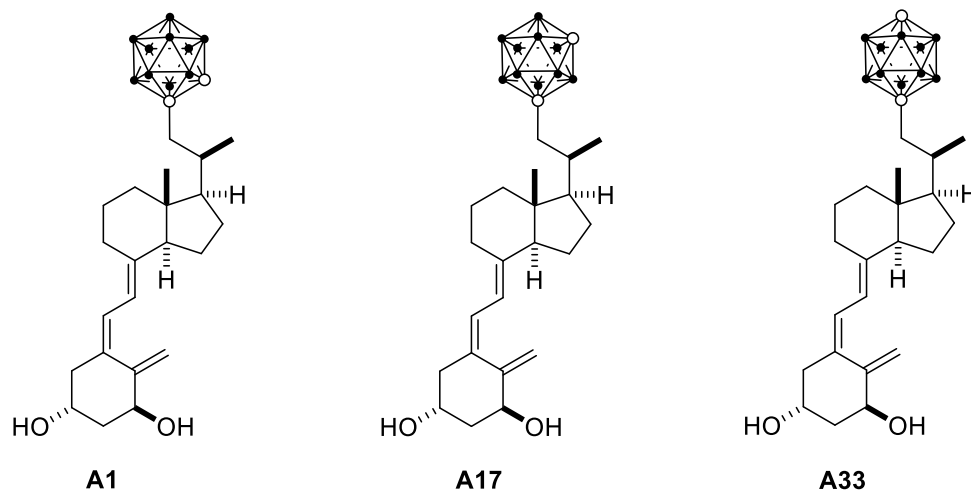


Fig. 14. Target compounds

RESULTS AND DISCUSSION

Results and Discussion

1. CHAPTER I: Design and Docking of carborane-containing vitamin D analogs

1.1. Design of carborane-containing vitamin D analogs

New carborane-containing calcitriol analogs were designed and docked into the LBD of VDR (Fig. 15). In order to find the ligands that bind better to this receptor, several different parameters were investigated: 1) the carborane isomer connected to the side chain (*ortho*-, *meta*- or *para*-carborane); 2) the C-substituents attached to the carborane unit (R groups); 3) the length of the side chain connecting the carborane unit to the **CD**-ring system ($n=1$, $n=2$ or $n=3$).

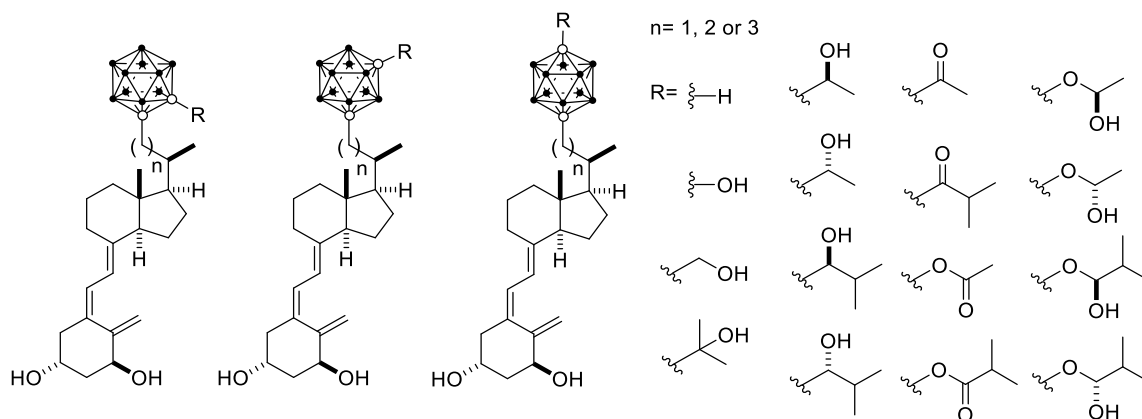


Fig. 15. Representation of carborane-containing analogs to analyze by docking in human VDR

Justification for the choice of parameters:

- 1) It is unknown whether the slight differences in electronic properties, hydrophobicity and acidity⁴⁶ between carborane isomers could influence the analogs' binding affinity. The orientation of the attached R groups could also affect the binding.
- 2) Analogues with different R groups could interact differently with the VDR, thus altering their binding affinity. The size and nature of the R groups were expected to have an impact on the chemical and physical properties of each analogue inside the VDR.
- 3) Given the size of the carborane moiety⁴⁹ and depending on the size of the different R groups attached, the length of the side chain ($n= 1, 2$ or 3) could influence the analogs' binding affinity for the VDR.

1.2. Building of the proposed carborane-containing vitamin D analogs

The ligands were built using the PyMol program.⁵⁰ The vitamin D part was obtained from the crystal structure of the complex of 1,25D-hVDR LBD (PDB code: 1DB1).¹¹ The carborane cage part of the ligands was obtained from the crystal structure of the corresponding *ortho* (PDB code: 5E7V),⁴⁹ *meta* (PDB code: 4MDL)⁵¹ and *para*-carboranes (PDB codes: 3VJS).⁵² The ligands were further treated by adding hydrogen atoms and checking atom valence using Chem3D. Energy minimization of the ligands was performed using the MM2 function of Chem3D.

1.3. Docking of the proposed carborane-containing vitamin D analogs

Docking studies to predict the affinity of the new ligands for the VDR were carried out using the GOLD program (version Suite 5.2). A modified crystal structure (addition of hydrogens, reconstitution of gaps and correction of His tautomers) of the complex between 1,25D-hVDR(LBD) was chosen as protein (PDB code: 1DB1).¹¹

The Ligand Binding Pocket of the mutant LBD was defined as Binding Site with the automatic active-site detection on, and the radius was set to 10 Å. The conformations for each ligand in the active site of the protein were sampled using a genetic algorithm (GA). The ligands were docked in 25 independent genetic algorithm (GA) runs, for each of which a maximum of 125000 GA operations were performed on a single population of 100 individuals. Operator weights for crossover, mutation, and migration in the entry box were used as default parameters (95, 95, and 10, respectively), as well as the hydrogen bonding (4.0 Å) and van der Waals (2.5 Å) parameters. The different poses were ranked according to the force-field-based CHEMPLP scoring function and GoldScore was used as a re-scoring function. The 3 best solutions for each ligand were obtained with an associated score and these results were compared with the solutions for 1,25D.

1.4. Docking Results

The best obtained poses for each ligand were analyzed in terms of score, adopted conformation inside the receptor and interactions with the different residues.

In appendix 1 (page 83), the chosen conformation for each ligand was superimposed to the natural ligand 1,25D (represented in grey) into the ligand binding pocket of VDR. The interactions with His305 and His397 are shown for all analogs. The interactions

between the C3-OH and C1-OH of the analogs and Tyr143, Ser237, Arg274 and Ser278 were only shown when the interactions of the **A** ring of the analog changed significantly.

In summary, analogs **B2**, **C2**, **B4**, **B8**, **A13**, **A14**, **C17**, **B18**, **C18**, **A19**, **B19**, **A20**, **A21**, **A23**, **B30**, **A31**, **A32**, **B33** and **C33** are the most promising in terms of adopted conformation, interactions with the VDR and score. Therefore, they are good candidates for synthesis and biological assays (Fig. 16).

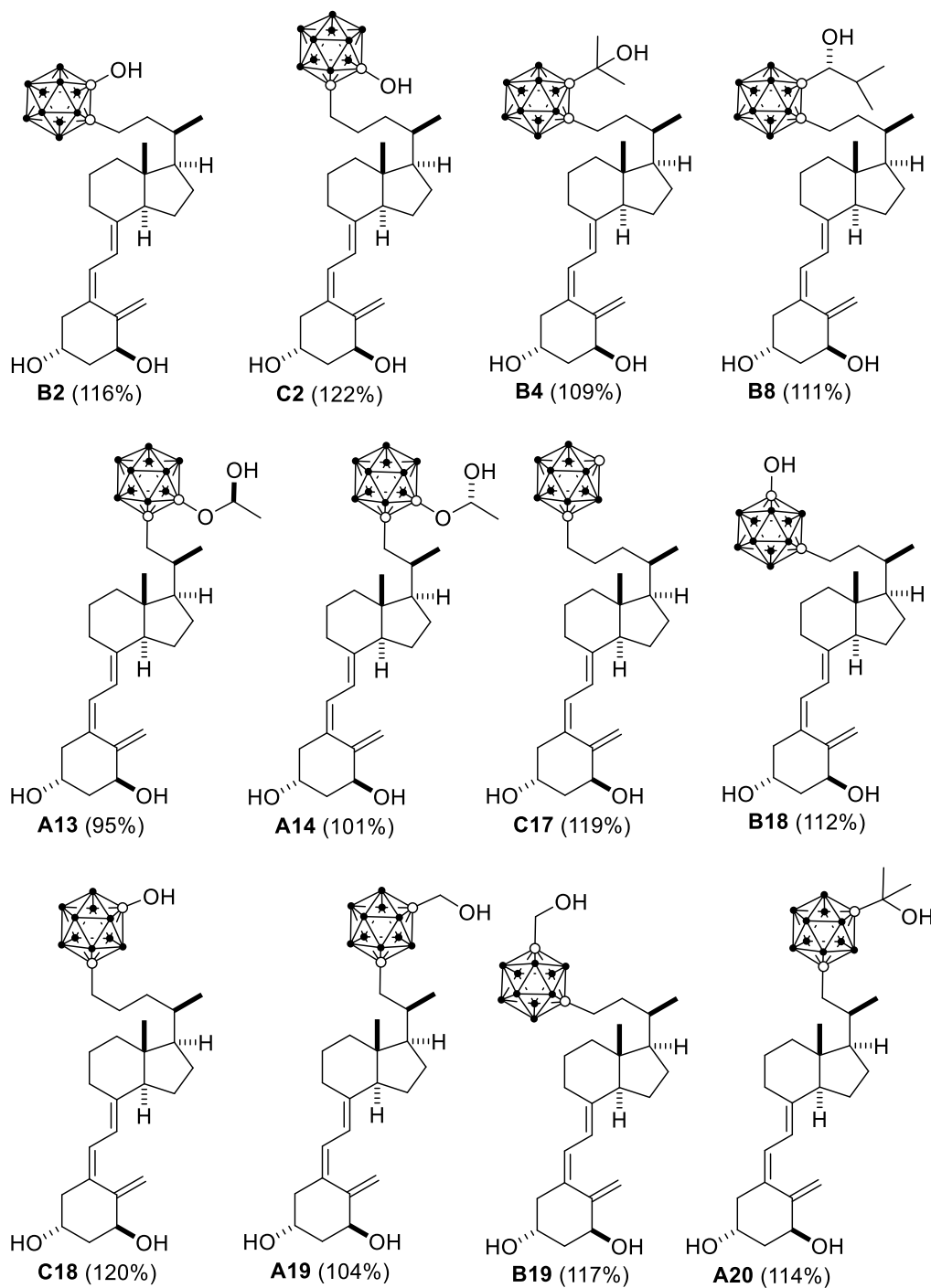


Fig. 16. Conformation of the most promising docked analogs

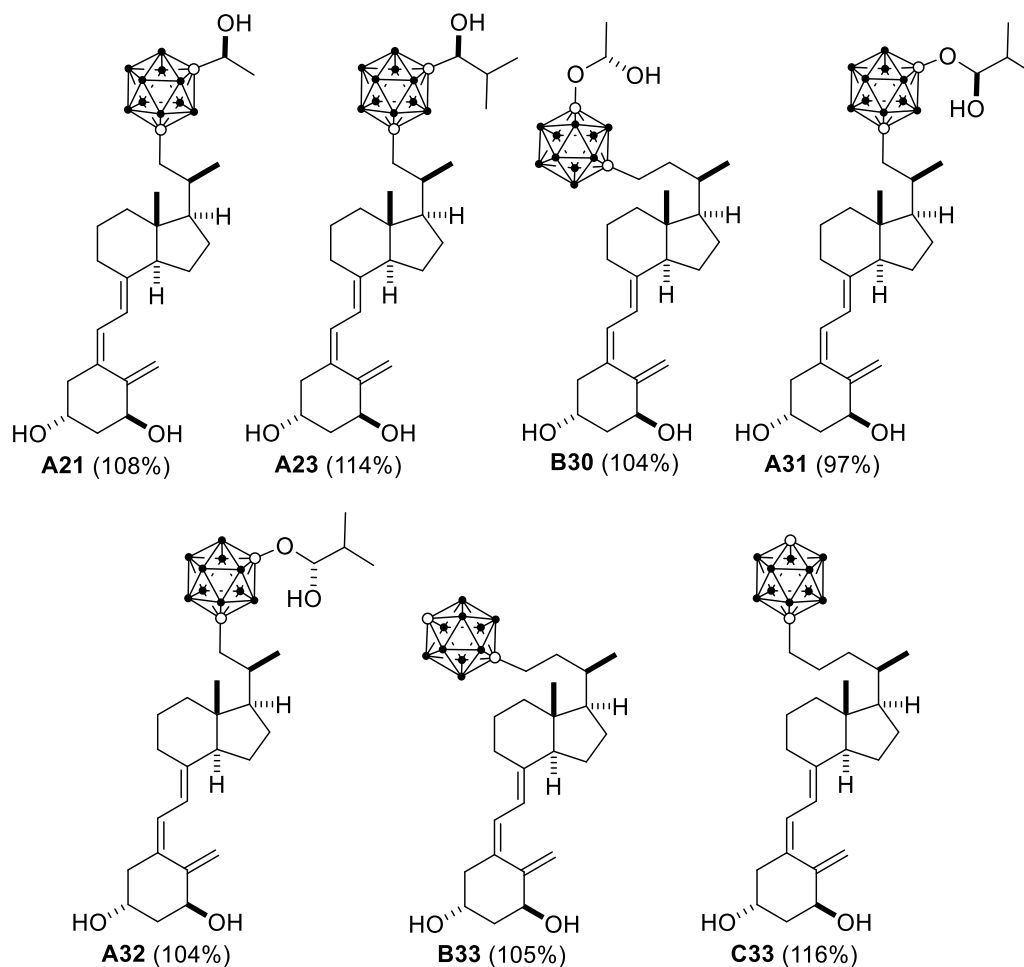


Fig. 16. Conformation of the most promising docked analogs (*continuation*)

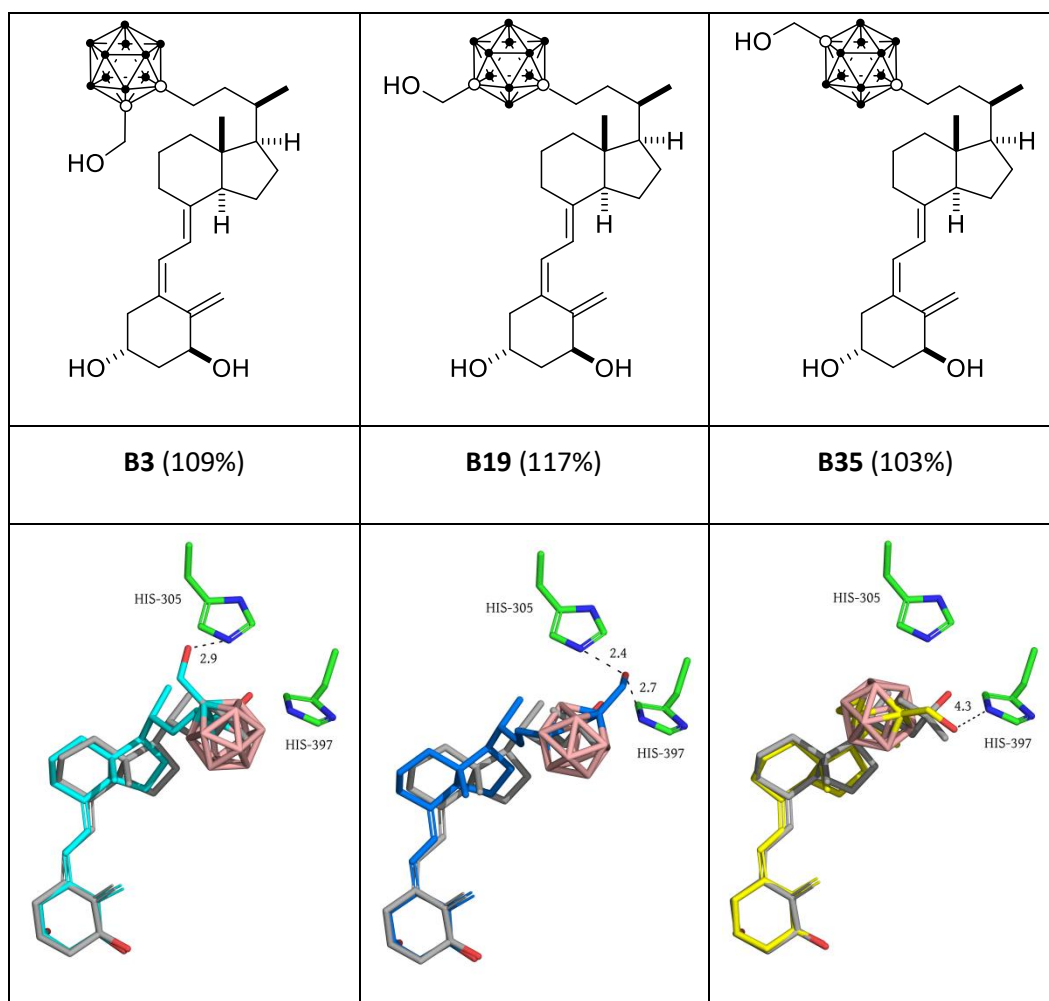
The different conditions tested also provided some interesting information, which is explored next.

1.4.1. Docking results of analogs depending on the carborane isomers

Regarding the distinct conditions tested, it is possible to conclude that, overall, analogs with *meta*-carboranes appear to fit better in the binding pocket of VDR, as the connected R groups impart a favorable orientation. On the contrary, *para*-carborane containing analogs fit worse in the binding pocket, as most R groups do not interact with residues His305 and His397. This preference is detected in regards to both ligand poses, interaction with the VDR and docking scores.

For example, when comparing analogs **B3** (*ortho*-carborane), **B19** (*meta*-carborane) and **B35** (*para*-carborane, Table 1), it is possible to see that analog **B19** fits better, has a better score and its R group forms more stable hydrogen bonds with the receptor.

Table 1. Comparison of docking scores for analogs containing different carborane isomers. First line shows a representation of the docked analog. Last line shows the docking result for each ligand superimposed with calcitriol inside the VDR binding pocket. Calcitriol is represented in grey.



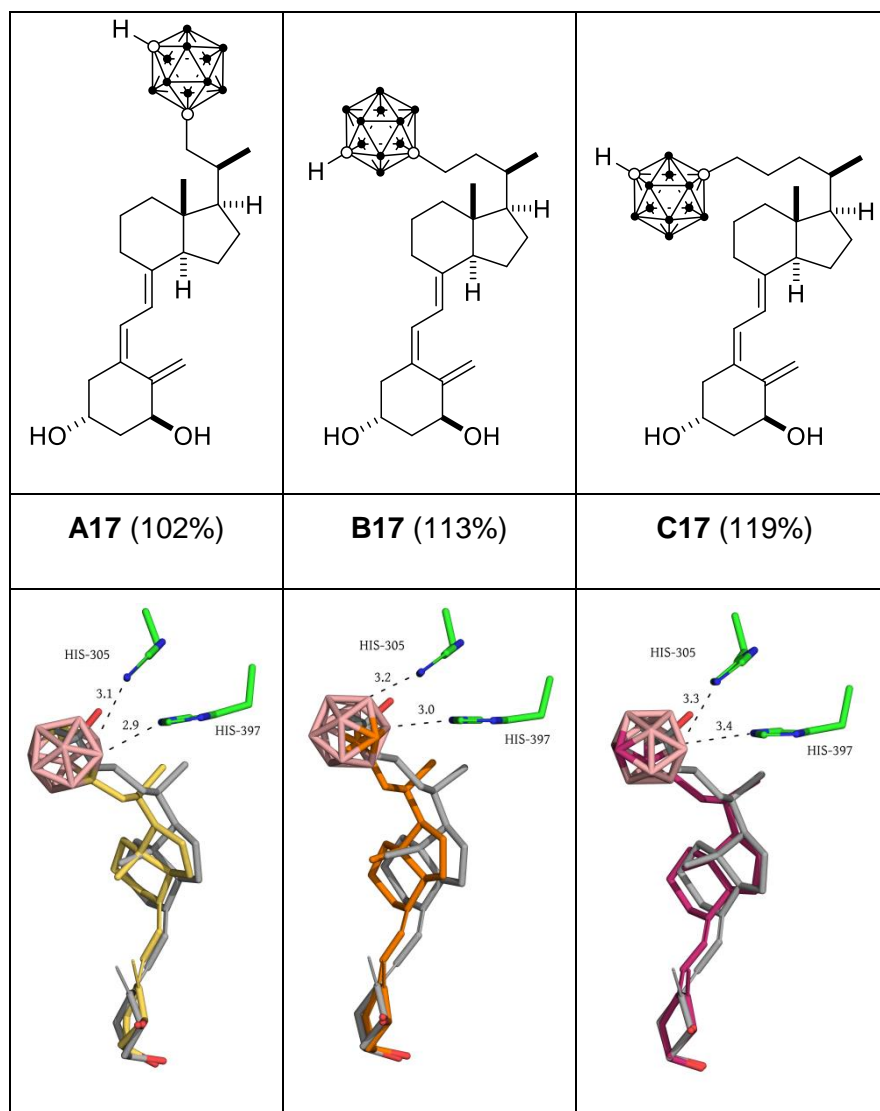
From these docking results, it is possible to observe that the theoretical binding affinity for the VDR depends on the carborane isomer attached to the side chain. Thus, these *in silico* results postulate that similar compounds containing distinct carborane isomers could have different biological properties. Therefore, we decided to synthesize *ortho*-, *meta*- and *para*-carborane analogs.

1.4.2. Docking results of analogs with different side chain sizes and R groups

Regarding the size of the side chain, it was concluded that the preferred length of the side chain (n) greatly depends on the size of the R groups. Analogs with smaller R groups (-H or -OH) benefit from larger side chains (n=3), while analogs with intermediate to large R groups (alcohols, esters or hemiacetals) fit better inside the VDR when combined with smaller side chains (n=1 or n=2).

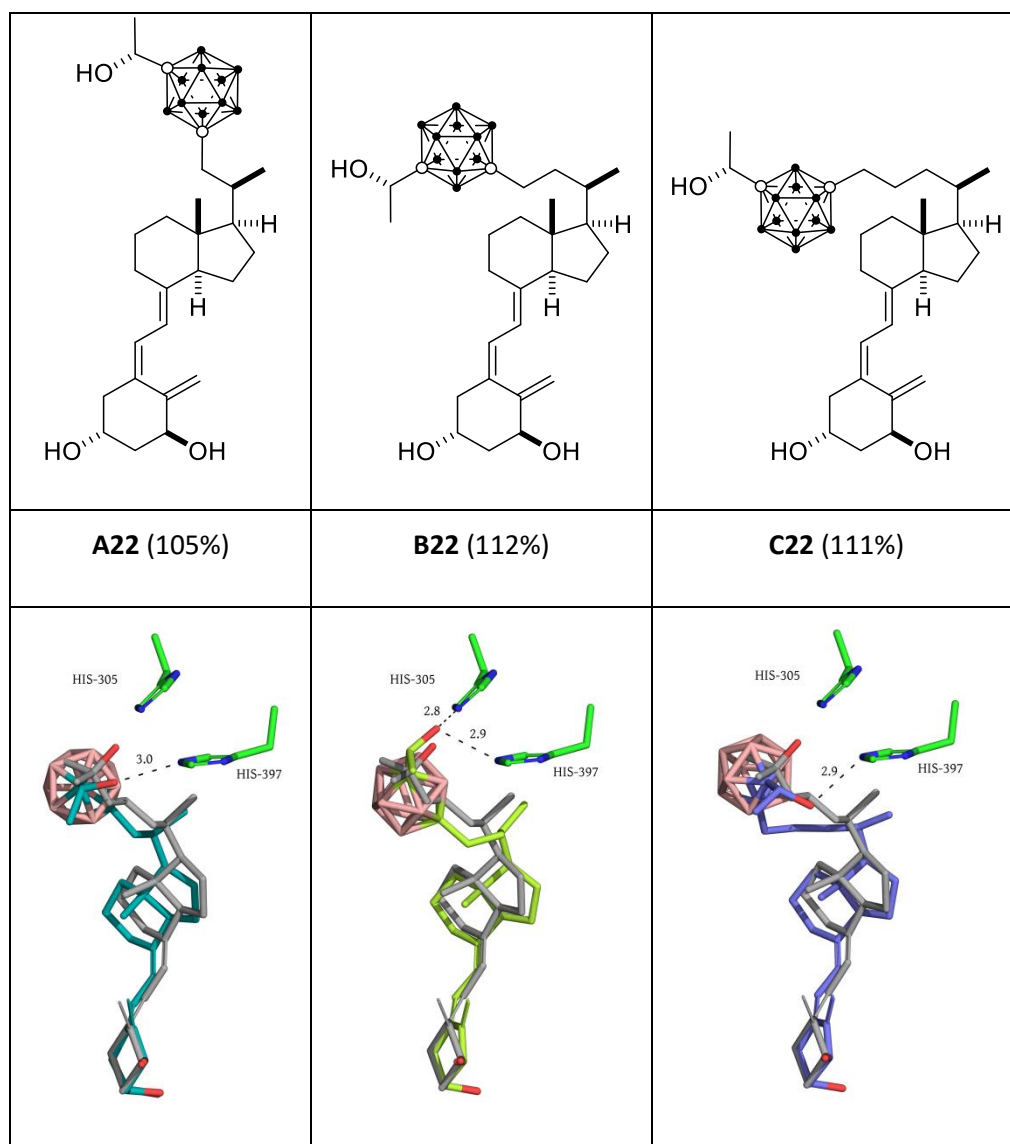
For example, with regard to small R groups (Table 2), analog **C17** (n=3) has a better score than the other two analogs, **A17** (n=1) and **B17** (n=2), as it fits better inside the binding pocket.

Table 2. Comparison of docking score for analogs with small R groups. First line shows a representation of the docked analog. Last line shows the docking result for each ligand superimposed with calcitriol (grey) inside the VDR binding pocket.

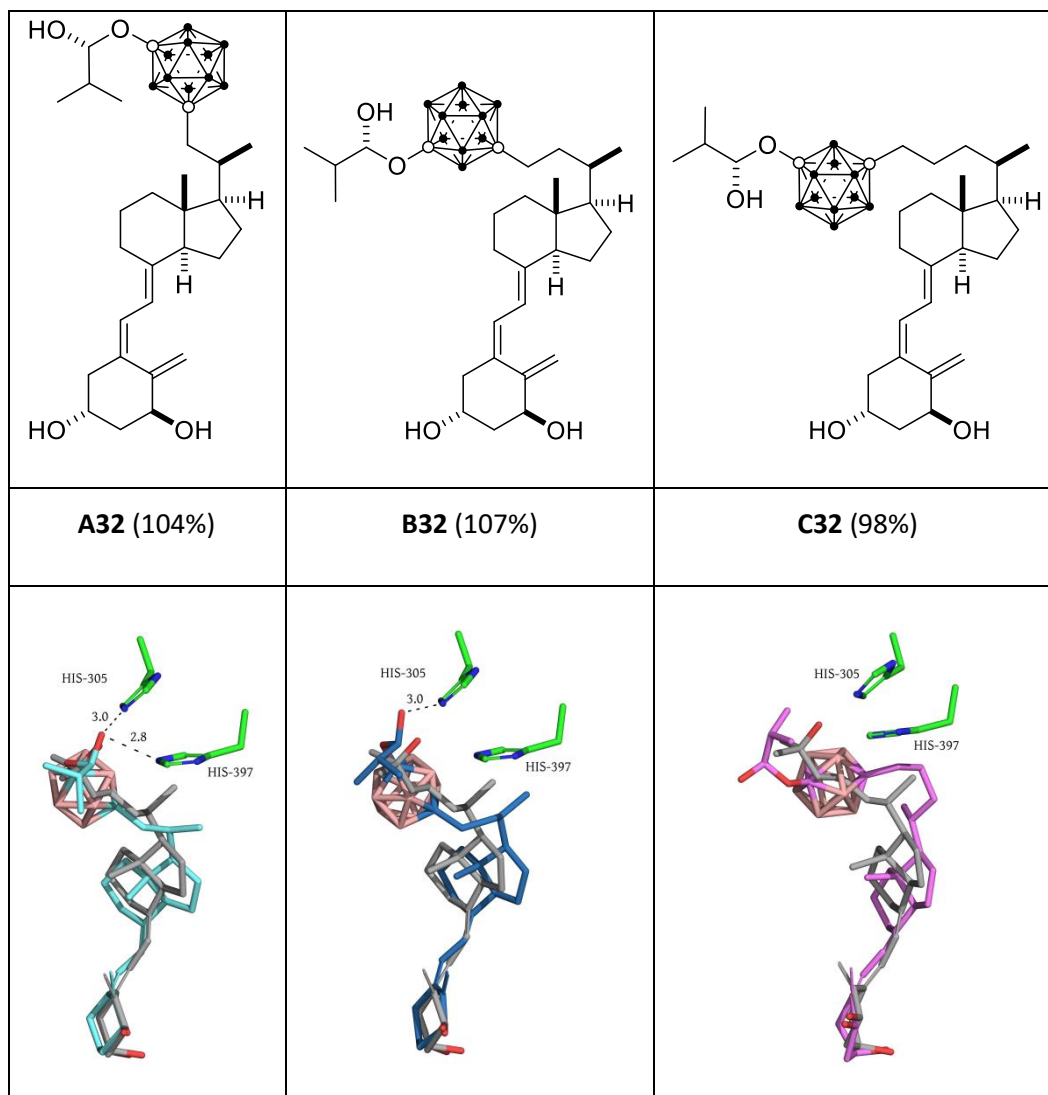


Intermediate sized groups, such as small alcohols, are better in combination with an intermediate side chain length (Table 3). For example, analog **B22** (n=2) has a better score than analogs **A22** (n=1) and **C22** (n=3), which contain smaller and larger side chains, respectively. Analog **B22** is able to adopt a conformation similar to that of calcitriol, while forming similar hydrogen bonds with His305 and His397.

Table 3. Comparison of docking score for analogs with intermediate R groups. First line shows a representation of the docked analog. Last line shows the docking result for each ligand superimposed with calcitriol (grey) inside the VDR binding pocket



When it concerns larger **R** groups, such as large ketone, acetal and hemiacetal substituents, a smaller side chain ($n=1$) is often favourable (Table 4). In this case, analogs **A32** ($n=1$) and **B32** ($n=2$) have similar docking results. However, analog **A32** binds to both His305 and His397 and adopts a more preferable conformation inside the pocket. On the contrary, analog **C32** is clearly too large to fit the binding pocket, as seen from its distorted side chain and **CD** bicycle.

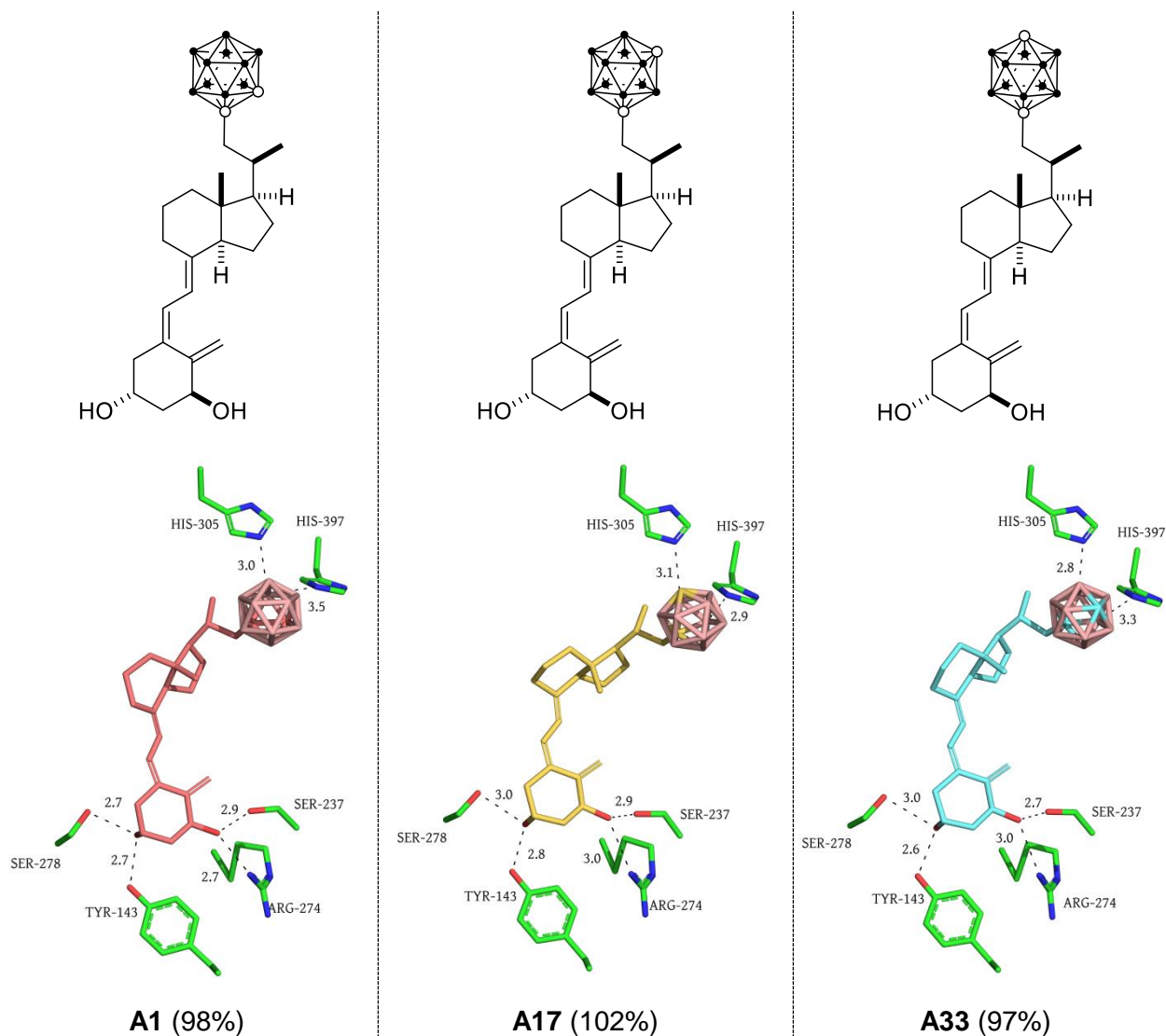
Table 4. Comparison of docking score for analogs with large R groups. First line shows a representation of the docked analog. Last line shows the docking result for each ligand superimposed with calcitriol (grey) inside the VDR binding pocket

These results demonstrate that the choice of side chain size depends on the R group.

1.5. Choice of target analogs for synthesis

Compounds **A1**, **A17** and **A33** (Table 5) were investigated as possible targets to study the biological role of the *ortho*-, *meta*- and *para*-carboranes. Since they have a different side chain length ($n=1$) than the previously synthesized **RO** analog ($n=3$), these compounds would also be useful to study the effect of the side chain length in the analogs' biological behavior.

Table 5. Target analogs for synthesis. . First line shows a representation of the docked analog. Last line shows the docking result for each ligand inside the VDR binding pocket



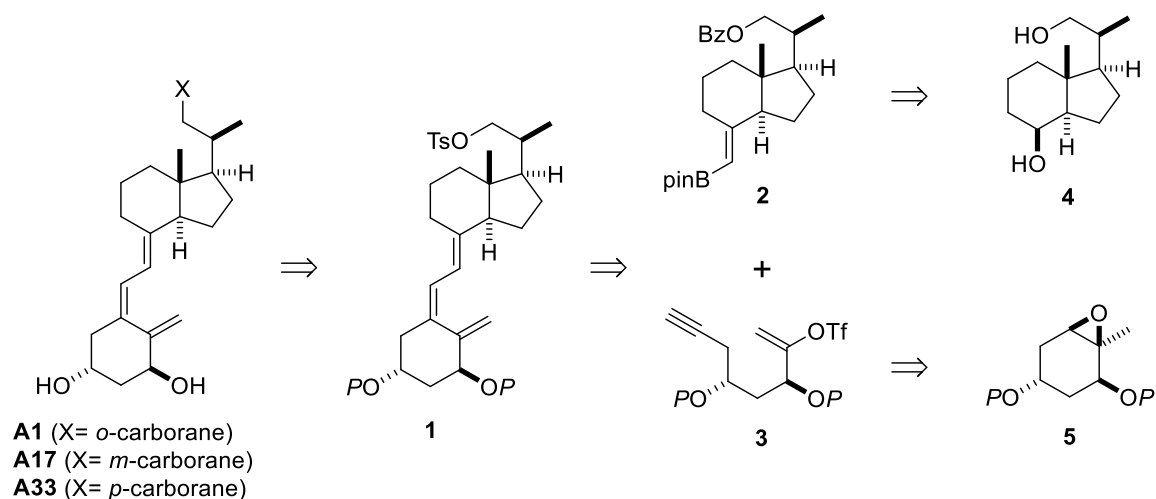
In addition, these analogs could be used as precursors of promising hemiacetal analogs. One of the long term goals of this research group is the synthesis of carborane-containing calcitriol analogs with stable hemiacetal substituents on the carborane, to test their stability and biological properties. From the hemiacetal analogs tested, compounds **A13**, **A14**, **A31** and **A32**, which have *ortho*- or *meta*-carboranes and a side chain length of $n=1$, were the most promising (Fig. 16). Since analogs **A1**, **A17** and **A33** have the same side chain length and carborane isomers, they could be used as precursors to these hemiacetal compounds.

In terms of docking results, these analogs have docking scores similar to 1,25D. They adopt a favorable conformation inside the receptor and bind to the same amino acids as calcitriol. Therefore, they should have binding affinity towards the VDR and should induce transcription.

2. CHAPTER II: Synthesis of Carborane Analogs **A1**, **A17** and **A33**

2.1. Retrosynthesis

The retrosynthesis analysis for the preparation of the target compounds **A1**, **A17** and **A33** is depicted in Scheme 9.



Scheme 9. Retrosynthetic analysis planned for the synthesis of compounds **A1**, **A17** and **A33**. P = protecting group

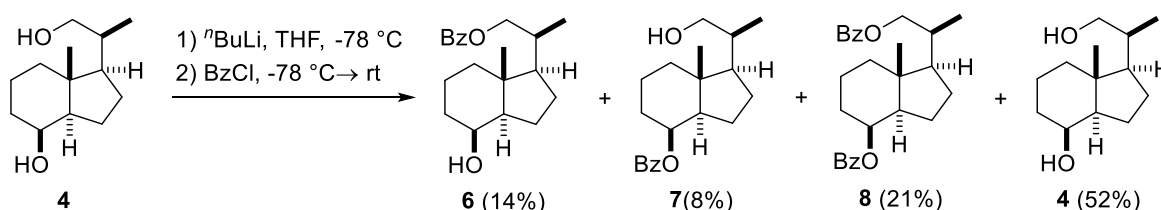
The key step of the synthesis is the introduction of the carborane moiety at the end of the synthesis by reaction of the corresponding carboranyl lithium on tosylate **1**.

The triene system would be built by a stereoselective Pd-catalyzed ring closure on enol-triflate **3** and subsequent Suzuki-Miyaura coupling with alkenyl-boronic ester **2**. The enol-triflate **3** would arise from epoxide **5**, following procedures previously developed in this laboratory.⁵³ The required boronic ester **2** would be prepared from Inhoffen-Lythgoe diol **4** by oxidation, Wittig chemistry and Pd-catalysed Br-B interchange.⁵⁴

2.2. Synthesis of benzoate 6

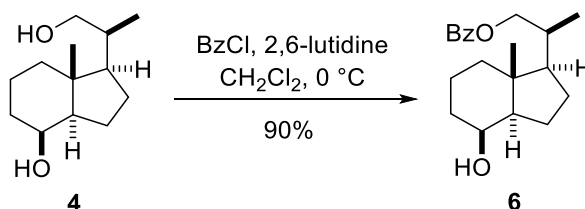
The synthesis started with known Inhoffen-Lythgoe diol (**4**), prepared from reductive ozonolysis of commercial vitamin D₂,⁵⁵ which was converted to benzoate **6** (Scheme 10).

Diol **4** was treated with ⁿBuLi, at low temperature, followed by addition of benzoyl chloride to give compounds **6** (14%), **7** (8%) and **8** (21%), together with starting material **4** (52%).



Scheme 10. Synthesis of benzoate **6** by metalation of diol **4**

We next tried to improve the yield of the desired benzoate **6**. Thus, treatment of diol **4** with benzoyl chloride in the presence of 2,6-lutidine, in dichloromethane, provided benzoate **6** in a good yield (Scheme 11).



Scheme 11. Selective synthesis of benzoate **6**

Fig. 17 shows the most significant ¹H-NMR and ¹³C-NMR signals of benzoate **6**

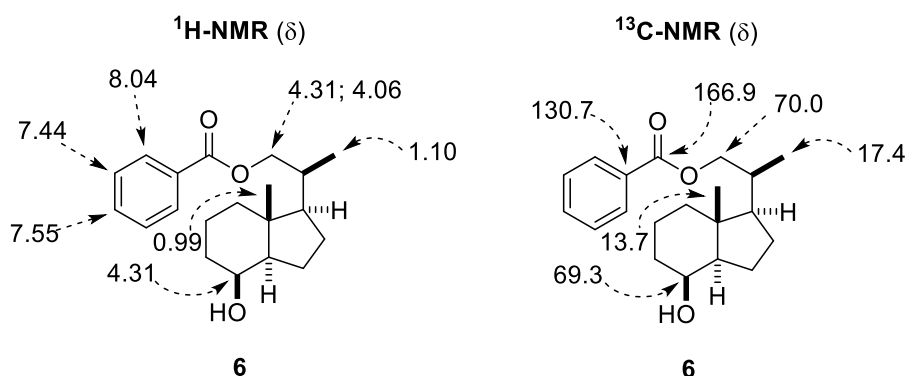
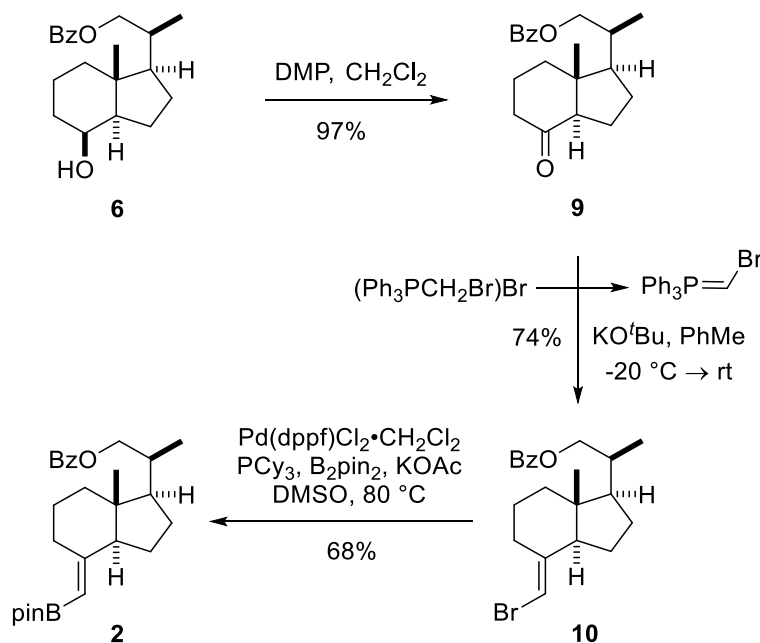


Fig. 17. ¹H-NMR and ¹³C-NMR main signals for compound **6**

2.3. Synthesis of boronic ester 2

Boronic ester **2** was then prepared in 50% overall yield, following previously developed procedures of this laboratory, which involve Dess-Martin oxidation, Wittig chemistry and Miyaura borylation (Scheme 12).⁵⁶⁻⁵⁷



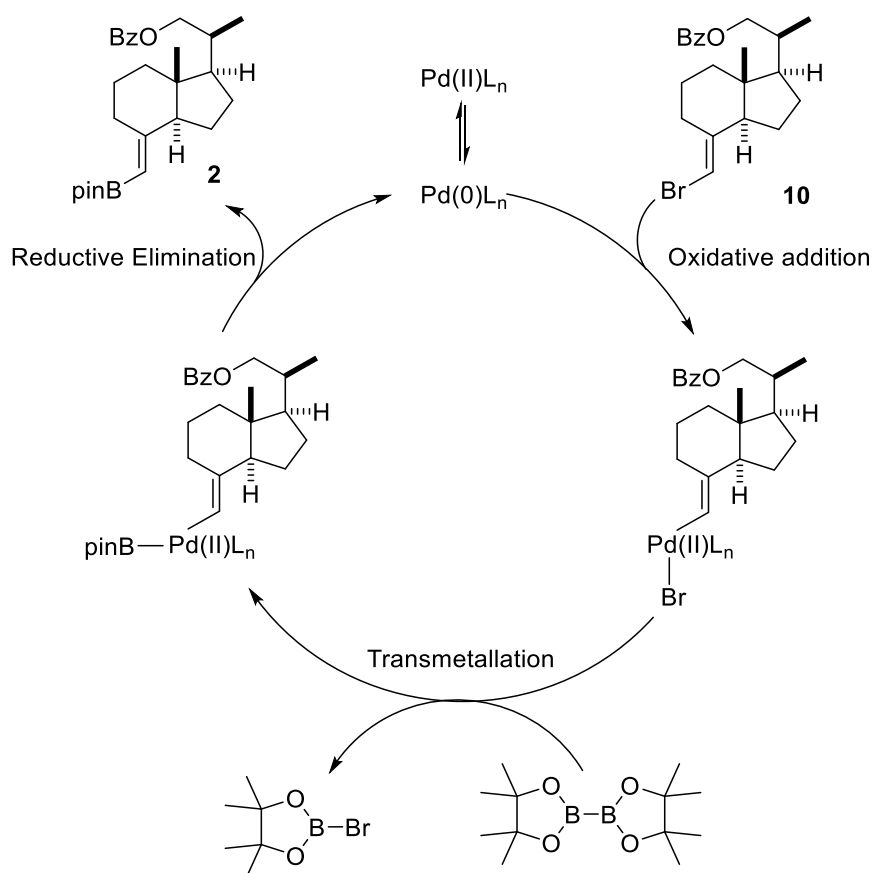
Scheme 12. Synthesis of boronic ester **2**

The oxidation of alcohol **6** with Dess-Martin periodinane in CH₂Cl₂ afforded ketone **9** in excellent yield.

Wittig chemistry between ketone **9** and ylide Ph₃P=CHBr, generated *in situ* by treatment of (bromomethyl)triphenylphosphonium bromide with potassium *tert*-butoxide in toluene, provided vinyl bromide **10** in a 74% yield.

The alkenyl bromide **10** was then converted to boronate **2** in 68% yield by a Pd(0) catalyzed cross-coupling reaction employing bis(pinacolate)diboron and PdCl₂(dppf)·CH₂Cl₂, as the catalyst, in the presence of tricyclohexylphosphine and KOAc in DMSO.⁵⁷

Scheme 13 depicts the proposed mechanism for this Miyaura borylation.



Scheme 13. Proposed mechanism for the Miyaura borylation reaction in the synthesis of boronic ester **2**

The reaction starts with the *in situ* formation of the Pd(0) catalyst, which is then inserted in the C-Br bond of the vinyl halide through oxidative addition. Then, transmetallation with bis(pinacolate)diboron, followed by reductive elimination, furnishes boronate **2** and leads to the regeneration of Pd(0).

Fig. 18 shows the most significant ¹H-NMR and ¹³C-NMR signals of boronic ester **2**.

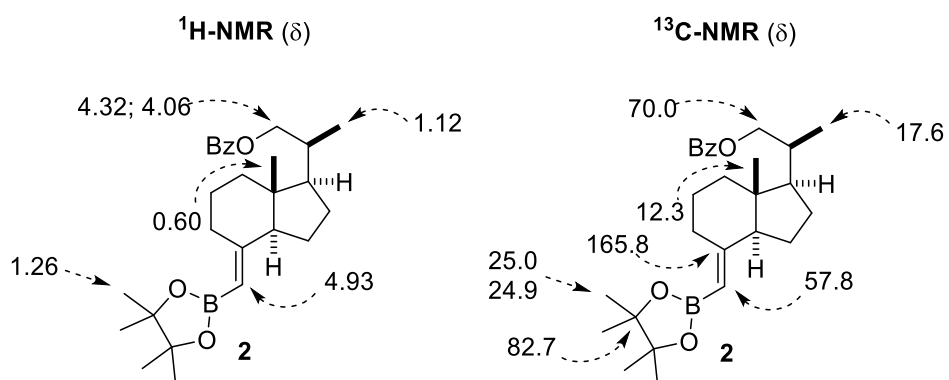
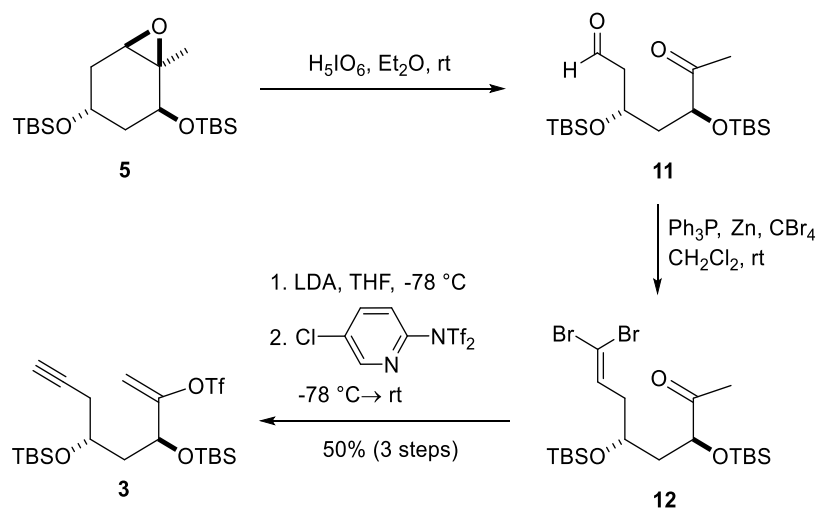


Fig. 18. Main ¹H-NMR and ¹³C-NMR signals for boronic ester **2**

2.4. Synthesis of enol-triflate 3

The enol-triflate **3** was prepared from the diprotected epoxide **5**, following previously developed procedures (Scheme 14).⁵⁸



Scheme 14. Synthesis of enol triflate **3**

Epoxide **5** was converted to dibromide **12** by a two-step sequence. Periodic acid-oxidative cleavage of the epoxide **5** in Et_2O gave aldehyde **11**, which was transformed into dibromide **12** by Corey-Fuchs' conditions.⁵⁹

Finally, the enol-triflate **3** was obtained in moderate yield from dibromide **12**, by treatment with lithium diisopropylamide (LDA), followed by reaction of the resulting enolate with *N*-(5-chloro-2-pyridyl)triflimide (Comins' reagent).

Fig. 19 shows the most significant $^1\text{H-NMR}$ and $^{13}\text{C-NMR}$ signals of enol-triflate **3**.

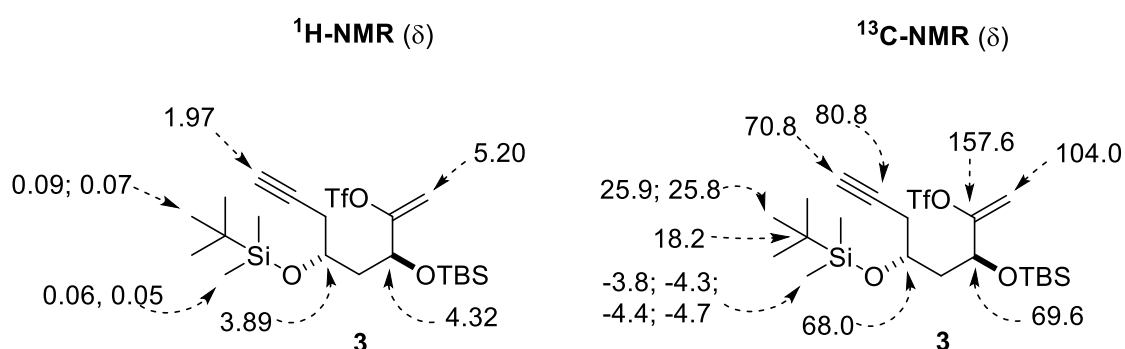
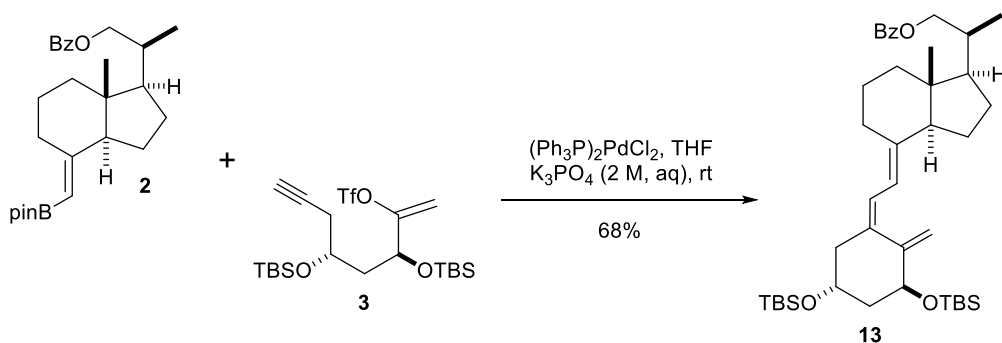


Fig. 19. $^1\text{H-NMR}$ and $^{13}\text{C-NMR}$ signals of enol-triflate **3**

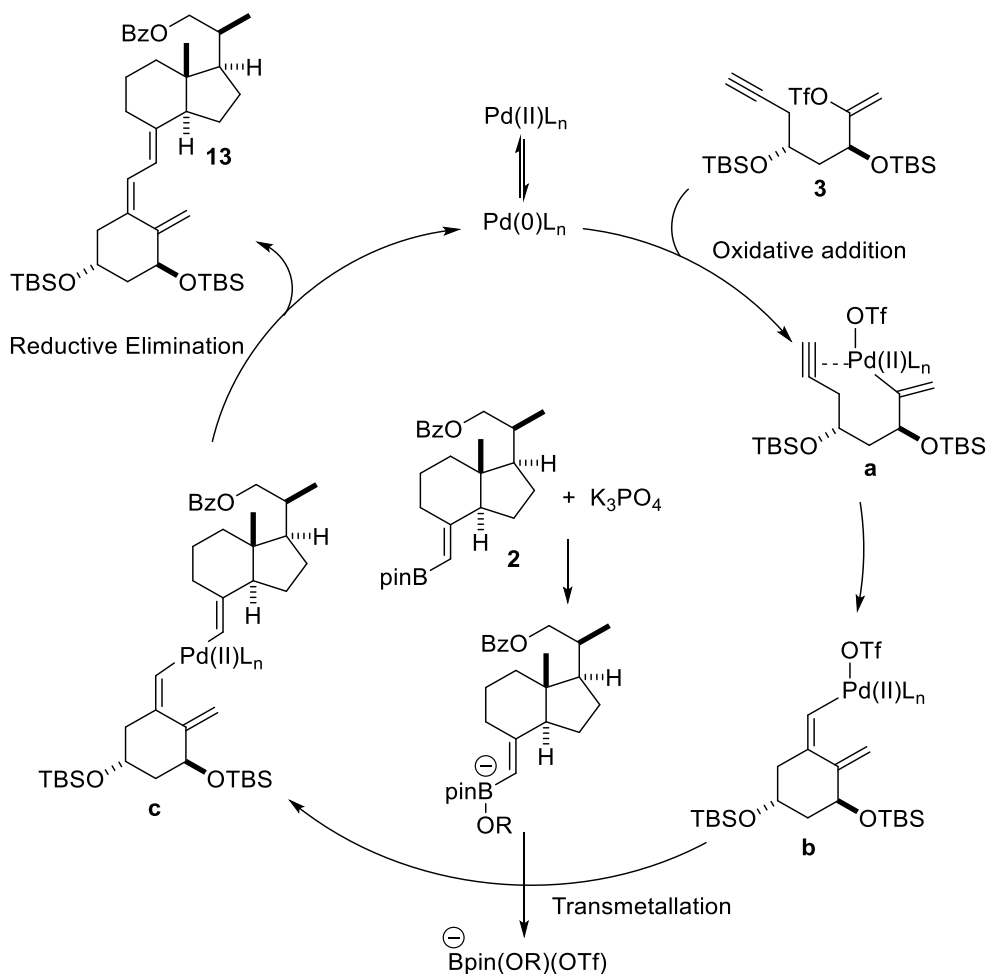
2.5. Synthesis of tosylate 1

With the upper and lower fragments in hand, we proceeded to build the vitamin D triene system by a Pd-catalyzed ring closure of enol-triflate **3**, followed by Suzuki Miyaura cross-coupling with boronate **2**, in the presence of aqueous K_3PO_4 , to give **13** in 68% yield (Scheme 15).



Scheme 15. Synthesis of benzoate **13** via carbocyclization and Suzuki-Miyaura cross-coupling of **2** and **3**

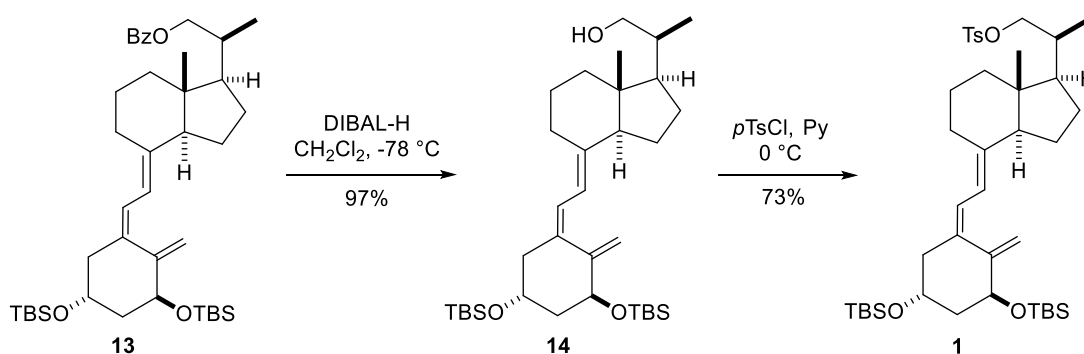
The proposed mechanism for this reaction is shown in Scheme 16.



Scheme 16. Proposed mechanism of action of the Suzuki Miyaura cross-coupling to afford **13**

The Pd(0) complex coordinates with the alkyne group of enol-triflate **3**, which is followed by oxidative addition to the triflate group to furnish intermediate compound **a**. Then, a Pd-catalyzed Heck-type addition produces the Pd(II) intermediate (**b**), which undergoes a transposition with an activated boronate to produce intermediate **c**. Finally, this intermediate is transformed into benzoate **13** by reductive elimination, which is accompanied by the regeneration of the Pd(0) complex.

To facilitate the introduction of the carborane moiety in the side chain, tosylate **1**, which contains a good leaving group at C-22, was prepared from benzoate **13** in a two-step sequence (71% yield, Scheme 17).



Scheme 17. Synthesis of tosylate **1**

Ester **13** was reduced with DIBAL-H to alcohol **14**, which upon tosylation afforded the desired compound **1** in good yield.

Fig. 20 shows the most significant ¹H-NMR and ¹³C-NMR signals of tosylate **1**.

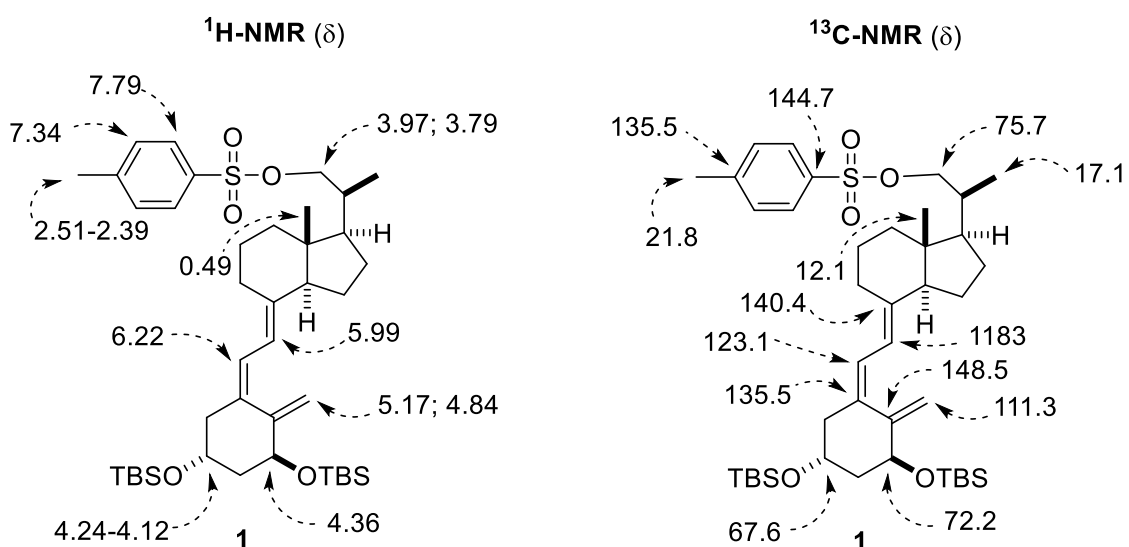
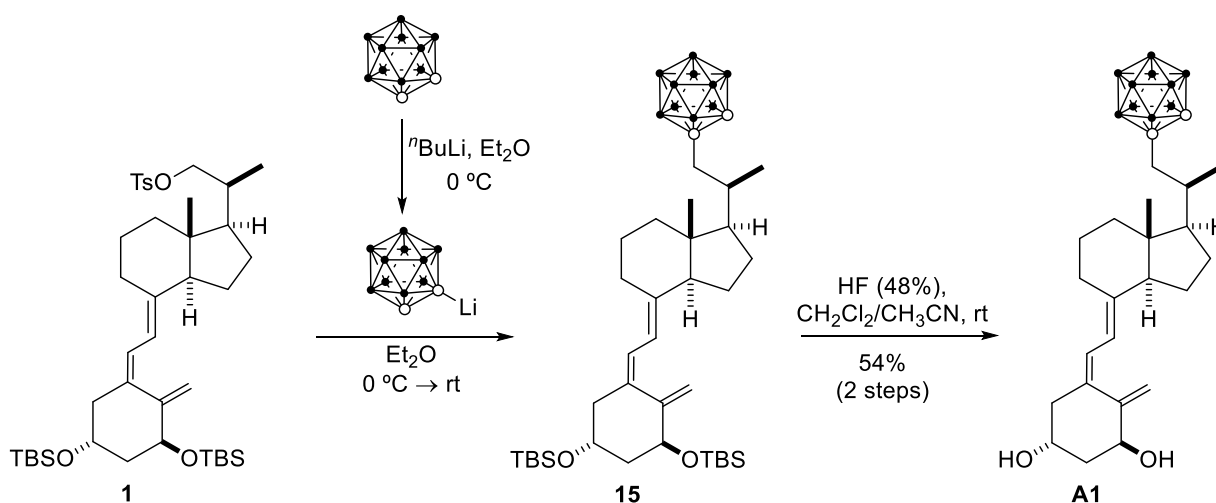


Fig. 20. Main ¹H-NMR and ¹³C-NMR signals of tosylate **1**

2.6. Synthesis of analogs A1, A17 and A33

As mentioned in the introduction, the carborane unit was previously introduced in the side chain of a vitamin D analog *via* reaction of an alkyne with decaborane ($B_{10}H_{14}$), in the presence of *N,N*-dimethylaniline.⁴⁹ However, this methodology had some drawbacks, including low reaction yields and high toxicity of decaborane. Additionally, this reaction only allows the production of *ortho*-substituted derivatives. Since one of the purposes of this work is the synthesis of analogs with *ortho*, *meta* and *para*-carborane units at the side chain, we focused on an alternative method to directly introduce the carborane moiety. A S_N2 reaction between tosylate **1** and a carboranyl lithium was found suitable for this purpose.

Thus, direct displacement of the tosylate group of **1** with *ortho*-carboranyl lithium, generated by reaction of the *ortho*-carborane with n BuLi, provided the *ortho*-carborane derivative **15**, which was deprotected with aqueous HF to furnish the desired vitamin D analog **A1** in good yield (54%, 2 steps, Scheme 18).



Scheme 18. Synthesis of analog **A1**

The *ortho*-carborane analog **A1** was obtained from the Inhoffen-Lythgoe in 9 steps and 12% overall yield.

Fig. 21 shows the ^1H -NMR spectrum of vitamin D analog **A1**.

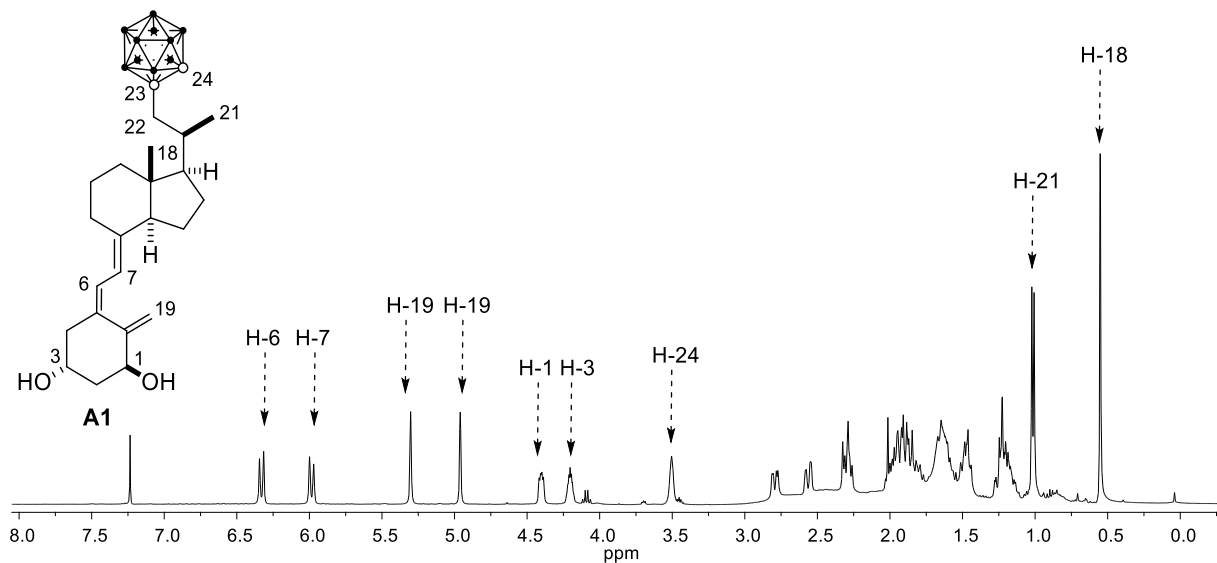


Fig. 21. ¹H-NMR spectrum of analog **A1**

The well-defined singlet at 3.53 ppm corresponds to the C-24 proton of the *ortho*-carborane unit. The 10 H of the carborane moiety, present at the 10 BH vertices, appear as a wide band between 3.0-1.0 ppm, as seen by the increase of the baseline of the spectrum.

The ¹¹B-NMR spectrum of analog **A1** (Fig. 22) shows that the 10 BH protons of the carborane unit are divided in 5 signals that integrate in the ratio 1:1:2:4:2 (-2.3, -5.6, -9.3, -11.6 and -13.1 ppm). This spectrum is similar to the known spectrum of free *ortho*-carborane, which confirms the successful introduction of this moiety in the target analog.^{46, 60}

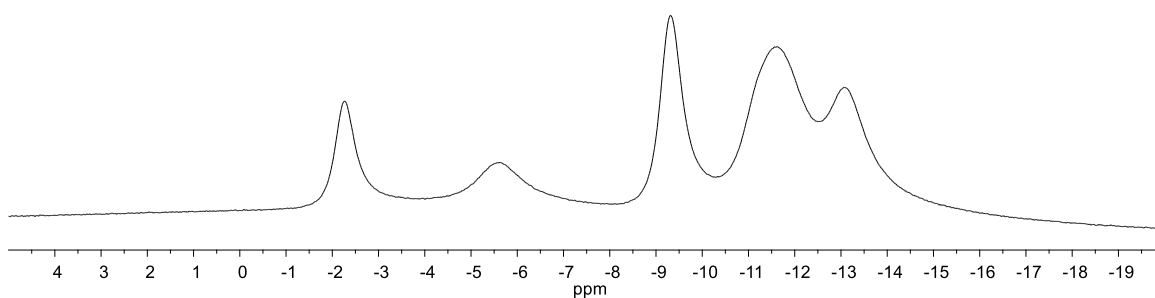
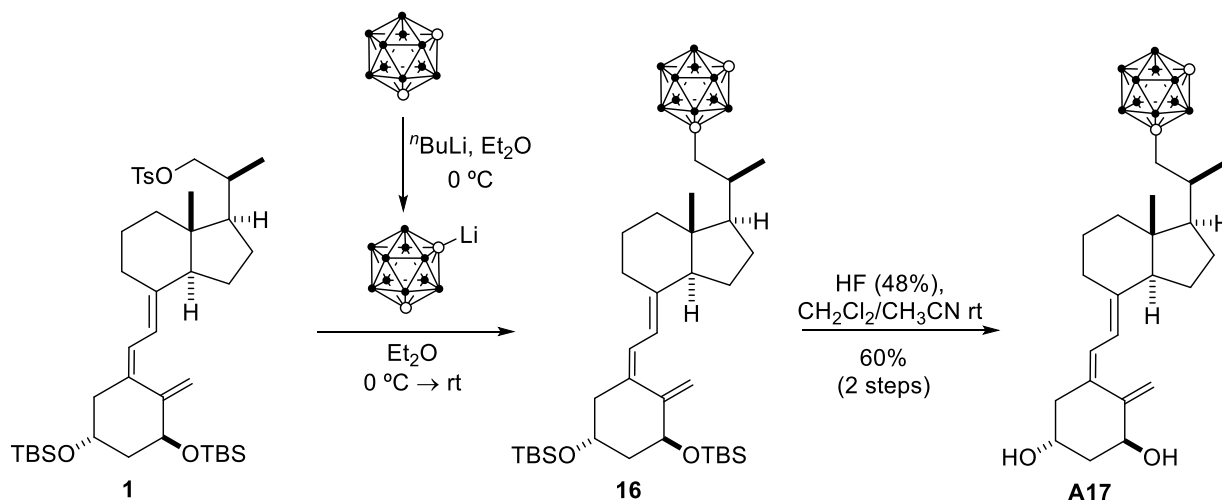


Fig. 22. ¹¹B-NMR spectrum of analog **A1**

Following the same methodology, analog **A17** was synthesized from tosylate **1** in a 60% yield (2 steps, Scheme 19).



Scheme 19. Synthesis of analog **A17**

The *meta*-carborane analog **A17** was obtained from the Inhoffen-Lythgoe in 9 steps and 13% overall yield.

Fig. 23 shows the $^1\text{H-NMR}$ spectrum of vitamin D analog **A17**

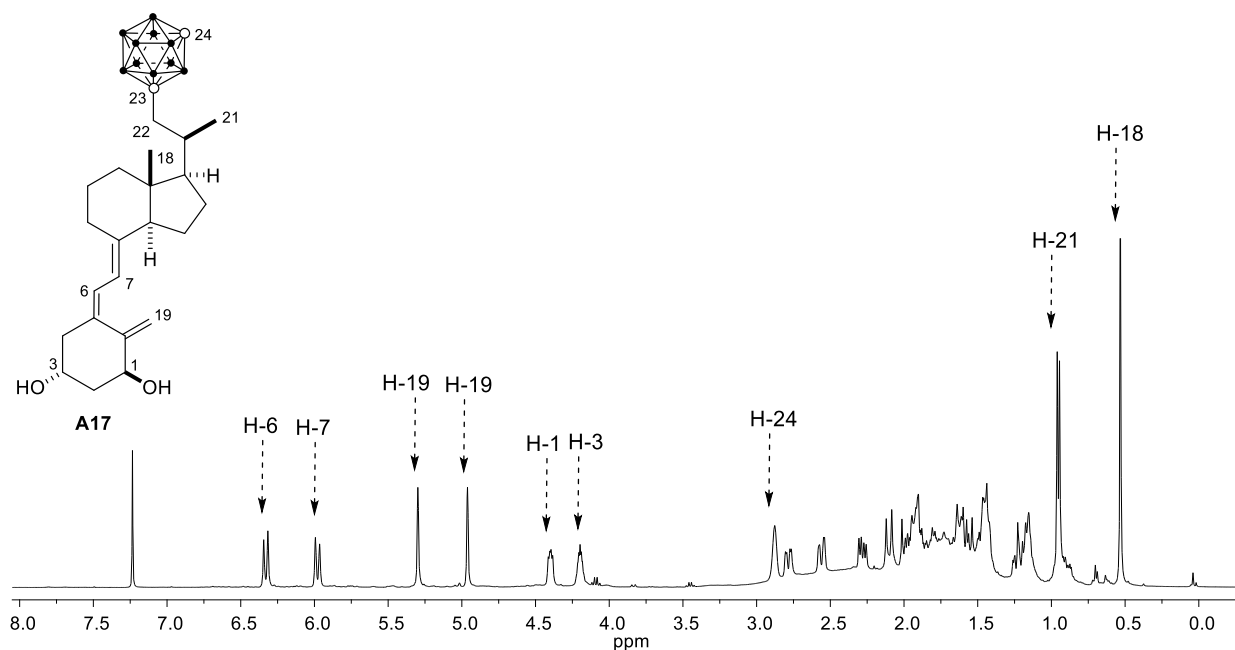


Fig. 23. $^1\text{H-NMR}$ spectrum of analog **A17**

The well-defined singlet at 2.90 ppm corresponds to the proton of C-24. The wide band between 3.00 and 1.00 ppm, observed by the increase of the baseline of the spectrum, corresponds to the 10 BH protons.

The ^{11}B -NMR spectrum of analog **A17** (Fig. 24) shows that the 10 BH protons of the *meta*-carborane unit of the analog **A17** are divided in 4 different sets in the ratio 2:4:2:2 (-3.8, -10.7, -13.7, -15.1 ppm), which is similar to the spectrum obtained for the free *meta*-carborane.⁴⁶

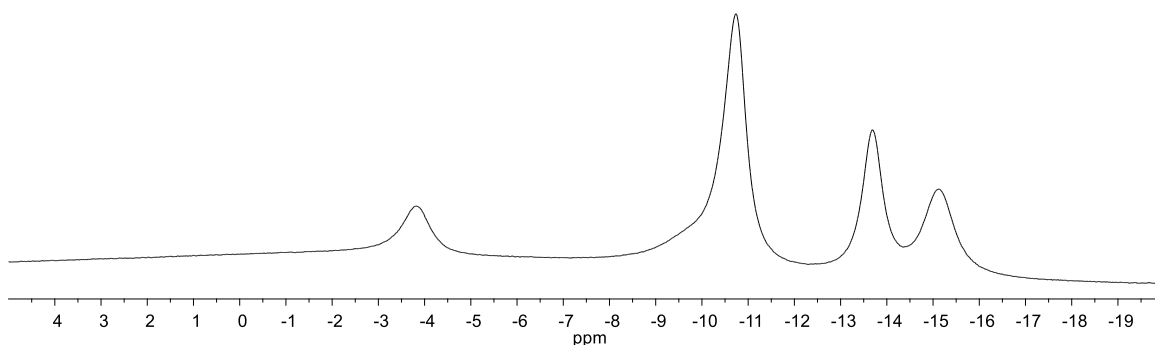
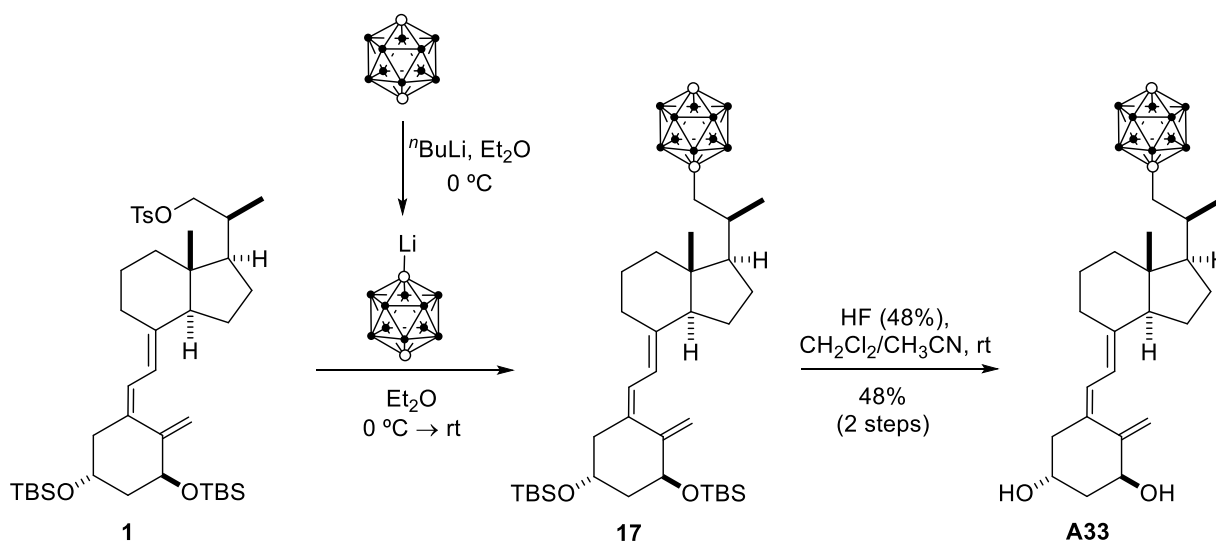


Fig. 24. ^{11}B -NMR spectrum of analog **A17**

Following the same methodology, analog **A33** was prepared from tosylate **1** in a 48% yield (2 steps, Scheme 20).



Scheme 20. Synthesis of analog **A33**

The synthesis of **A33** was accomplished in 9 steps and a 12% overall yield from the Inhoffen-Lythgoe diol.

Fig. 25 shows the ^1H -NMR spectrum of vitamin D analog **A33**.

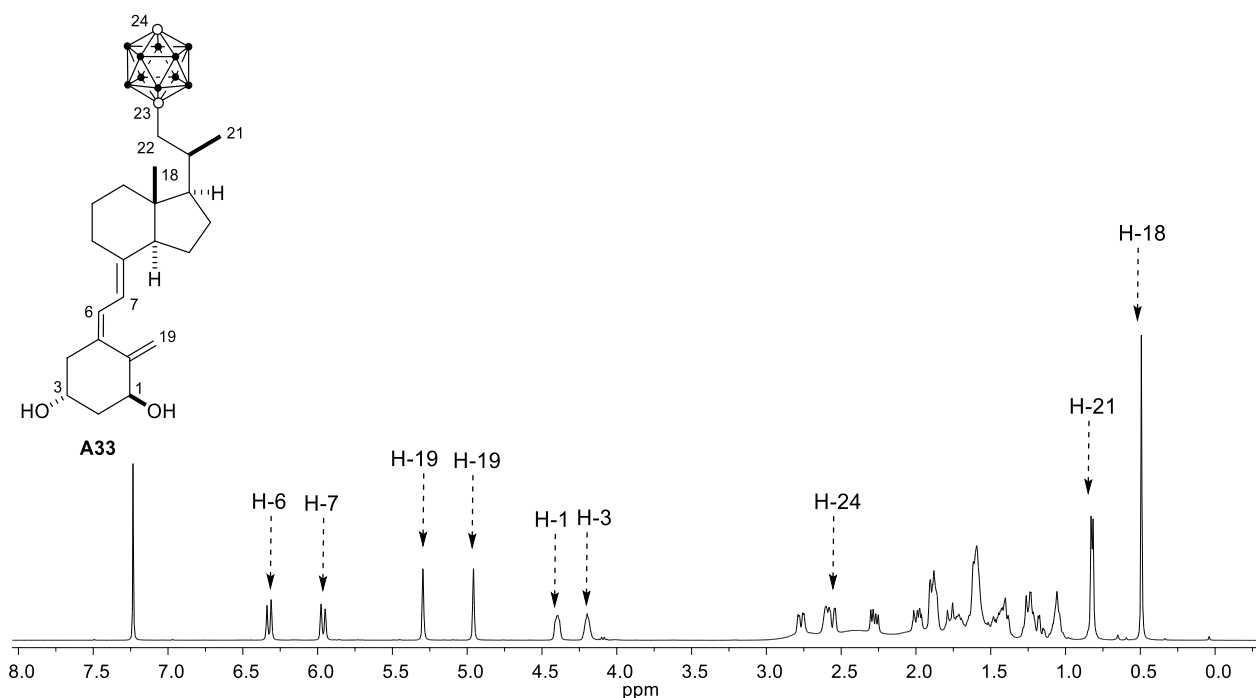


Fig. 25. $^1\text{H-NMR}$ spectrum of analog **A33**

The proton of C-24 of the *para*-carborane moiety appears as a singlet at 2.59 ppm. The 10 H of the BH units appear as a wide band between 3.0-1.0 ppm, similarly to the other analogs.

The decoupled $^{11}\text{B-NMR}$ spectrum of analog **A33** (Fig. 26) shows that the 10 BH protons of the *para*-carborane unit of the analog **A33** are divided in 2 different sets in the ratio 5:5 (-12.3; -15.2 ppm). One of the signals is assigned to the 5 boron atoms closer to the free CH group and the other signal is assigned to the BH vertices closer to C-23.

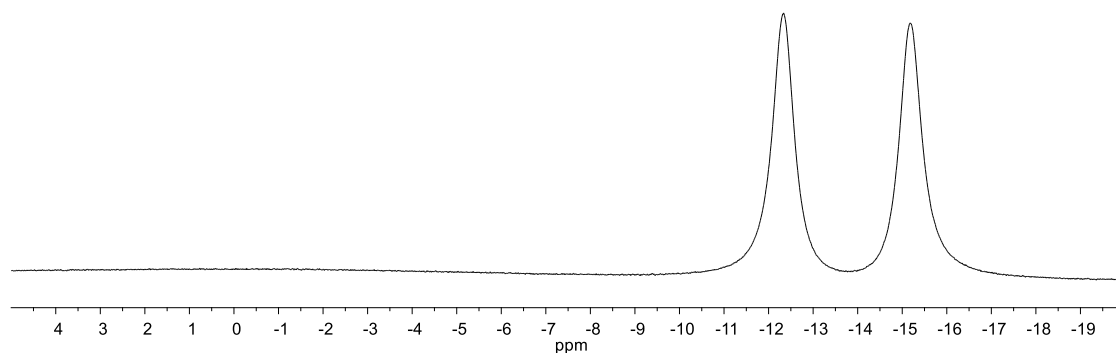


Fig. 26. $^{11}\text{B-NMR}$ spectrum of analog **A33**

The biological properties of these compounds could not be evaluated in time to be included in this work, but the analogs are currently taking part in different biological tests (competitive binding assays, ability to induce transcription activity, cellular proliferation and differentiation in several cell lines and the capacity to modulate calcium serum levels in mice).

CONCLUSIONS

Conclusions

Docking calculations of 144 carborane-containing vitamin D analogs into the binding pocket of human vitamin D receptor [hVDR(LBD)] were accomplished. Several analogs, namely **B2, C2, B4, B8, A13, A14, C17, B18, C18, A19, B19, A20, A21, A23, B30, A31, A32, B33** and **C33**, bind to hVDR(LBD) better than 1 α ,25-dihydroxyvitamin D₃ (1,25D). Therefore, they are good candidates for synthesis and biological testing.

Analogs **A1, A17** and **A33** were synthesized to investigate whether the *ortho*, *meta* and *para*-carborane unit and the side chain size could impart different biological properties, and based on docking calculations.

These secosteroid analogs (**A1, A17** and **A33**), bearing an *ortho*, *meta* and *para*-carborane at the side chain, respectively, were synthesized from the Inhoffen-Lythgoe diol, in a total of 9 steps and about 12% overall yield. The key step was the introduction of the carborane unit at the end of the synthesis by S_N2 displacement of a tosylate group by a carboranylithium, which proved to be an improvement on the published synthetic approach.

This work allowed the establishment of a good synthetic methodology for the synthesis of vitamin D analogs with *ortho*, *meta* and *para* carboranes attached at the side chain.

Future endeavors include the *in vitro* and *in vivo* biological testing of the synthesized compounds, as well as the synthesis of new promising carborane-containing analogs, following the synthetic approach developed in this work.

EXPERIMENTAL SECTION

Experimental Section

1. Docking Calculations

The receptor and the ligands were used as MOL2 files. Energy minimization was not performed on the protein. The ligands were built using the PyMol program,⁵⁰ by modification of the crystal structure of 1,25D. The vitamin D part was obtained from the crystal structure of the complex of 1,25D-hVDR LBD (PDB code: 1DB1).¹¹ The carborane cage part of the ligands was obtained from the crystal structure of the corresponding *ortho* (PDB code: 5E7V)⁴⁹, *meta* (PDB code: 4MDL)⁵¹ and *para*-carboranes (PDB codes: 3VJS).⁵² The ligands were further treated by adding hydrogen atoms and checking atom valence using Chem3D. Energy minimization of the ligands was performed using the MM2 function of Chem3D. The boron atoms “B” were considered as carbon sp³ atoms only for the empirical potential energy function.

Docking studies to predict the affinity of the new ligands for the VDR were carried out using the GOLD program (version Suite 5.2). A modified crystal structure (addition of hydrogen, reconstituted gaps and corrected His tautomers) of the complex between 1,25D-hVDR LBD was chosen as protein (PDB code: 1DB1).¹¹

The Ligand Binding Pocket of the mutant LBD was defined as Binding Site with the automatic active-site detection on, and the radius was set to 10 Å. Ligand was docked in 25 independent genetic algorithm (GA) runs, for each of which a maximum of 125000 GA operations were performed on a single population of 100 individuals. Operator weights for crossover, mutation, and migration in the entry box were used as default parameters (95, 95, and 10, respectively), as well as the hydrogen bonding (4.0 Å) and van der Waals (2.5 Å) parameters. The “flip ring corners” flag was switched off, while all the other flags were on. CHEMPLP was used as a scoring function and GoldScore as a re-scoring function. The best 3 solutions were obtained with an associated score. These results were compared with the solutions for 1,25D.

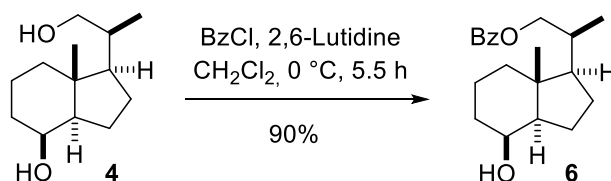
2. General Procedures

All reactions involving oxygen- or moisture-sensitive compounds were carried out under a dry Ar atmosphere using oven-dried or flame-dried glassware and standard syringe/septa techniques, unless when indicated. Liquid reagents or solutions of reagents were added by syringe or cannula techniques. Reaction temperatures refer to external bath temperatures. Reactions at low temperatures were performed in methanol baths cooled with a CRYOCOOL immersion cooler CC-90 (EK-90 de Thermo Fisher Scientific), provided with a temperature regulator. Reactions at high temperatures were carried out using silicon baths, with a temperature regulator. All dry solvents were distilled under Ar immediately prior to use. Tetrahydrofuran (THF), Et₂O and toluene were distilled from Na/benzophenone. Pyridine and 2,6-Lutidine were distilled from CaH₂. CH₂Cl₂ was distilled from P₂O₅. DMSO was distilled from CaH₂ at low pressure and kept over 4 Å molecular sieves. *tert*-Butyl methyl ether (MTBE) and CH₂Cl₂ for extractions was used as received. Solutions of ⁿBuLi in hexanes were titrated with *N*-benzylbenzamide before use. The organic extracts were dried over anhydrous Na₂SO₄, filtered and concentrated using a rotary evaporator at aspirator pressure (20-30 mmHg). Reactions were monitored by thin-layer chromatography (TLC) using aluminum-backed MERCK 60 silica gel plates (0.2 mm thickness). The chromatograms were visualized first with ultraviolet light (254 nm) and then by immersion in solutions of ceric ammonium molybdate or *p*-anisaldehyde followed by heating with a heater gun. Flash column chromatography was performed with Merck silica gel 60 (230-400 mesh). All NMR spectra were measured with solutions in CDCl₃ in a Bruker DPX-250 (250 MHz), Varian Inova 400 (400 MHz) or Bruker DRX-500 (500 MHz) spectrometers. Chemical shifts are reported on the δ scale (ppm) downfield from tetramethylsilane (δ = 0.0 ppm) using the residual solvent signal at δ = 7.26 ppm (¹H, s, CDCl₃) or δ = 77.0 ppm (¹³C, t, CDCl₃). Coupling constants (*J*) are reported in Hz. Distortionless Enhancement by Polarization Transfer (DEPT-135) was used to assign carbon types. NMR signals have been assigned using steroidal numbering. High resolution mass spectra (HRMS) were performed in a Micromass Instruments Autospec, Thermo Finnigan MAT95XP and Applied Biosystems QSTAR Elite spectrometers. IR spectra were recorded on a silicon disc on a Bruker IFS-66V and VECTOR 22 FT-IR spectrometers. Optical rotations were measured on a Jasco DIP-370 polarimeter in a 1 dm cell. [α] and *c* are given in cm³.g⁻¹.dm⁻¹ and g.cm⁻³, respectively. HPLC purifications were performed on a Shimadzu preparative liquid chromatograph model LC-8A equipped with a TSP UV-1 absorbance detector, using

HPLC Phenomenex Luna 5u Silica column (SiO₂, 5 μ, 100A, Ø 250 mm x 21.2 mm).
Yields refer to chromatographically purified compounds, unless otherwise stated.

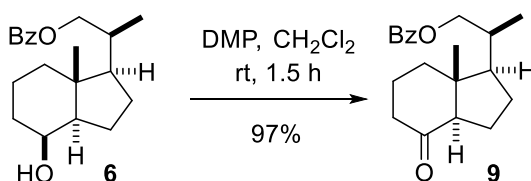
The reference and distributor for each reactant used in this work is listed below:

2,6-Lutidine, Acros, EW-88124-07	HF, 48-51%, Acros, Ref.223335000
B ₂ Pin ₂ , Aldrich, Ref. 47,329-4	KOAc, Merck, Ref. 104820
ⁿ BuLi, Acros, 18127	KO ^t Bu, Fluka, Ref. 60100
K ₃ PO ₄ ·3H ₂ O, Aldrich, Ref. P5629	<i>m</i> -Carborane, Katchem, Ref. 200
BzCl, Aldrich, 259950	<i>o</i> -Carborane, Katchem, Ref. 199
CBr ₄ , Aldrich, Ref. C11081	<i>p</i> -Carborane, Katchem, Ref.201
DIBAL-H, Aldrich, Ref. 214973	PCy ₃ , Aldrich, Ref. 261971
DMAP, Fluka, Ref. 29224	PdCl ₂ (dppf)·CH ₂ Cl ₂ , Aldrich, Ref. 379670
H ₅ IO ₆ , Fluka, Ref. 77310	PdCl ₂ (PPh ₃) ₂ , Fluka, Ref. 15253
HF, Acros, Ref.423805000	PPh ₃ , Aldrich, Ref. T84409
DMP, Carbolution, Ref.CC03024	TsCl, Aldrich, Ref. T35955
	Zn, Strem, Ref. 933056

(S)-2-[(1R,3aR,4S,7aR)-4-hydroxy-7a-methyloctahydro-1H-inden-1-yl]propyl benzoate (6)

Benzoyl chloride (1.3 mL, 11.3 mmol, 2 equiv) was added dropwise to a 0 °C cooled solution of diol **4** (1.2 g, 5.6 mmol, 1 equiv) and 2,6-lutidine (2.0 mL, 17.0 mmol, 3 equiv) in CH₂Cl₂ (20 mL). The reaction mixture was stirred for 5 h and then quenched by the addition of aqueous HCl (5%, 10 mL). The mixture was extracted with MTBE (3x10 mL) and the combined organic layers were dried, filtered and concentrated. The residue was purified by flash chromatography (SiO₂, Ø 2.5x5 cm, 0-20% EtOAc/hexanes) to afford **6** [1.6 g, 5.1 mmol, 90%, yellowish oil; R_f = 0.69 (30% EtOAc/hexanes), [α]_D²⁵ = + 30.2 (c 1.12, CHCl₃)].

¹H NMR (250 MHz, CDCl₃): δ 8.04 (d, *J* = 7.4 Hz, 2H, H_{ar}), 7.55 (dd, *J* = 8.2 and 6.4 Hz, 1H, H_{ar}), 7.44 (t, *J* = 7.6 Hz, 2H, H_{ar}), 4.31 (dd, *J* = 10.7 and 3.4 Hz, 1H, H-22), 4.06 (dd, *J* = 10.7 and 7.1 Hz, 2H, H-8 and H-22), 2.04 – 1.20 (m, 14H), 1.10 (d, *J* = 6.6 Hz, 3H, CH₃-21), 0.99 (s, 3H, CH₃-18). **¹³C NMR** (63 MHz, CDCl₃): δ 166.9 (C, C=O), 132.9 (CH, CH_{ar}), 130.7 (C, C_{ar}), 129.6 (CH, 2xCH_{ar}), 128.5 (CH, 2xCH_{ar}), 70.0 (CH₂, C-22), 69.3 (CH, C-8), 53.5 (CH), 52.5 (CH), 42.1 (C, C-13), 40.4 (CH₂), 35.7 (CH), 33.7 (CH₂), 26.9 (CH₂), 22.71 (CH₂), 17.54 (CH₂), 17.38 (CH₃, CH₃-21), 13.71 (CH₃, CH₃-18). **IR** (film, cm⁻¹): 3533 (ν_{O-H}), 2941 (ν_{C-H}), 2871 (ν_{C-H}), 1718 (ν_{C=Oester}). **HRMS** ([ESI-TOF]⁺, *m/z*) [M+H]⁺ calcd for C₂₀H₂₉O₃, 317.2111; found 317.2110.

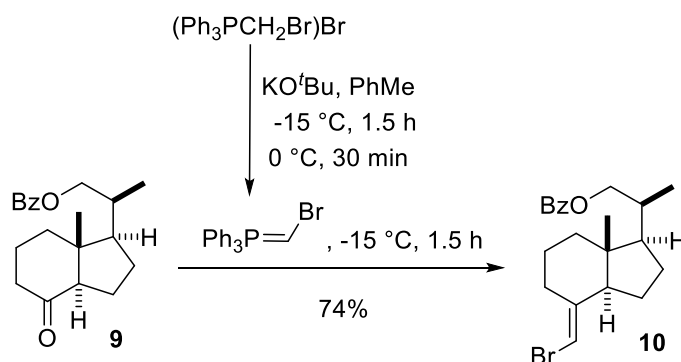
(S)-2-[(1R,3aR,7aR)-7a-methyl-4-oxooctahydro-1H-inden-1-yl]propyl benzoate (9)

Dess–Martin periodinane (DMP, 2.4 g, 5.8 mmol, 1.1 equiv) was added to a solution of **6** (1.6 mg, 5.1 mmol, 1 equiv) in CH₂Cl₂ (40 mL). The reaction mixture was stirred at rt for 1.5 h and then concentrated. The residue was purified by flash chromatography (SiO₂, Ø 3x6 cm, 30% EtOAc/hexanes) to give ketone **9** [1.5 g, 4.9 mmol, 97%, colorless oil; R_f = 0.70 (20% EtOAc/hexanes), [α]_D²⁵ = + 0.67 (c 0.92, CHCl₃)].

¹H NMR (250 MHz, CDCl₃): δ 8.04 – 7.96 (m, 2H, H_{ar}), 7.57 – 7.48 (m, 1H, H_{ar}), 7.41 (t, *J* = 7.4 Hz, 2H, H_{ar}), 4.29 (dd, *J* = 10.8 and 3.4 Hz, 1H, H-22), 4.05 (dd,

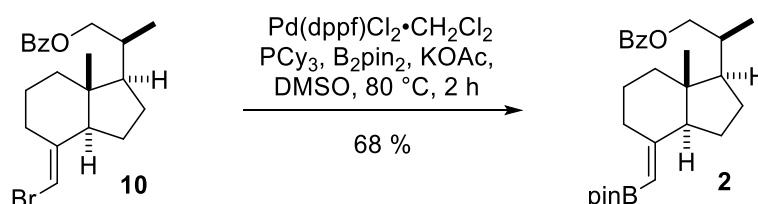
$J = 10.8$ and 6.8 Hz, 1H, H-22), 2.45 (dd, $J = 11.4$ and 7.5 Hz, 1H), 2.24 – 1.39 (m, 12H), 1.12 (d, $J = 6.6$ Hz, 3H, CH₃-21), 0.65 (s, 3H, CH₃-18). ¹³C NMR (63 MHz, CDCl₃): δ 211.7 (C, C=O, C-8), 166.6 (C, C=O), 132.9 (CH, CH_{ar}), 130.4 (C, C_{ar}), 129.5 (CH, 2xCH_{ar}), 128.4 (CH, 2xCH_{ar}), 69.6 (CH₂, C-22), 61.6 (CH), 53.4 (CH), 49.9 (C, C-13), 40.9 (CH₂), 38.8 (CH₂), 35.8 (CH), 27.0 (CH₂), 24.0 (CH₂), 19.2 (CH₂), 17.4 (CH₃, CH₃-21), 12.5 (CH₃, CH₃-18). IR (film, cm⁻¹): 2962 (ν_{C-H}), 2873 (ν_{C-H}), 1714 ($\nu_{C=O\text{ester}}$), 1601 ($\nu_{C=O\text{ketone}}$). HRMS ([ESI-TOF]⁺, m/z) [M+H]⁺ calcd for C₂₀H₂₇O₃, 315.1955; found 315.1956.

(S)-2-[(1R,3aR,7aR,E)-4-(bromomethylene)-7a-methyloctahydro-1H-inden-1-yl]propyl benzoate (10)



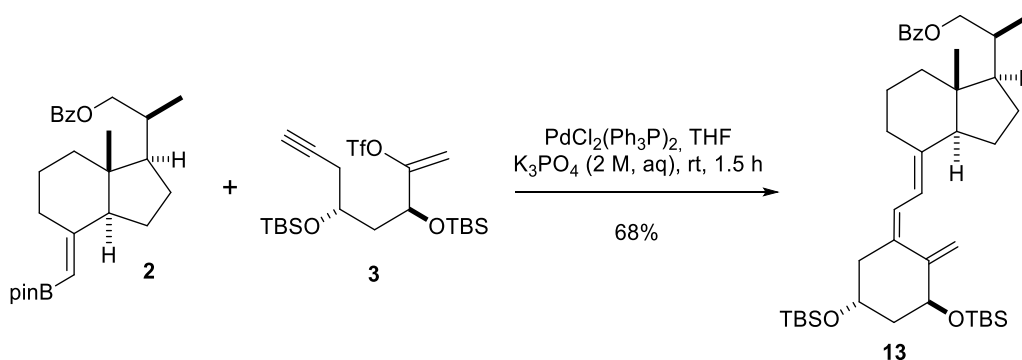
A suspension of (bromomethylene)triphenylphosphonium bromide (2.0 g, 4.5 mmol, 5 equiv) in toluene (18 mL) was sonicated for 30 min and then cooled to -15 °C. After 10 min, a solution of KO^tBu in THF (4.5 mL, 4.5 mmol, 1M, 4.9 equiv) was added dropwise. The yellow mixture was stirred at -15 °C for 1.5 h and at 0 °C for 30 min. The ylide was cooled to -15 °C. A 0 °C cooled solution of ketone **9** (286 mg, 0.910 mmol, 1 equiv) in toluene (9 mL) was added dropwise *via* canula. The mixture was stirred at -15 °C for 1.5 h. The reaction was quenched by addition of sat NH₄Cl (5 mL). The mixture was filtered through a short pad of silica gel, rinsed with EtOAc and concentrated. The residue was purified by flash chromatography (SiO₂, Ø 2x6 cm, 0-3% EtOAc/hexanes) to give bromide **10** [262 mg, 0.670 mmol, 74%, R_f = 0.71 (20% EtOAc/hexanes), colorless oil, $[\alpha]_D^{25} = +85.0$ (c 1.1, CHCl₃)].

¹H NMR (250 MHz, CDCl₃): δ 8.10 – 8.00 (m, 2H, H_{ar}), 7.57 (t, $J = 7.3$ Hz, 1H, H_{ar}), 7.45 (t, $J = 7.6$ Hz, 2H, H_{ar}), 5.67 (s, 1H, H-7), 4.33 (dd, $J = 10.8$ and 3.3 Hz, 1H, H-22), 4.08 (dd, $J = 10.7$ and 7.0 Hz, 1H, H-22), 2.90 (dd, $J = 10.2$ and 2.8 Hz, 1H), 2.08 – 1.24 (m, 12H), 1.14 (d, $J = 6.6$ Hz, 3H, CH₃-21), 0.62 (s, 3H, CH₃-18). ¹³C NMR (63 MHz, CDCl₃): δ 166.8 (C, C=O), 144.9 (C, C-8), 133.0 (CH, CH_{ar}), 130.6 (C, C_{ar}), 129.7 (CH, 2xCH_{ar}), 128.5 (CH, 2xCH_{ar}), 97.8 (CH, C-7), 69.9 (CH₂, C-22), 55.7 (CH), 52.7 (CH), 45.8 (C, C-13), 39.9 (CH₂), 36.4 (CH), 31.1 (CH₂), 27.3 (CH₂), 22.6 (CH₂), 22.3 (CH₂), 17.6 (CH₃, CH₃-21), 12.1 (CH₃, CH₃-18). IR (film, cm⁻¹): 2947 (ν_{C-H}), 2870 (ν_{C-H}), 1718 ($\nu_{C=O}$). HRMS ([ESI-TOF]⁺, m/z) [M+H]⁺ calcd for C₂₁H₂₈BrO₂, 319.1254; found 319.1264.

(S)-2-((1R,3aS,7aR,E)-7a-methyl-4-[(4,4,5,5-tetramethyl-1,3,2-dioxaborolan-2-yl)methylene]octahydro-1H-inden-1-yl)propyl benzoate (2)

Tricyclohexylphosphine (PCy_3 , 10.7 mg, 0.038 mmol, 0.06 equiv) and $\text{PdCl}_2(\text{dppf}) \cdot \text{CH}_2\text{Cl}_2$ (15.7 mg, 0.019 mmol, 0.03 equiv) were dissolved in dry DMSO (2 mL). The mixture was stirred at rt for 20 min. A solution of **10** (250 mg, 0.639 mmol, 1 equiv) in DMSO (5 mL) was added *via* canula. B_2pin_2 (324 mg, 1.28 mmol, 2 equiv) and KOAc (251 mg, 2.55 mmol, 4 equiv) were successively added. The reaction mixture was stirred at 80 °C for 2 h, cooled to rt and then diluted with H_2O (10 mL). The mixture was extracted with MTBE (3x10 mL) and the combined organic layers were dried, filtered and concentrated. The residue was purified by flash chromatography (SiO_2 , \varnothing 1.5x6 cm, hexanes) to give **2** [191 mg, 0.44 mmol, 68%, $R_f = 0.58$ (10% EtOAc/hexanes), yellowish wax, $[\alpha]_D^{25} = +62.4$ (c 1.0, CHCl_3)].

^1H NMR (250 MHz, CDCl_3): δ 8.04 (d, $J = 7.0$ Hz, 2H, H_{ar}), 7.61 – 7.50 (m, 1H, H_{ar}), 7.44 (t, $J = 7.2$ Hz, 2H, H_{ar}), 4.93 (s, 1H, H-7), 4.32 (dd, $J = 9.9$ and 2.0 Hz, 1H, H-22), 4.06 (dd, $J = 10.4$ and 7.0 Hz, 1H, H-22), 3.19 (d, $J = 12.8$ Hz, 1H, H-14), 2.12 – 1.37 (m, 12H), 1.26 (s, 12H, 4x CH_3COB), 1.12 (d, $J = 6.4$ Hz, 3H, CH_3 -21), 0.60 (s, 3H, CH_3 -18). **^{13}C NMR** (63 MHz, CDCl_3): δ 166.9 (C, C-8), 165.8 (C=O, C_{ar}), 132.9 (CH, CH_{ar}), 130.6 (C, C_{ar}), 129.6 (CH, 2x CH_{ar}), 128.5 (CH, 2x CH_{ar}), 82.7 (C, 2x CH_3COB), 70.0 (CH_2 , C-22), 57.8 (CH, C-7), 53.6 (CH), 46.4 (C, C-13), 40.4 (CH_2), 36.4 (CH, C-20), 33.3 (CH_2), 27.1 (CH_2), 25.0 (CH_3 , 2x CH_3COB), 24.9 (CH_3 , 2x CH_3COB), 24.4 (CH_2), 22.5 (CH_2), 17.6 (CH_3 , CH_3 -21), 12.3 (CH_3 , CH_3 -18). **IR** (film, cm^{-1}): 2980 ($\nu_{\text{C-H}}$), 2870 ($\nu_{\text{C-H}}$), 1780 ($\nu_{\text{C=O}}$), 1639 ($\nu_{\text{C=C}}$). **HRMS** ([ESI-TOF] $^+$, m/z) [$\text{M}+\text{H}$] $^+$ calcd for $\text{C}_{27}\text{H}_{40}\text{BO}_4$, 439.3014; found 439.3020.

(S)-2-((1*R*,3*aS*,7*aR*,*E*)-4-[(*Z*)-2-8((3*S*,5*R*)-3,5-bis((*tert*-butyldimethylsilyloxy)-2-methylenecyclohexylidene)ethylidene]-7*a*-methyloctahydro-1*H*-inden-1-yl)propyl benzoate (13**)**

An aqueous solution of K_3PO_4 (5 mL, 2M, 15 equiv) was added to a solution of boronate **2** (300 mg, 0.684 mmol, 1 equiv) and enol-triflate **3** (424 mg, 0.821 mmol, 1.2 equiv) in THF (5 mL). Then, $\text{PdCl}_2(\text{PPh}_3)_2 \cdot \text{CH}_2\text{Cl}_2$ (24 mg, 0.034 mmol, 0.05 equiv) was added. The reaction mixture was vigorously stirred for 1.5 h, in the dark. The reaction was quenched by addition of H_2O (10 mL). The mixture was extracted with MTBE (3x10 mL) and the combined organic layers were dried, filtered and concentrated. The residue was purified by flash chromatography (SiO_2 , \varnothing 2,5x6 cm, hexanes) to give **13** [300 mg, 0.440 mmol, 68%, $R_f = 0.77$ (5% EtOAc/hexanes), white foam, $[\alpha]_D^{25} = +2.2$ (c 0.48, CHCl_3)].

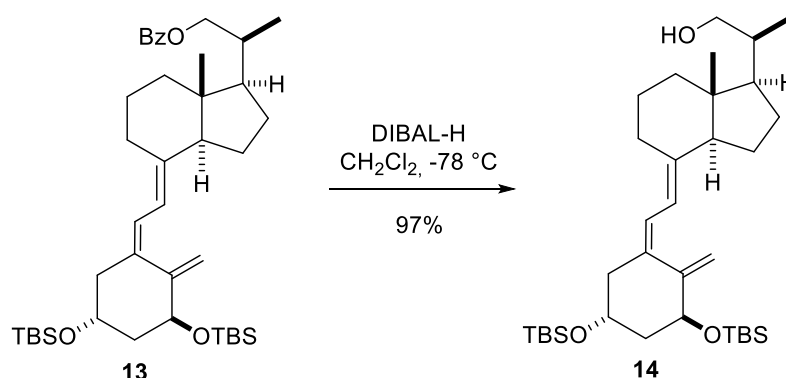
$^1\text{H NMR}$ (250 MHz, CDCl_3): δ 8.06 (d, $J = 8.0$ Hz, 2H, H_{ar}), 7.57 (t, $J = 6.9$ Hz, 1H, H_{ar}), 7.45 (t, $J = 7.7$ Hz, 2H, H_{ar}), 6.25 (d, $J = 11.4$ Hz, 1H, H-6), 6.04 (d, $J = 11.1$ Hz, 1H, H-7), 5.22 – 5.14 (s, 1H, H-19), 4.87 (s, $J = 2.2$ Hz, 1H, H-19), 4.41 – 4.29 (m, 2H, H-22), 4.25 – 4.14 (m, 1H, H-1), 4.10 – 4.02 (m, 1H, H-3), 2.90 – 2.78 (m, 1H, H-9), 2.46 (dd, $J = 13.1$ and 3.3 Hz, 1H, H-4), 2.22 (dd, $J = 13.1$ and 7.2 Hz, 1H, H-4), 1.92 – 1.45 (m, 14H), 1.14 (d, $J = 6.4$ Hz, 3H, CH_3 -21), 0.90 – 0.81 (m, 18H, $2 \times \text{CH}_3\text{CSi}$), 0.59 (s, 3H, CH_3 -18), 0.11 – 0.00 (m, 12H, $4 \times \text{CH}_3\text{Si}$).

$^{13}\text{C NMR}$ (63 MHz, CDCl_3): δ 166.9 (C=O, C_{ar}), 148.4 (C, C-10), 140.7 (C, C-8), 135.4 (C, C-5), 133.0 (CH, CH_{ar}), 130.7 (C, C_{ar}), 129.7 (CH, $2 \times \text{CH}_{\text{ar}}$), 128.5 (CH, $2 \times \text{CH}_{\text{ar}}$), 123.2 (=CH, C-6), 118.2 (=CH, C-7), 111.4 (CH_2 , C-19), 72.2 (CH, C-1), 70.1 (CH_2 , C-22), 67.7 (CH, C-3), 56.2 (CH), 53.4 (CH), 46.2 (CH_2), 46.0 (C, C-13), 44.9 (CH_2), 40.6 (CH_2), 36.5 (CH), 29.0 (CH_2), 27.4 (CH_2), 26.0 (CH_3 , $3 \times \text{CH}_3\text{CSi}$), 25.96 (CH_3 , $3 \times \text{CH}_3\text{CSi}$), 23.6 (CH_2), 22.4 (CH_2), 18.4 (C, CH_3CSi), 18.3 (C, CH_3CSi), 17.7 (CH_3 , CH_3 -21), 12.2 (CH_3 , CH_3 -18), -4.5 (CH_3 , $2 \times \text{CH}_3\text{Si}$), -4.6 (CH_3 , CH_3Si), -4.9 (CH_3 , CH_3Si).

IR (film, cm^{-1}): 2918 ($\nu_{\text{C-H}}$), 2849 ($\nu_{\text{C-H}}$), 1724 ($\nu_{\text{C=O}}$).

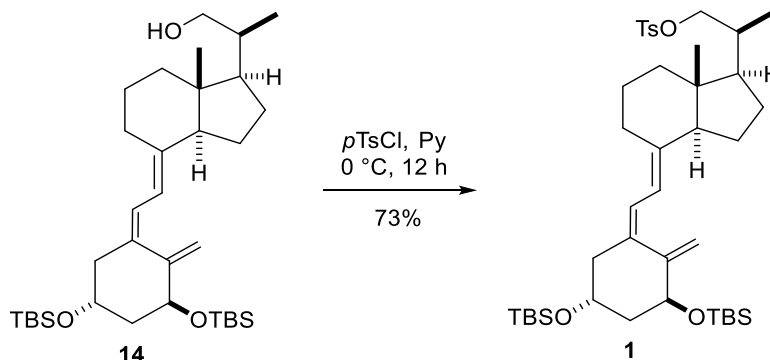
HRMS ($[\text{APCI-TOF}]^+$, m/z) $[\text{M}+\text{H}]^+$ calcd for $\text{C}_{41}\text{H}_{67}\text{O}_4\text{Si}_2$, 679.4572; found 679.4574.

(S)-2-((1R,3aS,7aR,E)-4-[(Z)-2-((3S,5R)-3,5-bis((tert-butyl)dimethylsilyloxy)-2-methylenecyclohexylidene)ethylidene]-7a-methyloctahydro-1H-inden-1-yl)propan-1-ol (14)



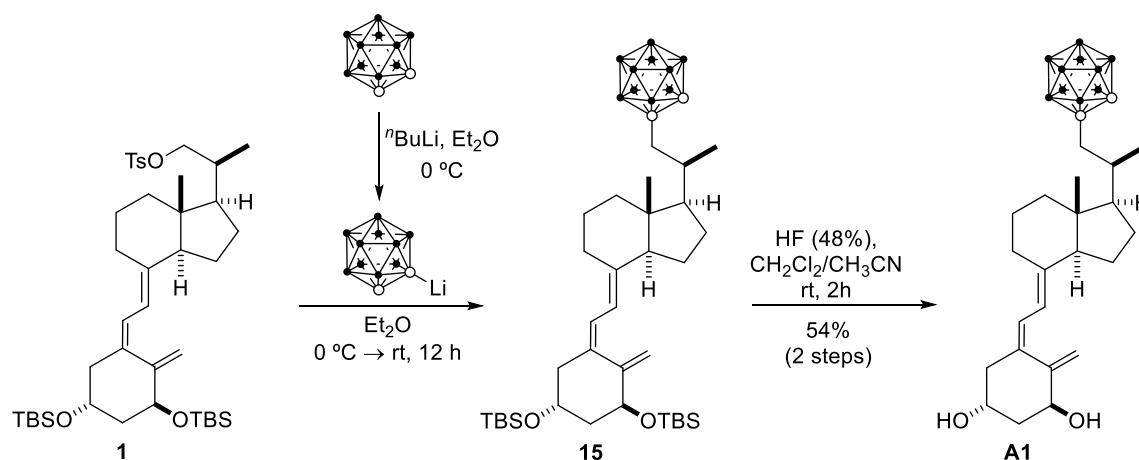
A solution of DIBAL-H (1.5 mL, 1M, 3 equiv) was added dropwise to a -78 °C cooled solution of **13** (300 mg, 0.442 mmol, 1 equiv) in CH₂Cl₂ (10 mL). The reaction mixture was stirred in dark for 1 h and then allowed to reach rt. The reaction was quenched by addition of H₂O (20 mL) and aqueous HCl (10 mL, 5%). The mixture was stirred for 15 min and then extracted with CH₂Cl₂ (3x10 mL). The combined organic layers were dried, filtered and concentrated. The residue was purified by flash chromatography (SiO₂, Ø 2x6 cm, hexanes) to give **14** [247 mg, 0.430 mmol, 97%, yellow foam, R_f = 0.14 (5% EtOAc/hexanes), [α]_D²⁵ = + 42.8 (c 0.60, CHCl₃)].

¹H NMR (250 MHz, CDCl₃): δ 6.24 (d, *J* = 11.3 Hz, 1H, H-6), 6.02 (d, *J* = 11.2 Hz, 1H, H-7), 5.18 (s, 1H, H-19), 4.86 (s, 1H, H-19), 4.37 (dd, *J* = 6.3 and 3.8 Hz, 1H, H-1), 4.19 (ddd, *J* = 10.8, 7.2 and 3.8 Hz, 1H, H-3), 3.65 (dd, *J* = 10.5 and 3.0 Hz, 1H, H-22), 3.38 (dd, *J* = 10.5 and 6.7 Hz, 1H, H-22), 2.87 – 2.77 (m, 1H, H-9), 2.44 (dd, *J* = 13.0 and 3.3 Hz, 1H), 2.21 (dd, *J* = 13.0 and 7.1 Hz, 1H, H-4), 2.03 – 1.24 (m, 15H), 1.05 (d, *J* = 6.5 Hz, 3H, CH₃-21), 0.88 (s, 18H, 2x CH₃CSi), 0.55 (s, 3H, CH₃-18), 0.06 (s, 12H, 4x CH₃Si). **¹³C NMR** (63 MHz, CDCl₃): δ 148.5 (C, C-10), 140.9 (C, C-8), 135.3 (C, C-5), 123.2 (=CH, C-6), 118.1 (=CH, C-7), 111.3 (=CH₂, C-19), 72.2 (CH, C-1), 68.1 (CH₂, C-22), 67.7 (CH, C-3), 56.2 (CH), 52.9 (CH), 46.2 (CH₂), 46.0 (C, C-13), 44.9 (CH₂), 40.6 (CH₂), 39.24 (CH), 29.0 (CH₂), 27.4 (CH₂), 26.00 (CH₃, 3xCH₃CSi), 25.96 (CH₃, 3xCH₃CSi), 23.6 (CH₂), 22.4 (CH₂), 18.4 (C, CH₃CSi), 18.3 (C, CH₃CSi), 17.0 (CH₃, CH₃-21), 12.2 (CH₃, CH₃-18), -4.5 (CH₃, 2xCH₃Si), -4.6 (CH₃, CH₃Si), -4.9 (CH₃, CH₃Si). **HRMS** ([ESI-TOF]⁺, *m/z*) [M+H]⁺ calcd for C₃₄H₆₃O₃Si₂, 575.4310; found 575.4309.

(S)-2-((1R,3aS,7aR,E)-4-[(Z)-2-((3S,5R)-3,5-bis((tert-butyl)dimethylsilyloxy)-2-methylenecyclohexylidene)ethylidene]-7a-methyloctahydro-1H-inden-1-yl)propyl 4-methylbenzenesulfonate (1)

p-Toluenesulfonyl chloride (120 mg, 0.629 mmol, 2.4 equiv) was added to a 0 °C cooled solution of **14** (154 mg, 0.268 mmol, 1 equiv) in pyridine. The bright yellow reaction mixture was stirred overnight at -4 °C, in dark. The reaction was quenched by addition of sat CuSO₄ (20 mL). The mixture was extracted with MTBE (3x10 mL). The combined organic phases were dried, filtered and concentrated. The residue was purified by flash chromatography (SiO₂, Ø 2x6 cm, hexanes) to give **1** [143 mg, 0.196 mmol, 73%, colorless foam, R_f = 0.72 (20% EtOAc/hexanes), [α]_D²⁵ = + 3.2 (c 0.20, CHCl₃)].

¹H NMR (250 MHz, CDCl₃): δ 7.79 (d, *J* = 8.3 Hz, 2H, H_{ar}), 7.34 (d, *J* = 8.4 Hz, 2H, H_{ar}), 6.22 (d, *J* = 11.3 Hz, 1H, H-6), 5.99 (d, *J* = 11.6 Hz, 1H, H-7), 5.17 (s, 1H, H-19), 4.84 (s, 1H, H-19), 4.36 (dd, *J* = 6.5 and 4.1 Hz, 1H, H-1), 4.24 – 4.12 (m, 1H, H-3), 3.97 (dd, *J* = 9.2 and 2.9 Hz, 1H, H-22), 3.79 (dd, *J* = 9.2 and 6.3 Hz, 1H, H-22), 2.85 – 2.75 (m, 1H), 2.51 – 2.39 (m, 3H), 2.20 (dd, *J* = 13.2 and 6.9 Hz, 2H), 2.03 – 1.06 (m, 17H), 1.01 – 0.79 (m, 18H, 2xCH₃CSi), 0.49 (s, 3H, CH₃-18), 0.05 (s, 12H, 4xCH₃Si). **¹³C NMR** (63 MHz, CDCl₃): δ 148.5 (C, C-10), 144.7 (C, C_{ar}), 140.4 (C, C-8), 135.5 (C, C-5), 133.2 (C, C_{ar}), 129.9 (2xCH, C_{ar}), 128.1 (2xCH, C_{ar}), 123.1 (=CH, C-6), 118.3 (=CH, C-7), 111.3 (=CH₂, C-19), 75.7 (CH₂, C-22), 72.2 (CH, C-1), 67.6 (CH, C-3), 56.0 (CH), 52.3 (CH), 46.1 (C, C-13), 45.9 (CH₂), 44.9 (CH₂, C-2), 40.4 (CH₂, C-12), 36.7 (CH), 28.9 (CH₂), 27.1 (CH₂), 25.99 (CH₃, 3xCH₃CSi), 25.96 (CH₃, 3xCH₃CSi), 23.5 (CH₂), 22.2 (CH₂), 21.8 (CH₃, CH₃-Ts), 18.37 (C, CH₃CSi), 18.30 (C, CH₃CSi), 17.1 (CH₃, CH₃-21), 12.1 (CH₃, CH₃-18), -4.5 (CH₃, 2xCH₃Si), -4.6 (CH₃, CH₃Si), -4.9 (CH₃, CH₃Si). **HRMS** ([APCI-TOF]⁺, *m/z*) [M+H]⁺ calcd for C₄₁H₆₉O₅SSi₂, 729.4399; found 729.4399.

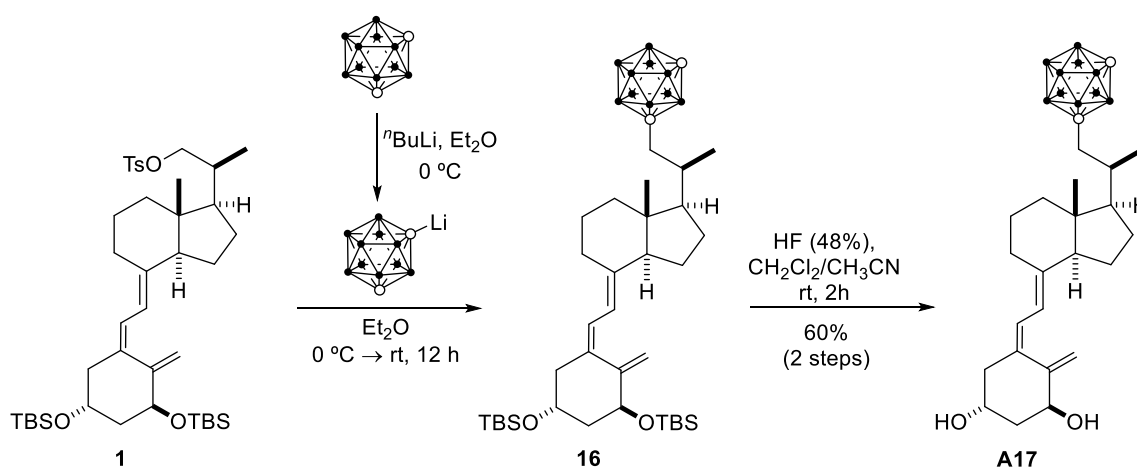
1-[(R)-2-((1R,3aS,7aR,E)-4-((Z)-2-((3S,5R)-3,5-dihydroxy-2-methylenecyclohexylidene)ethylidene)-7a-methyloctahydro-1H-inden-1-yl)propyl]-1,2-dicarba-closo-dodecaborane (A1)

A solution of n BuLi (78 μ L, 2.5 M, 2 equiv) was added dropwise to a 0 $^{\circ}$ C cooled solution of *o*-carborane (28 mg, 0.20 mmol, 2 equiv) in Et₂O (2.5 mL). The bath was removed and the cloudy mixture was stirred at rt for 1 h. The reaction mixture was cooled to 0 $^{\circ}$ C and, after 5 min, a solution of **1** (71 mg, 0.097 mmol, 1 equiv) in Et₂O (1.5 mL) was added *via* canula. The yellow mixture was stirred in dark at 0 $^{\circ}$ C for 2 h. Then, the bath was removed and the reaction mixture was stirred overnight at rt. The reaction was quenched by addition of H₂O (10 mL) and extracted with MTBE (3x10 mL). The combined organic layers were dried, filtered and concentrated. The residue was purified by flash chromatography (SiO₂, \varnothing 1.5x8 cm, 1-5% EtOAc/hexanes) to give the protected analog **15** [45 mg, 0.064 mmol, 66%, R_f = 0.55 (10% EtOAc/hexanes)]. A solution of compound **15** (45 mg, 0.064 mmol, 1 equiv) in CH₂Cl₂/CH₃CN (4 mL, 1:3) was treated with aqueous HF (48%, 15 drops). The mixture was stirred at rt for 2 h and then poured into sat NaHCO₃ (50 mL). The mixture was stirred for 30 min and then extracted with CH₂Cl₂ (3x20 mL). The combined organic layers were dried, filtered and concentrated. The residue was purified by flash chromatography (SiO₂, \varnothing 1.5x7 cm, 60% EtOAc/hexanes) and then repurified by HPLC (Phenomenex SiO₂, Luna Silica(2) 5 μ m, 20% *i*PrOH/hexanes) to afford **A1** [25 mg, 0.053 mmol, 82%, 54% 2 steps, white wax, R_f = 0.55 (60% EtOAc/hexanes), $[\alpha]_D^{25}$ = + 6.7 (*c* 2.4, CHCl₃)].

¹H NMR (400 MHz, CDCl₃): δ 6.35 and 6.01 (d, J = 11.2 Hz, 2H, H-6 and H-7), 5.33 (s, 1H, H-19), 4.99 (s, 1H, H-19), 4.43 (dd, J = 7.7 and 4.2 Hz, 1H, H-1), 4.23 (dq, J = 9.5 and 3.3 Hz, 1H, H-3), 3.53 (s, 1H, H-24), 2.82 (dd, J = 12.2 and 3.7 Hz, 1H), 2.59 (dd, J = 13.4 and 2.8 Hz, 1H), 2.36 – 2.28 (m, 3H), 2.07 – 1.78 (m, 11H), 1.73 – 1.58 (m, 7H), 1.50 (dd, J = 18.9 and 9.8 Hz, 3H), 1.31 – 1.16 (m, 5H), 1.04 (d, J = 6.3 Hz, 3H, CH₃-21), 0.58 (s, 3H, CH₃-18). **¹³C NMR** (63 MHz, CDCl₃): δ 147.8 (C, C-10), 142.3 (C, C-8), 133.6 (C, C-5), 124.9 (=CH, C-6),

117.6 (=CH, C-7), 111.9 (=CH₂, C-19), 75.7 (C, C-23), 70.8 (CH, C-1), 67.0 (CH, C-3), 62.2 (CH, C-24), 56.5 (CH), 56.2 (CH, 45.9 (C, C-13), 45.3 (CH₂, C-4), 44.5 (CH₂), 43.0 (CH₂), 40.4 (CH₂), 37.7 (CH), 29.0 (CH₂), 28.0 (CH₂), 23.5 (CH₂), 22.3 (CH₂), 20.6 (CH₃, CH₃-21), 12.1 (CH₃, CH₃-18). **IR** (film, cm⁻¹): 3361 (ν_{O-H}), 2955, 2918 (ν_{C-H}), 2849 (ν_{C-H}), 2594 (ν_{B-H}), 1462. **HRMS** ([APCI-TOF]⁺, m/z) [M]⁺ calcd for C₂₄H₄₄B₁₀O₂, 474.4266; found 474.4304.

1-[[[(R)-2-((1R,3aS,7aR,E)-4-((Z)-2-((3S,5R)-3,5-dihydroxy-2-methylenecyclohexylidene)ethylidene)-7a-methyloctahydro-1H-inden-1-yl)propyl]]-1,7-dicarba-c/oso-dodecaborane (A17)

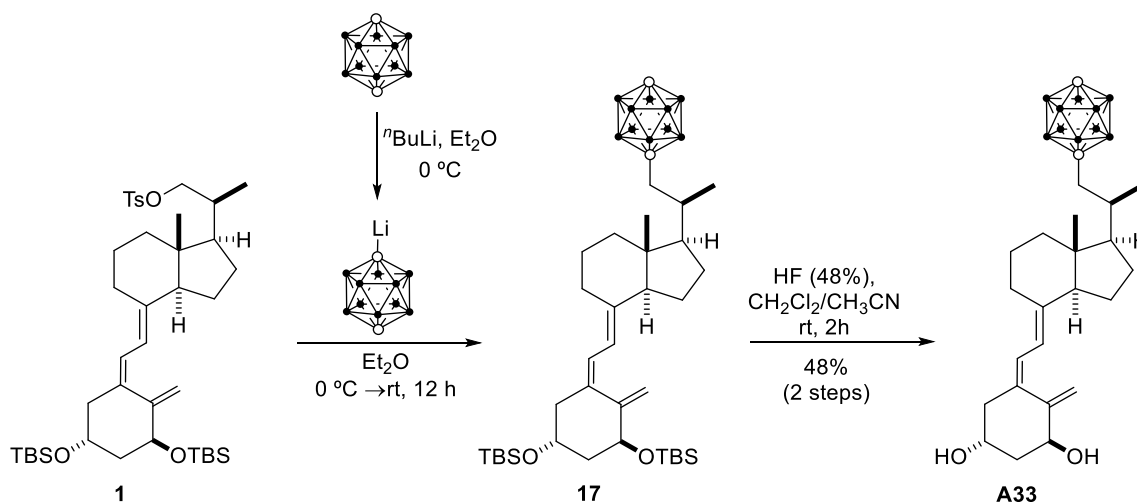


A solution of ⁿBuLi (104 μL, 2.5 M, 2 equiv) was added dropwise to a 0 °C cooled solution of *m*-carborane (50 mg, 0.35 mmol, 2.6 equiv) in Et₂O (3 mL). The bath was removed and the cloudy mixture was stirred at rt for 1 h. The reaction mixture was cooled to 0 °C and, after 5 min, a solution of **1** (95 mg, 0.13 mmol, 1 equiv) in Et₂O (2.5 mL) was added *via* canula. The yellow mixture was stirred in darkness for 30 min at 0 °C. Then, the bath was removed and the reaction mixture was stirred overnight at rt. The reaction was quenched by addition of H₂O (10 mL) and extracted with MTBE (3x10 mL). The combined organic layers were dried, filtered and concentrated. The residue was purified by flash chromatography (SiO₂, Ø 1,5x5 cm, 0-2% EtOAc/hexanes) to give the protected analog **16** [82 mg, 0.12 mmol, 90%, R_f = 0.88 (10% EtOAc/hexanes)]. A solution of compound **16** (82 mg, 0.12 mmol, 1 equiv) in CH₂Cl₂/CH₃CN (4 mL, 1:3) was treated with aqueous HF (48%, 15 drops). The reaction mixture was stirred at rt for 2 h and then poured into sat NaHCO₃ (50 mL). The mixture was stirred for 30 min and then extracted with CH₂Cl₂ (3x20 mL). The combined organic layers were dried, filtered and concentrated. The residue was purified by flash chromatography (SiO₂, Ø 1.5x4 cm, 60% EtOAc/hexanes) and then repurified by HPLC (Phenomenex SiO₂, Luna Silica(2) 5 μm,

20% i-PrOH/hexanes) to afford **A17** [37 mg, 0.053 mmol, 67%, white solid, $R_f = 0.38$ (60% EtOAc/hexanes), $[\alpha]_D^{25} = +8.5$ (c 0.92, CHCl_3)].

$^1\text{H NMR}$ (400 MHz, CDCl_3): δ 6.4 and 6.0 (d, $J = 11.2$ Hz, 2H, H-6 and H-7), 5.32 (s, 1H, H-19), 4.99 (s, 1H, H-19), 4.42 (dd, $J = 7.5$ and 4.2 Hz, 1H, H-1), 4.22 (dq, $J = 9.5$ and 3.3 Hz, 1H, H-3), 2.90 (s, 1H, H-24), 2.81 (dd, $J = 12.2$ and 3.6 Hz, 1H), 2.58 (dd, $J = 13.3$ and 2.7 Hz, 2H), 2.31 (dd, $J = 13.4$ and 6.4 Hz, 2H), 2.13 (d, $J = 14.8$ Hz, 2H), 2.05 – 1.41 (m, 18H), 1.32 – 1.12 (m, 4H), 0.98 (d, $J = 6.2$ Hz, 3H, CH_3 -21), 0.56 (s, 3H, CH_3 -18). **$^{13}\text{C NMR}$** (101 MHz, CDCl_3): δ 147.8 (C, C-10), 142.7 (C, C-8), 133.4 (C, C-5), 124.9 (=CH, C-6), 117.5 (=CH, C-7), 111.9 (=CH₂, C-19), 77.4 (C, C-23), 70.9 (CH, C-1), 67.0 (CH, C-3), 56.5 (CH), 56.4 (CH), 55.0 (CH, C-24), 45.9 (C, C-13), 45.3 (CH₂), 43.2 (CH₂), 43.0 (CH₂), 40.4 (CH₂), 37.9 (CH), 29.1 (CH₂), 27.8 (CH₂), 23.6 (CH₂), 22.4 (CH₂), 20.5 (CH₃, CH_3 -21), 12.1 (CH₃, CH_3 -18). **IR** (film, cm^{-1}): 3373 ($\nu_{\text{O-H}}$), 2931, 2851 ($\nu_{\text{C-H}}$), 2600 ($\nu_{\text{B-H}}$). **HRMS** ([APCI-TOF]⁺, m/z) [$\text{M}+\text{H}$]⁺ calcd for $\text{C}_{24}\text{H}_{45}\text{B}_{10}\text{O}_2$, 475.4345; found 475.4379.

1-[[*(R)*-2-((*1R,3aS,7aR,E*)-4-((*Z*)-2-((*3S,5R*)-3,5-dihydroxy-2-methylenecyclohexylidene)ethylidene]-7a-methyloctahydro-1*H*-inden-1-yl)propyl]]-1,12-dicarba-*c*-*loso*-dodecaborane (A33**)**



A solution of $^n\text{BuLi}$ (109 μL , 2.5 M, 2 equiv) was added dropwise to a 0 $^\circ\text{C}$ cooled solution of *p*-carborane (39 mg, 0.27 mmol, 2 equiv) in Et_2O (3 mL). The bath was removed and the cloudy mixture was stirred at rt for 1 h. The reaction mixture was cooled to 0 $^\circ\text{C}$ and, after 5 min, a solution of **1** (99 mg, 0.14 mmol, 1 equiv) in Et_2O (2.5 mL) was added *via* canula. The yellow mixture was stirred in dark at 0 $^\circ\text{C}$ for 2 h. Then, the bath was removed and the mixture was stirred overnight at rt. The reaction was quenched by addition of H_2O (10 mL). The mixture was extracted with MTBE (3x10 mL). The combined organic layers were dried, filtered and concentrated. The residue was purified by flash chromatography (SiO_2 , \varnothing 1.5x6 cm,

0-2% EtOAc/hexanes) to give the protected analog **17** [64 mg, 0.091 mmol, 67%, $R_f = 0.85$ (10% EtOAc/hexanes)]. A solution of compound **17** (64 mg, 0.091 mmol, 1 equiv) in $\text{CH}_2\text{Cl}_2/\text{CH}_3\text{CN}$ (4 mL, 1:3) was treated with aqueous HF (48%, 15 drops). The mixture was stirred at rt for 2 h and then poured into sat NaHCO_3 (50 mL). The mixture was stirred for 30 min and then extracted with CH_2Cl_2 (3x20 mL). The combined organic layers were dried, filtered and concentrated. The residue was purified by flash chromatography (SiO_2 , \varnothing 1.5x6 cm, 60% EtOAc/hexanes) and then repurified by HPLC (Phenomenex SiO_2 , Luna Silica(2) 5 μm , 20% i-PrOH/hexanes) to afford **A33** [31 mg, 0.066 mmol, 72%, white solid $R_f = 0.50$ (60% EtOAc/hexanes), $[\alpha]_D^{25} = +26.7$ (c 0.24, CHCl_3)].

$^1\text{H NMR}$ (400 MHz, CDCl_3): δ 6.35 and 5.99 (d, $J = 11.2$ Hz, 2H, H-6 and H-7), 5.32 (s, 1H, H-19), 4.98 (s, 1H, H-19), 4.46 – 4.39 (m, 1H, H-1), 4.26 – 4.19 (m, 1H, H-3), 2.79 (dd, $J = 12.2$ and 3.6 Hz, 1H), 2.63 (s, 1H, H-24), 2.59 (dd, $J = 14.0$ and 2.7 Hz, 1H), 2.30 (dd, $J = 13.4$ and 6.4 Hz, 2H), 2.01 (dd, $J = 13.6$ and 7.3 Hz, 2H), 1.96 – 1.86 (m, 4H), 1.84 – 1.70 (m, 3H), 1.63 (d, $J = 9.2$ Hz, 6H), 1.56 – 1.39 (m, 4H), 1.23 (ddd, $J = 16.4, 12.7$ and 6.8 Hz, 4H), 1.08 (d, $J = 6.4$ Hz, 2H), 0.85 (d, $J = 5.4$ Hz, 3H, CH_3 -21), 0.52 (s, 3H, CH_3 -18). **$^{13}\text{C NMR}$** (101 MHz, CDCl_3): δ 147.8 (C, C-10), 142.8 (C, C-8), 133.2 (C, C-5), 125.0 (=CH, C-6), 117.4 (=CH, C-7), 111.9 (=CH₂, C-19), 85.2 (C, C-23), 70.9 (CH, C-1), 67.0 (CH, C-3), 58.6 (CH, C-24), 56.5 (CH), 56.3 (CH), 45.9 (C, C-13), 45.4 (CH₂), 45.2 (CH₂), 43.0 (CH₂), 40.4 (CH₂), 37.2 (CH), 29.1 (CH₂), 27.7 (CH₂), 23.6 (CH₂), 22.3 (CH₂), 20.5 (CH₃, CH_3 -21), 12.0 (CH₃, CH_3 -18). **IR** (film, cm^{-1}): 3375 ($\nu_{\text{O-H}}$), 2916, 2851 ($\nu_{\text{C-H}}$), 2607 ($\nu_{\text{B-H}}$). **HRMS** ([APCI-TOF]⁺, m/z) [$\text{M}+\text{H}$]⁺ calcd for $\text{C}_{24}\text{H}_{45}\text{B}_{10}\text{O}_2$, 475.4345; found 475.4383.

REFERENCES

References

1. H. Pols, J. Birkenhäger, J. Foekens, J. Van Leeuwen, Vitamin D: a modulator of cell proliferation and differentiation. *J Steroid Biochem Mol Biol*, **1990**, 37 (6), 873-876.
2. D. Feldman, J. W. Pike, Vitamin D. *Academic Press: New York* **2005**.
3. G. Zhu, W. H. Okamura, Synthesis of vitamin D (calciferol). *Chem rev*, **1995**, 95 (6), 1877-1952.
4. M. Wacker, M. F. Holick, Sunlight and Vitamin D: A global perspective for health. *Dermatoendocrinol*, **2013**, 5 (1), 51-108.
5. A. Olmos-Ortiz, E. Avila, M. Durand-Carbajal, L. Díaz, Regulation of calcitriol biosynthesis and activity: focus on gestational vitamin D deficiency and adverse pregnancy outcomes. *Nutrients* **2015**, 7 (1), 443-480.
6. R. F. Chun, New perspectives on the vitamin D binding protein. *Cell Biochem Funct*, **2012**, 30 (6), 445-456.
7. D. D. Bikle, Vitamin D metabolism, mechanism of action, and clinical applications. *Chem Biol*, **2014**, 21 (3), 319-329.
8. D. E. Lawson, P. W. Wilson, Intranuclear localization and receptor proteins for 1, 25-dihydroxycholecalciferol in chick intestine. *Biochem J*, **1974**, 144 (3), 573-583.
9. D. Feldman, A. V. Krishnan, S. Swami, E. Giovannucci, The role of vitamin D in reducing cancer risk and progression. *Nat Rev Cancer*, **2014**, 14 (5), 342.
10. P. L. Shaffer, D. T. Gewirth, Structural analysis of RXR–VDR interactions on DR3 DNA. *J Steroid Biochem Mol Biol*, **2004**, 89, 215-219.
11. N. Rochel, J. Wurtz, A. Mitschler, B. Klaholz, D. Moras, The crystal structure of the nuclear receptor for vitamin D bound to its natural ligand. *Mol cell*, **2000**, 5 (1), 173-179.
12. F. Ciesielski, N. Rochel, D. Moras, Adaptability of the Vitamin D nuclear receptor to the synthetic ligand Gemini: remodelling the LBP with one side chain rotation. *J Steroid Biochem Mol Biol*, **2007**, 103 (3-5), 235-242.
13. J. L. Vanhooke, M. M. Benning, C. B. Bauer, J. W. Pike, Molecular structure of the rat vitamin D receptor ligand binding domain complexed with 2-carbon-substituted vitamin D₃ hormone analogues and a LXXLL-containing coactivator peptide. *Biochem*, **2004**, 43 (14), 4101-4110.
14. S. Yamada, M. Shimizu, K. Yamamoto, Structure–function relationships of vitamin D including ligand recognition by the vitamin D receptor. *Med Res Rev*, **2003**, 23 (1), 89-115.
15. M. R. Haussler, P. W. Jurutka, M. Mizwicki, A. W. Norman, Vitamin D receptor (VDR)-mediated actions of 1 α ,25(OH)₂ vitamin D₃: genomic and non-genomic mechanisms. *Best Pract Res Clin Endocrinol Metab*, **2011**, 25 (4), 543-559.
16. J. W. Pike, M. B. Meyer, The vitamin D receptor: new paradigms for the regulation of gene expression by 1 α ,25-dihydroxyvitamin D₃. *Endocrinol Metab Clin North Am*, **2010**, 39 (2), 255.
17. C. L. Smith, B. W. O'malley, Coregulator function: a key to understanding tissue specificity of selective receptor modulators. *Endocr Rev*, **2004**, 25 (1), 45-71.

18. S. V. Ramagopalan, A. Heger *et al*, A ChIP-seq defined genome-wide map of vitamin D receptor binding: associations with disease and evolution. *Genome Res*, **2010**, 20 (10), 1352-1360.
19. C. S. Hii, A. Ferrante, The non-genomic actions of vitamin D. *Nutrients* **2016**, 8 (3), 135.
20. B. Rohe, S. E. Safford, I. Nemere, M. C. Farach-Carson, Identification and characterization of 1 α ,25D₃-membrane-associated rapid response, steroid (1 α ,25D₃-MARRS)-binding protein in rat IEC-6 cells. *Steroids* **2005**, 70 (5), 458-463.
21. J. A. Huhtakangas, C. J. Olivera, J. E. Bishop, L. P. Zanello, A. W. Norman, The vitamin D receptor is present in caveolae-enriched plasma membranes and binds 1 α ,25(OH)₂-vitamin D₃ *in vivo* and *in vitro*. *Mol Endocrinol*, **2004**, 18 (11), 2660-2671.
22. J. Chen, M. Doroudi, J. Cheung, A. L. Grozier, Z. Schwartz, Plasma membrane Pdia3 and VDR interact to elicit rapid responses to 1 α ,25(OH)₂D₃. *Cell Signal*, **2013**, 25 (12), 2362-2373.
23. V. B. Sequeira, M. S. Rybchyn, *et al*, The role of the vitamin D receptor and ERp57 in photoprotection by 1 α ,25-dihydroxyvitamin D₃. *Mol Endocrinol*, **2012**, 26 (4), 574-582.
24. J. C. Fleet, Rapid, membrane-initiated actions of 1,25 dihydroxyvitamin D: what are they and what do they mean? *J Nutr*, **2004**, 134 (12), 3215-3218.
25. B. K. Nutchey, J. S. Kaplan *et al*, Molecular action of 1,25-dihydroxyvitamin D₃ and phorbol ester on the activation of the rat cytochrome P450C24 (CYP24) promoter: role of MAP kinase activities and identification of an important transcription factor binding site. *Biochem J*, **2005**, 389 (3), 753-762.
26. H. L. Henry, Regulation of vitamin D metabolism. *Best Pract Res Clin Endocrinol Metab*, **2011**, 25 (4), 531-541.
27. C. Zierold, J. A. Mings, H. F. DeLuca, Parathyroid hormone regulates 25-hydroxyvitamin D₃-24-hydroxylase mRNA by altering its stability. *Proc Nat Acad Sci*, **2001**, 98 (24), 13572-13576.
28. H. F. DeLuca, Overview of general physiologic features and functions of vitamin D. *Am J Clinl Nutr*, **2004**, 80 (6), 1689S-1696S.
29. T. Shimada, H. Hasegawa *et al*, FGF-23 is a potent regulator of vitamin D metabolism and phosphate homeostasis. *J Bone Min Res*, **2004**, 19 (3), 429-435.
30. S. S. Jensen, M. W. Madsen, J. Lukas, L. Binderup, J. Bartek, Inhibitory effects of 1 α ,25-dihydroxyvitamin D₃ on the G1-S phase-controlling machinery. *Mol Endocrinol*, **2001**, 15 (8), 1370-1380.
31. E. Gocek, G. P. Studzinski, Vitamin D and differentiation in cancer. *Crit Rev Clin Lab Sci*, **2009**, 46 (4), 190-209.
32. K. Kragballe, I. Wildfang, Calcipotriol (MC 903), a novel vitamin D₃ analogue stimulates terminal differentiation and inhibits proliferation of cultured human keratinocytes. *Arch Dermatol Res*, **1990**, 282 (3), 164-167.
33. N. Pendás-Franco, J. M. González-Sancho *et al*, Vitamin D regulates the phenotype of human breast cancer cells. *Differentiation*, **2007**, 75 (3), 193-207.
34. A. K. Bhalla, E. P. Amento, B. Serog, L. H. Glimcher, 1,25-Dihydroxyvitamin D₃ inhibits antigen-induced T cell activation. *J Immunol*, **1984**, 133 (4), 1748-1754.

35. S. Gregori, M. Casorati *et al*, Regulatory T cells induced by $1\alpha,25$ -dihydroxyvitamin D₃ and mycophenolate mofetil treatment mediate transplantation tolerance. *J Immunol*, **2001**, 167 (4), 1945-1953.
36. S. Chen, G. P. Sims, X. X. Chen, Y. Y. Gu, S. Chen, Modulatory effects of $1,25$ -dihydroxyvitamin D₃ on human B cell differentiation. *J Immunol*, **2007**, 179 (3), 1634-1647.
37. C. Almerighi, A. Sinistro, A. Cavazza, C. Ciaprini, G. Rocchi, $1\alpha, 25$ -dihydroxyvitamin D₃ inhibits CD40L-induced pro-inflammatory and immunomodulatory activity in human monocytes. *Cytokine*, **2009**, 45 (3), 190-197.
38. L. Piemonti, P. Monti *et al*, Vitamin D₃ affects differentiation, maturation, and function of human monocyte-derived dendritic cells. *J Immunol*, **2000**, 164 (9), 4443-4451.
39. D. Somjen, F. Kohen *et al*, A non-calcemic Vitamin D analog modulates both nuclear and putative membranous estrogen receptors in cultured human vascular smooth muscle cells. *J Steroid Biochem Mol Biol*, **2004**, 89, 397-399.
40. V. K. Ostrem, W. Lau *et al*, Induction of monocytic differentiation of HL-60 cells by $1,25$ -dihydroxyvitamin D analogs. *J Biol Chem*, **1987**, 262 (29), 14164-14171.
41. L. Binderup, E. Bramm, Effects of a novel vitamin D analogue MC 903 on cell proliferation and differentiation *in vitro* and on calcium metabolism *in vivo*. *Biochem Pharmacol*, **1988**, 37 (5), 889-895.
42. C. Leyssens, L. Verlinden, A. Verstuyf, The future of vitamin D analogs. *Front Physiol*, **2014**, 5, 122.
43. W. Yang, X. Gao, B. Wang, Boronic acid compounds as potential pharmaceutical agents. *Med Res Rev*, **2003**, 23 (3), 346-368.
44. S. J. Baker, C. Z. Ding *et al*, Therapeutic potential of boron-containing compounds. *Future Med Chem*, **2009**, 1 (7), 1275-1288.
45. P. Hunter, Not boring at all. *EMBO Rep*, **2009**, 10 (2), 125-128.
46. F. Issa, M. Kassiou, L. M. Rendina, Boron in drug discovery: carboranes as unique pharmacophores in biologically active compounds. *Chem Rev*, **2011**, 111 (9), 5701-5722.
47. R. L. Moss, Critical review, with an optimistic outlook, on Boron Neutron Capture Therapy (BNCT). *Appl Radiat Isot*, **2014**, 88, 2-11.
48. V. Byvaltsev, V. Kanygin, E. Belykh, S. Taskaev, Prospects in boron neutron capture therapy of brain tumors. *World Neurosurg*, **2012**, 78 (1-2), 8-9.
49. R. Otero, S. Seoane *et al*, Carborane-based design of a potent vitamin D receptor agonist. *Chem Sci*, **2016**, 7 (2), 1033-1037.
50. L. Schrödinger, The PyMOL Molecular Graphics System. Version: 2010.
51. J. Brynda, P. Mader *et al*, Carborane-Based Carbonic Anhydrase Inhibitors. *Angewandte Chemie*, **2013**, 125 (51), 14005-14008.
52. S. Fujii, H. Masuno *et al*, Boron cluster-based development of potent nonsteroidal vitamin D receptor ligands: direct observation of hydrophobic interaction between protein surface and carborane. *J Am Chem Soc*, **2011**, 133 (51), 20933-20941.

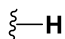
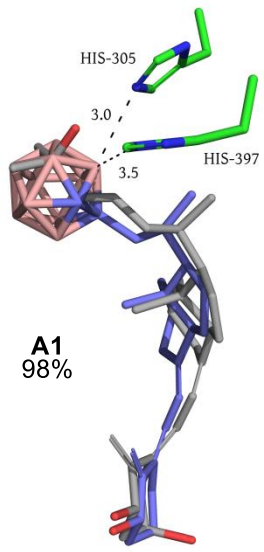
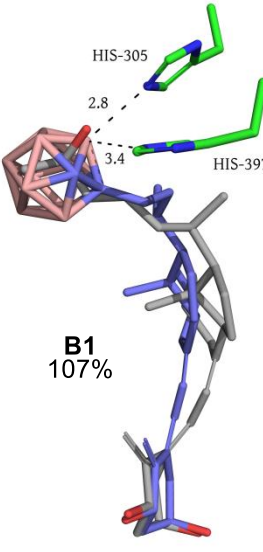
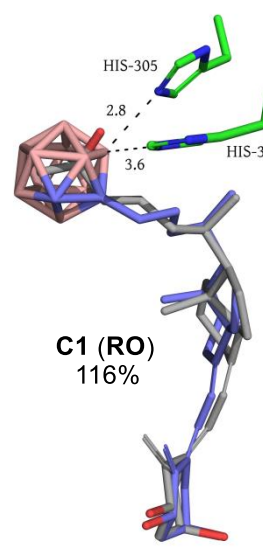
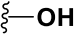
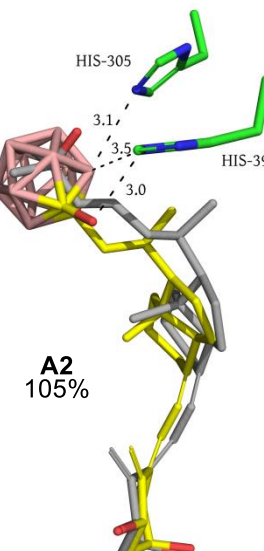
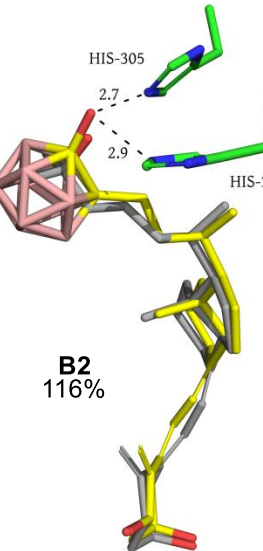
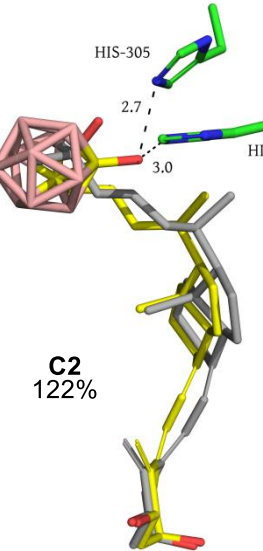
53. P. Gogoi, R. Sigüeiro, S. Eduardo, A. Mouriño, An Expeditious Route to 1 α ,25-Dihydroxyvitamin D₃ and Its Analogues by an Aqueous Tandem Palladium-Catalyzed A-Ring Closure and Suzuki Coupling to the C/D Unit. *Chem-Eur J*, **2010**, 16 (5), 1432-1435.
54. H. Inhoffen, H. Quinckerte, S. Schuzt, G. Friedrich, E. Tober, *Chemische Berichte* **1958**, 91, 781.
55. F. J. Sardina, A. Mourino, L. Castedo, Studies on the synthesis of side-chain hydroxylated metabolites of vitamin D. Stereocontrolled synthesis of 25-hydroxyvitamin D₂. *J Organic Chem*, **1986**, 51 (8), 1264-1269.
56. B. M. Trost, J. Dumas, M. Villa, New strategies for the synthesis of vitamin D metabolites via palladium-catalyzed reactions. *J Am Chem Soc*, **1992**, 114 (25), 9836-9845.
57. J. Takagi, K. Takahashi, T. Ishiyama, N. Miyaura, Palladium-catalyzed cross-coupling reaction of bis(pinacolato)diboron with 1-alkenyl halides or triflates: convenient synthesis of unsymmetrical 1,3-dienes via the borylation-coupling sequence. *J Am Chem Soc*, **2002**, 124 (27), 8001-8006.
58. A. Mouriño, M. Torneiro *et al*, Efficient and versatile synthesis of a-ring precursors of 1 α ,25-dihydroxy-vitamin D₃ and analogues. Application to the synthesis of Lythgoe-Roche phosphine oxide. *Tetrahedron Lett*, **1997**, 38 (26), 4713-4716.
59. E. Corey, P. Fuchs, A synthetic method for formyl \rightarrow ethynyl conversion (RCHO \rightarrow RC=CH or RC=CR'). *Tetrahedron Lett*, **1972**, 13 (36), 3769-3772.
60. S. Hermanek, Boron-11 NMR spectra of boranes, main-group heteroboranes, and substituted derivatives. Factors influencing chemical shifts of skeletal atoms. *Chem Rev*, **1992**, 92 (2), 325-362.

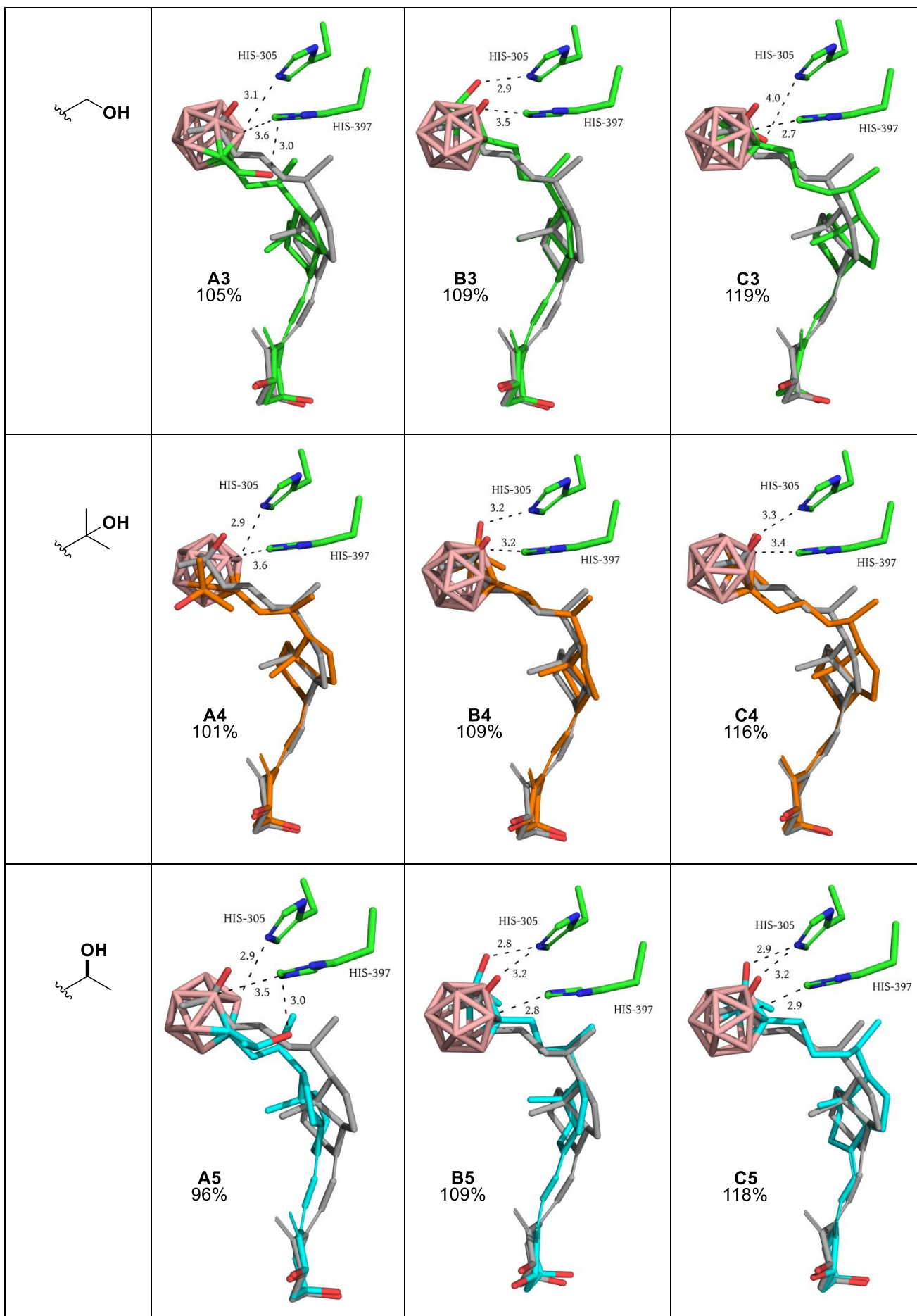
APPENDIX

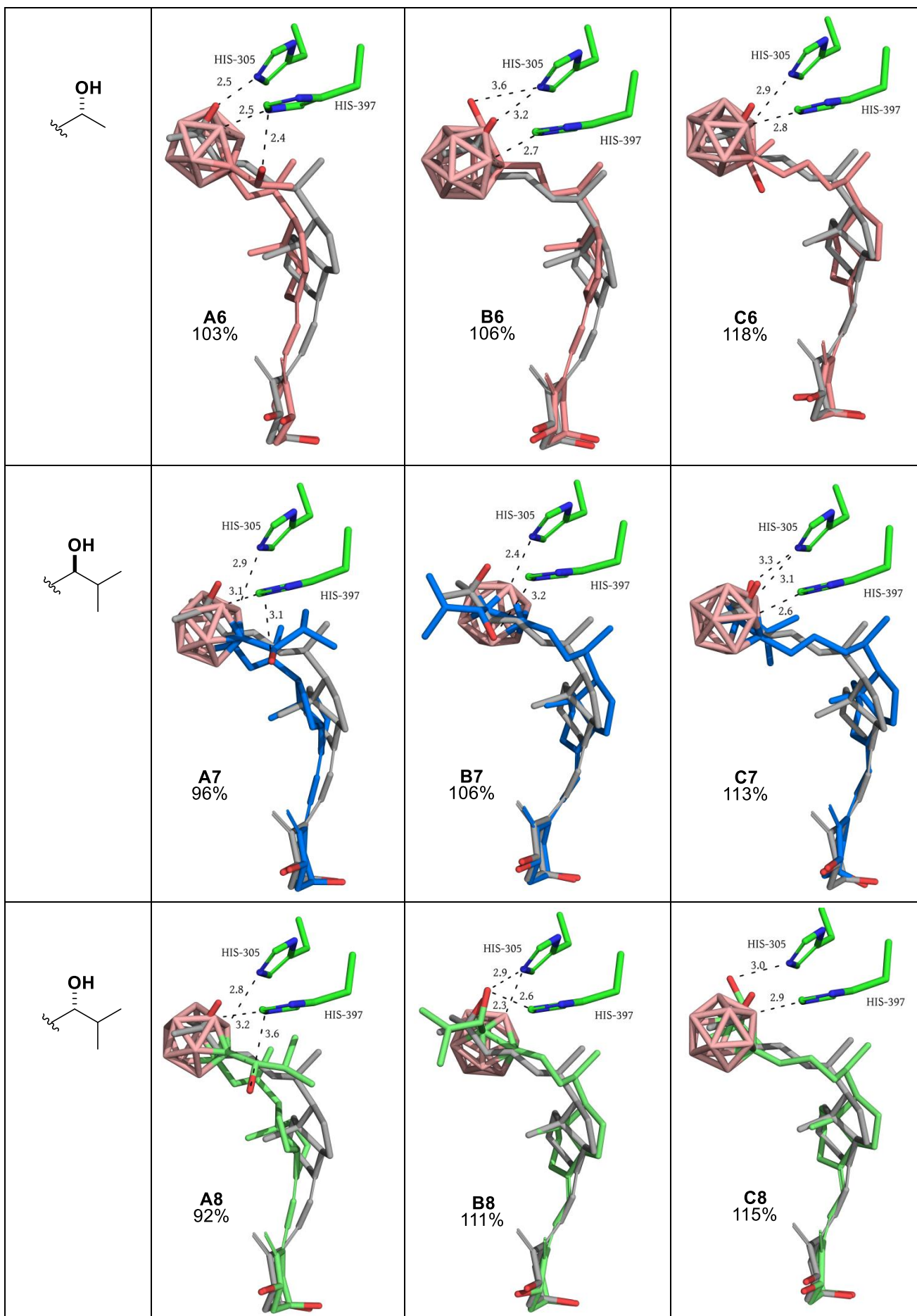
1. DOCKING RESULTS

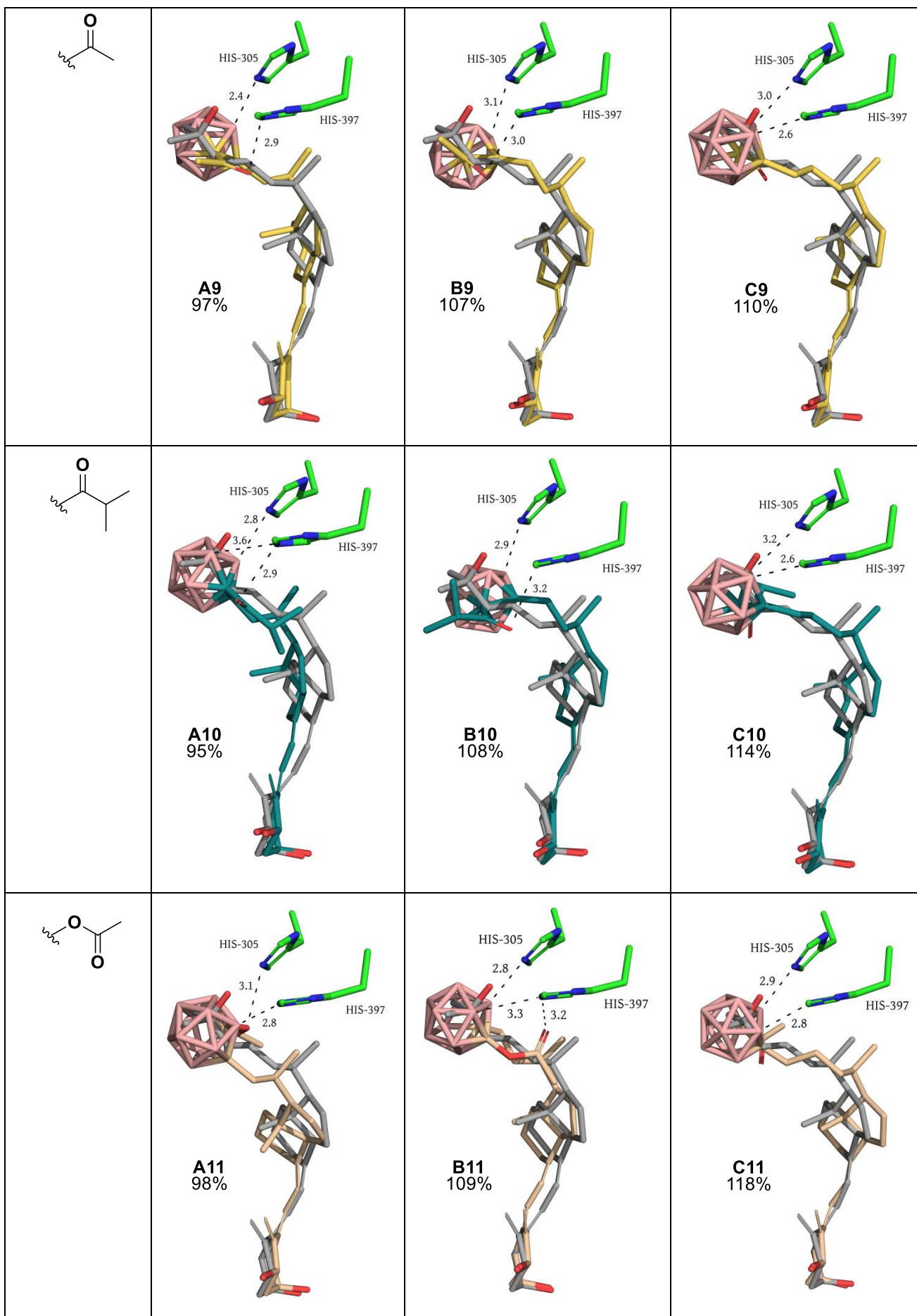
1. Docking Results

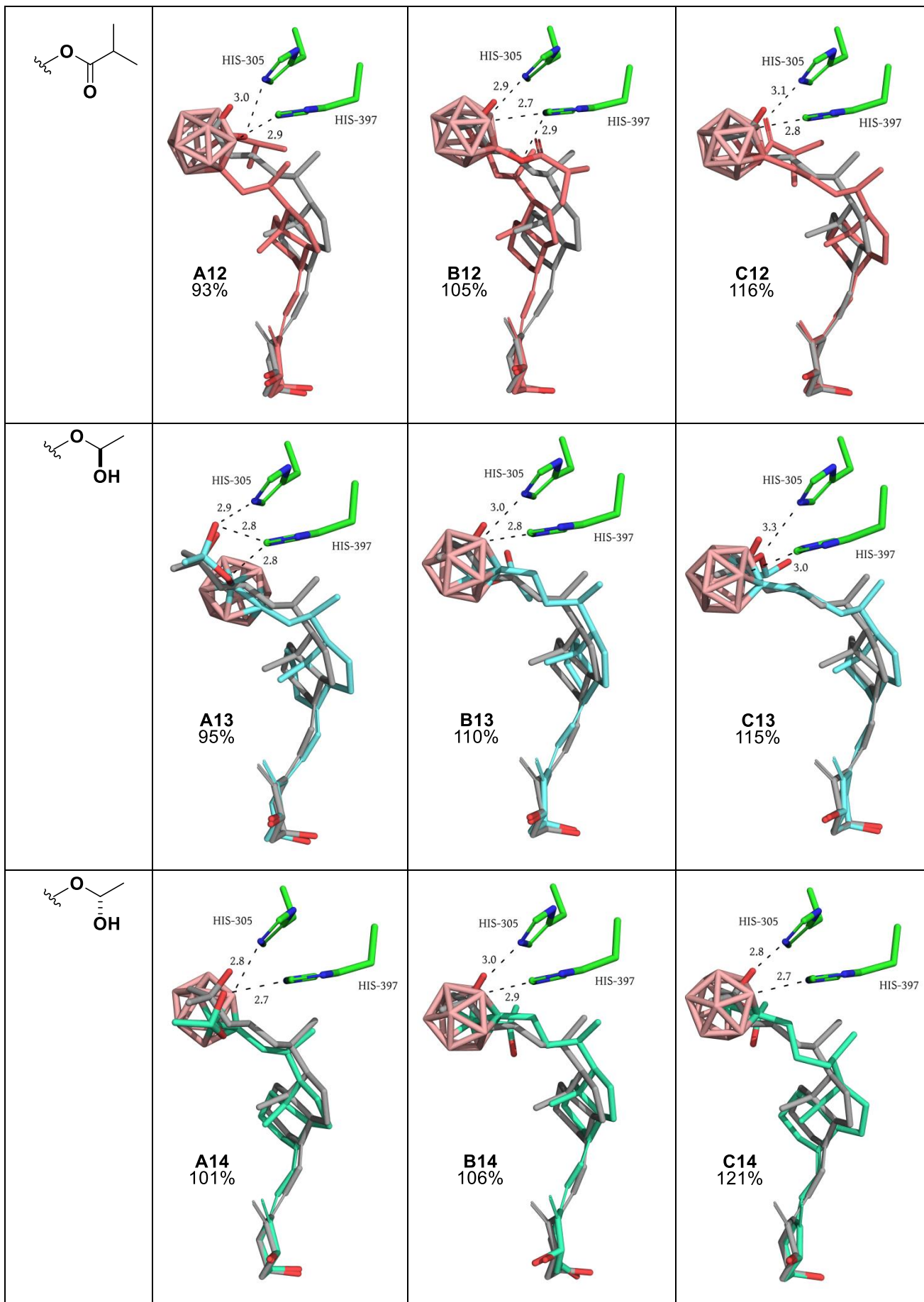
1.1. *Ortho* series

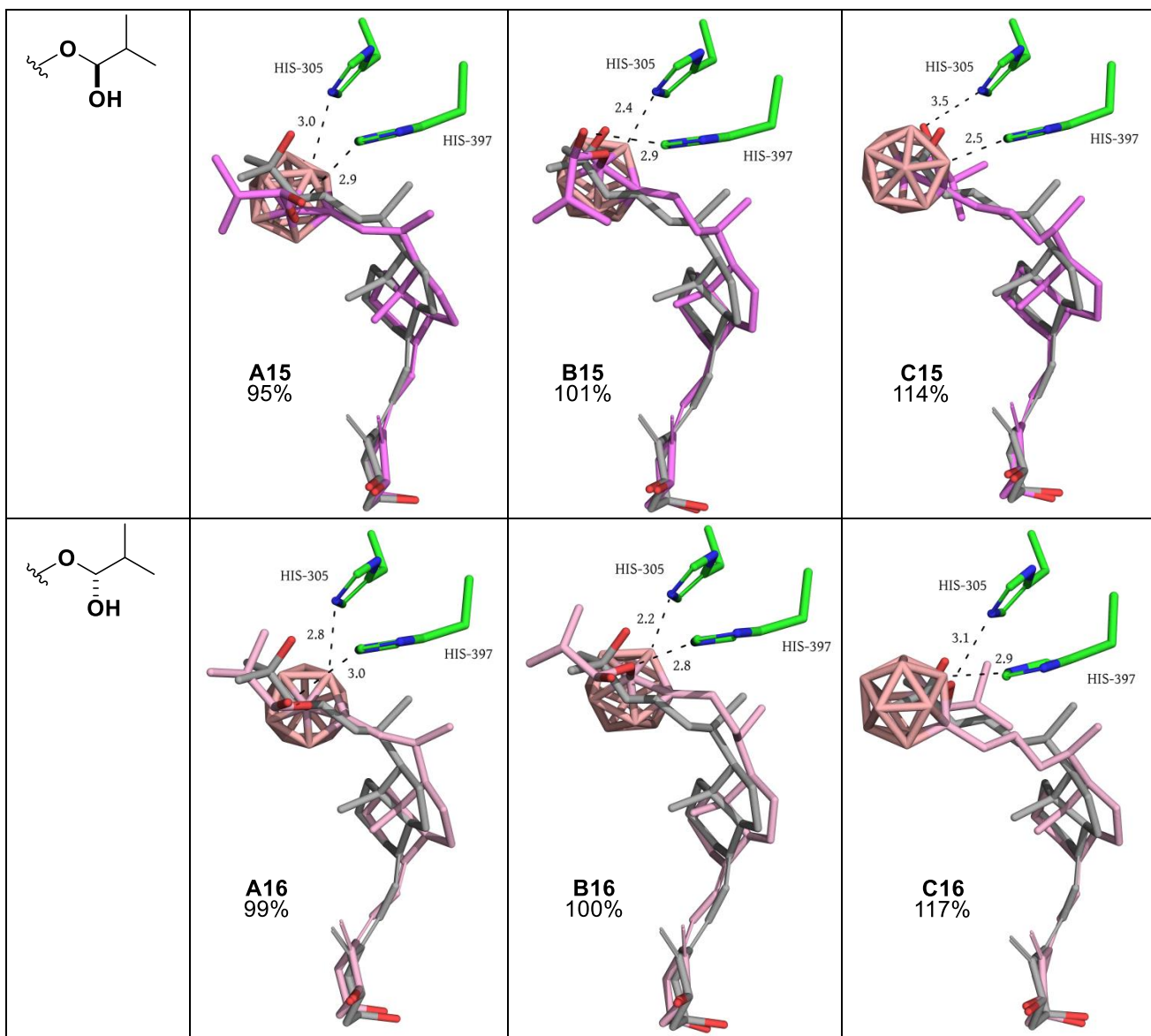
R	n=1	n=2	n=3
 ξ -H	 A1 98%	 B1 107%	 C1 (RO) 116%
 ξ -OH	 A2 105%	 B2 116%	 C2 122%



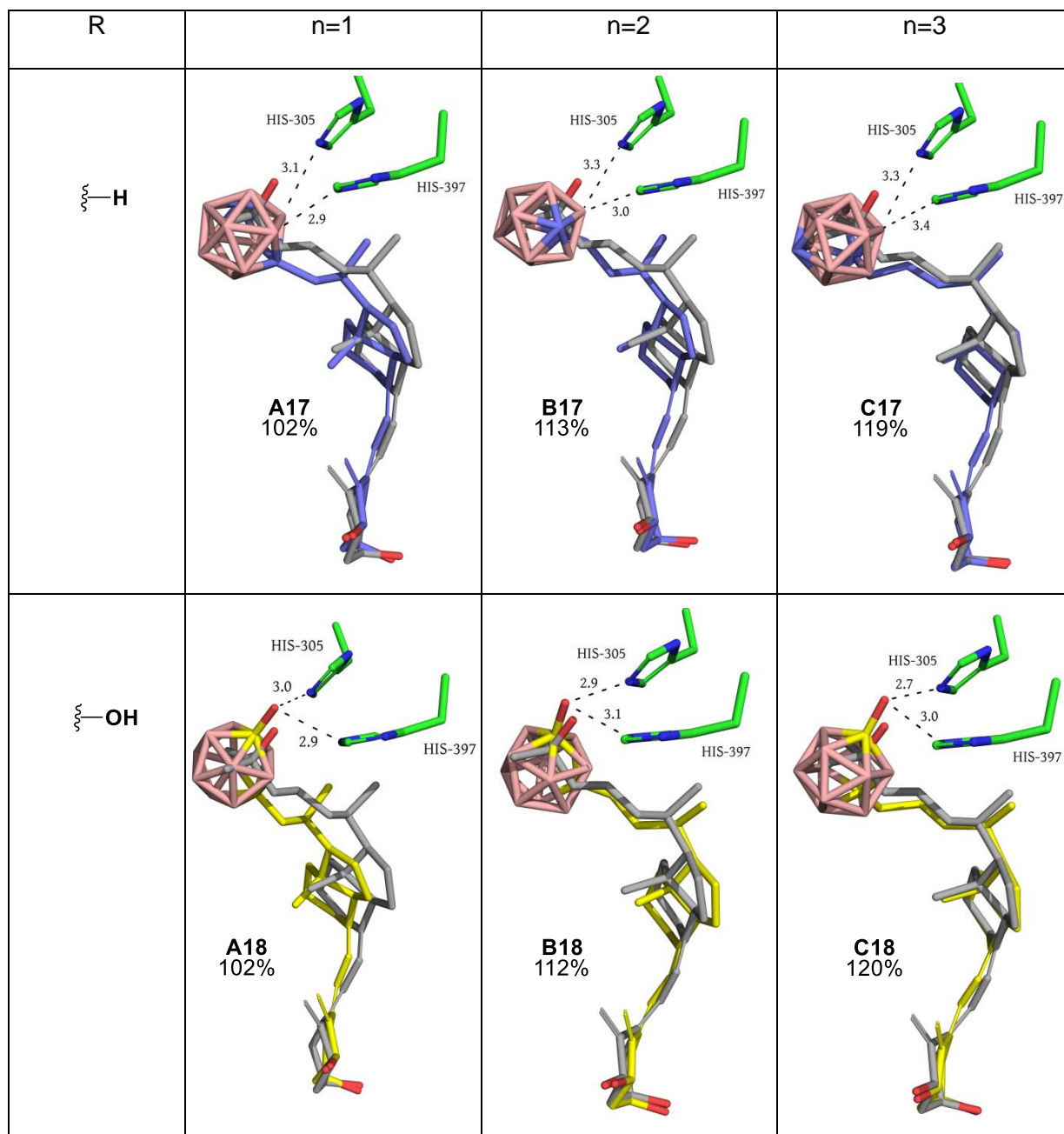


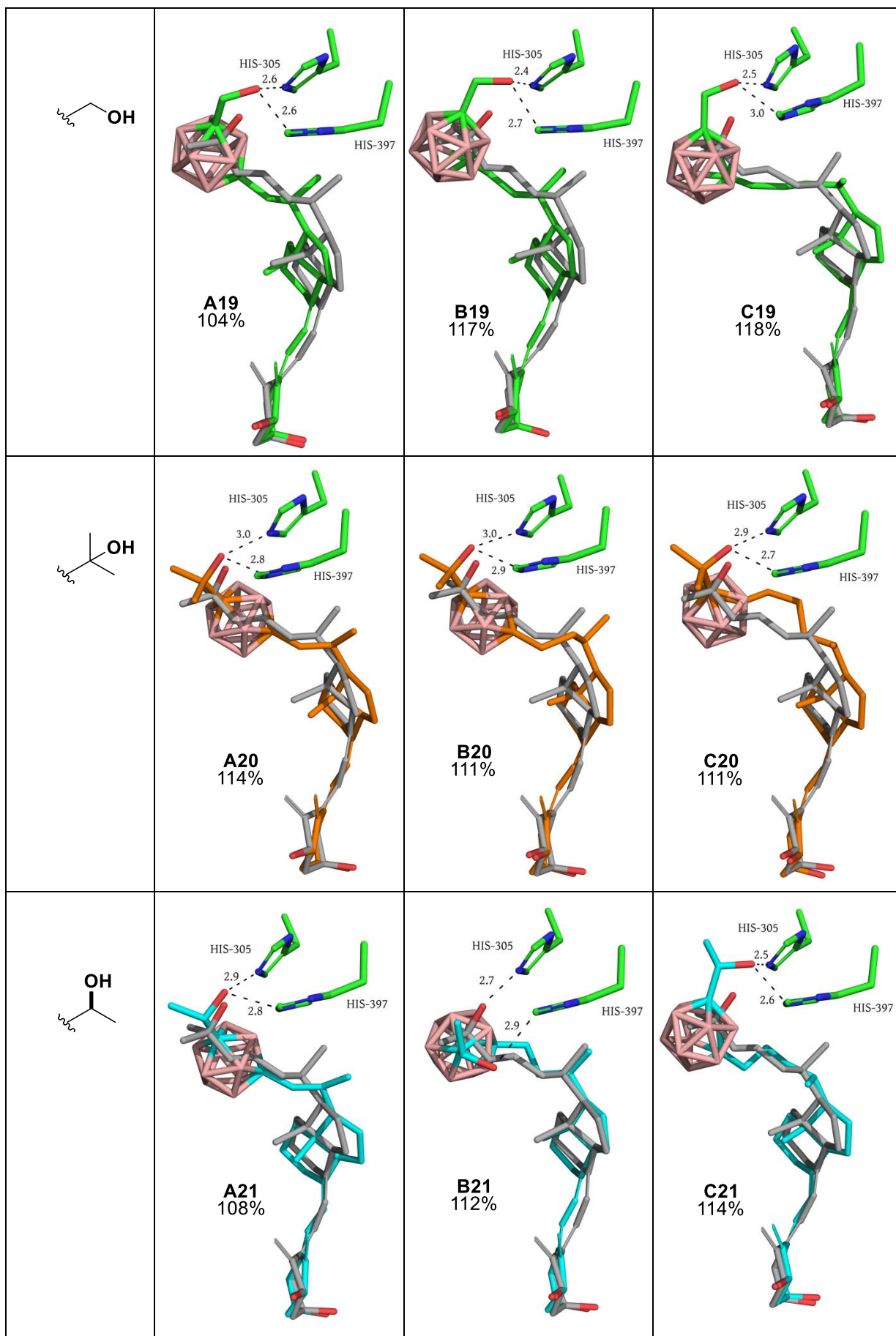


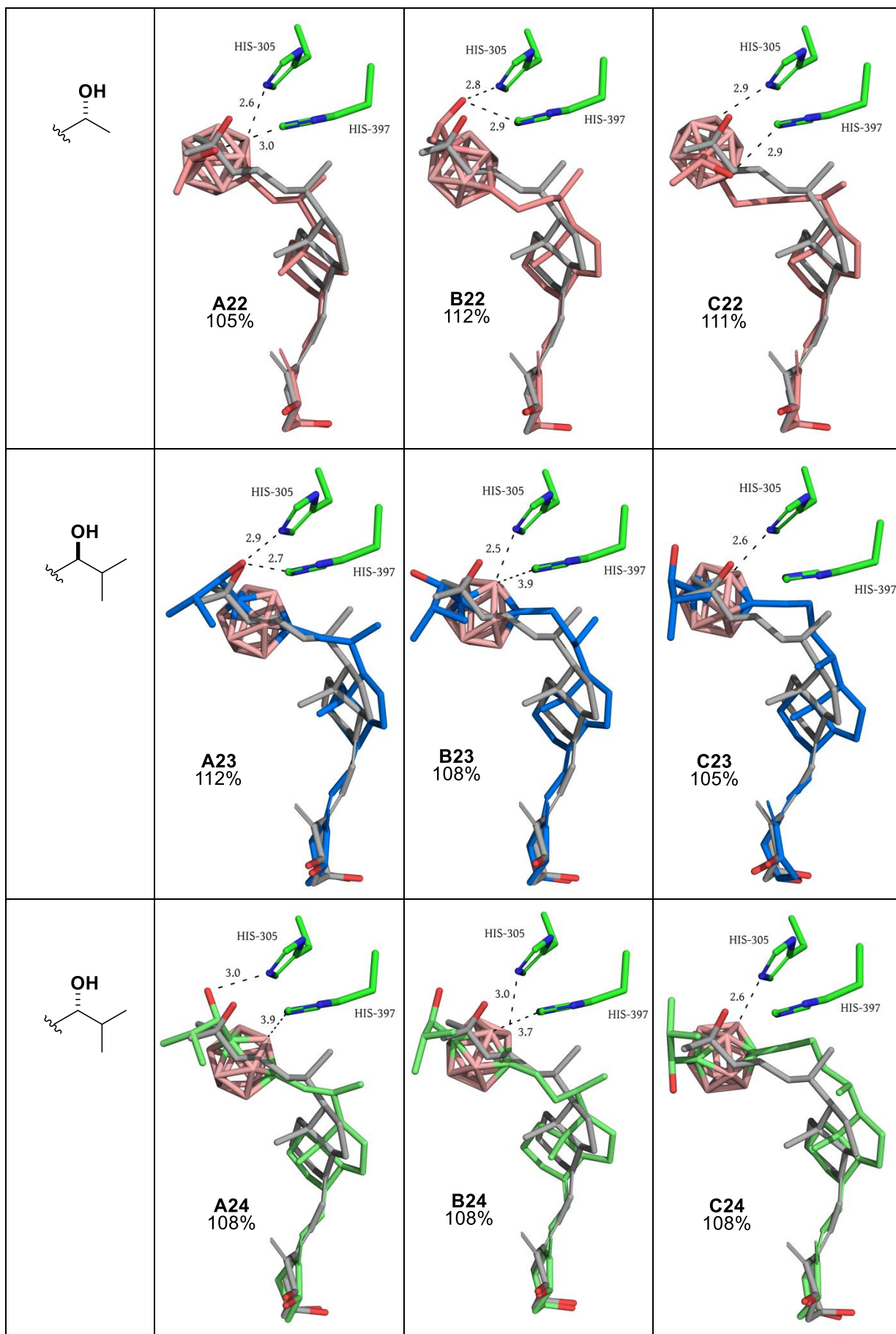


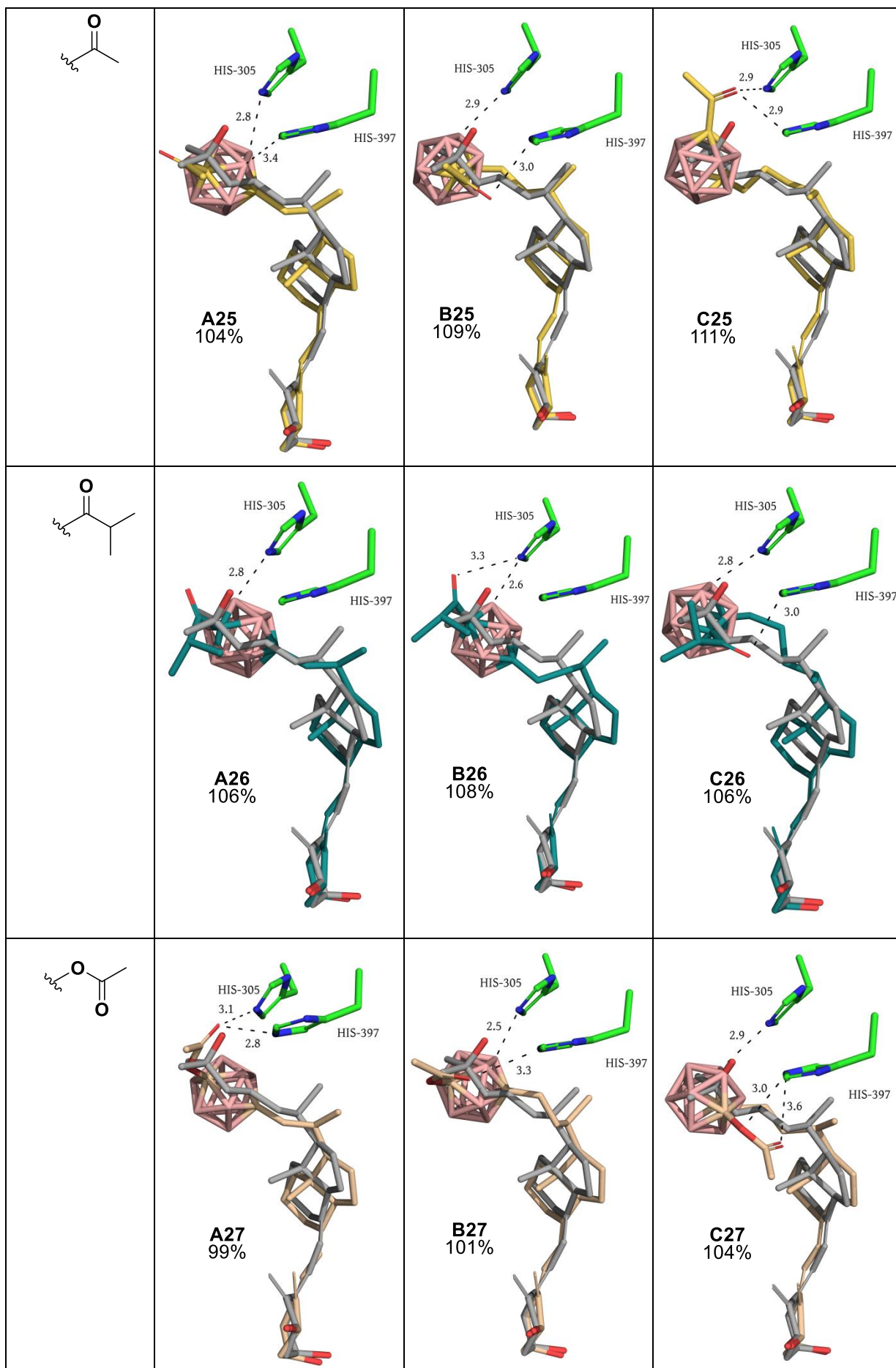


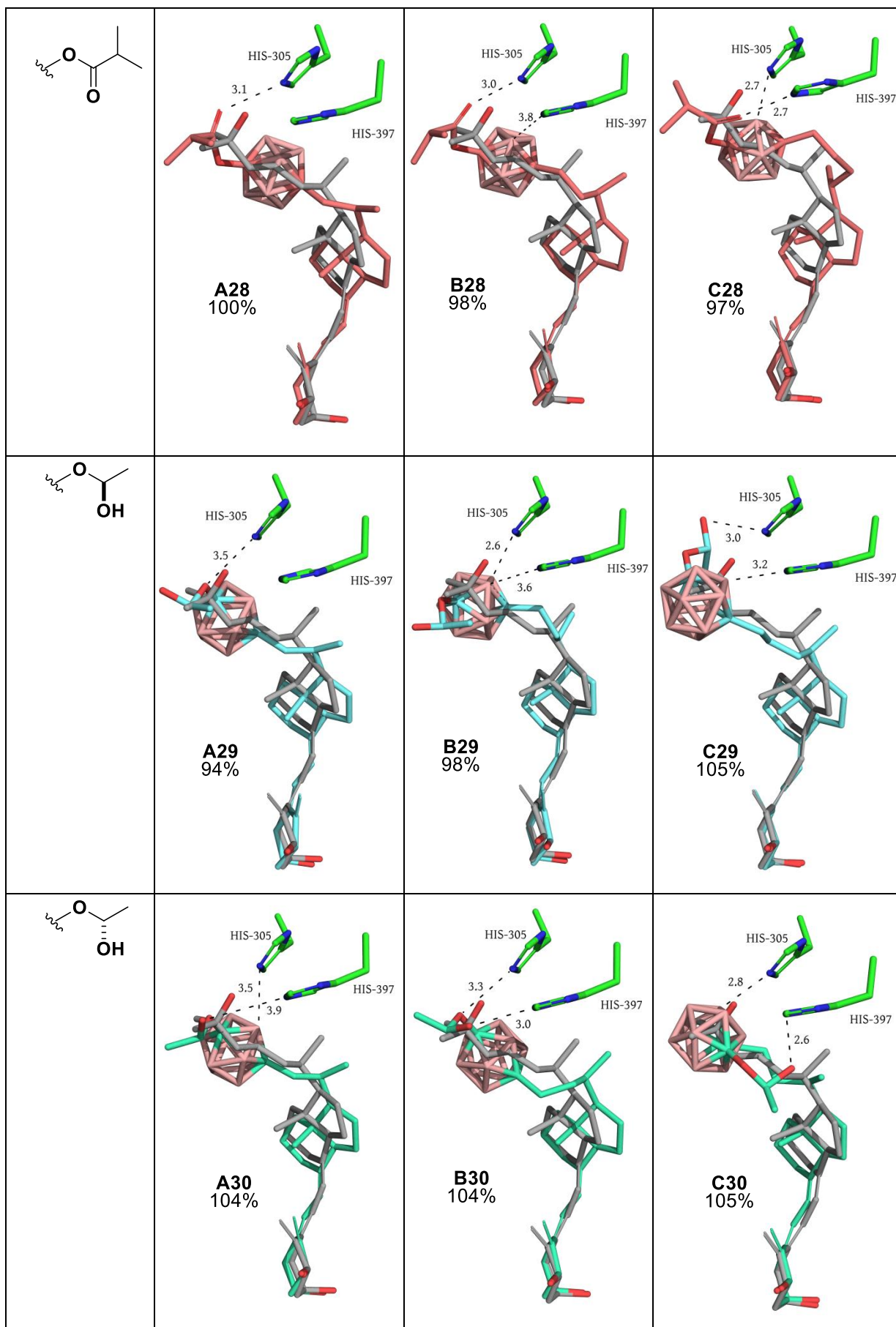
1.2. Meta series

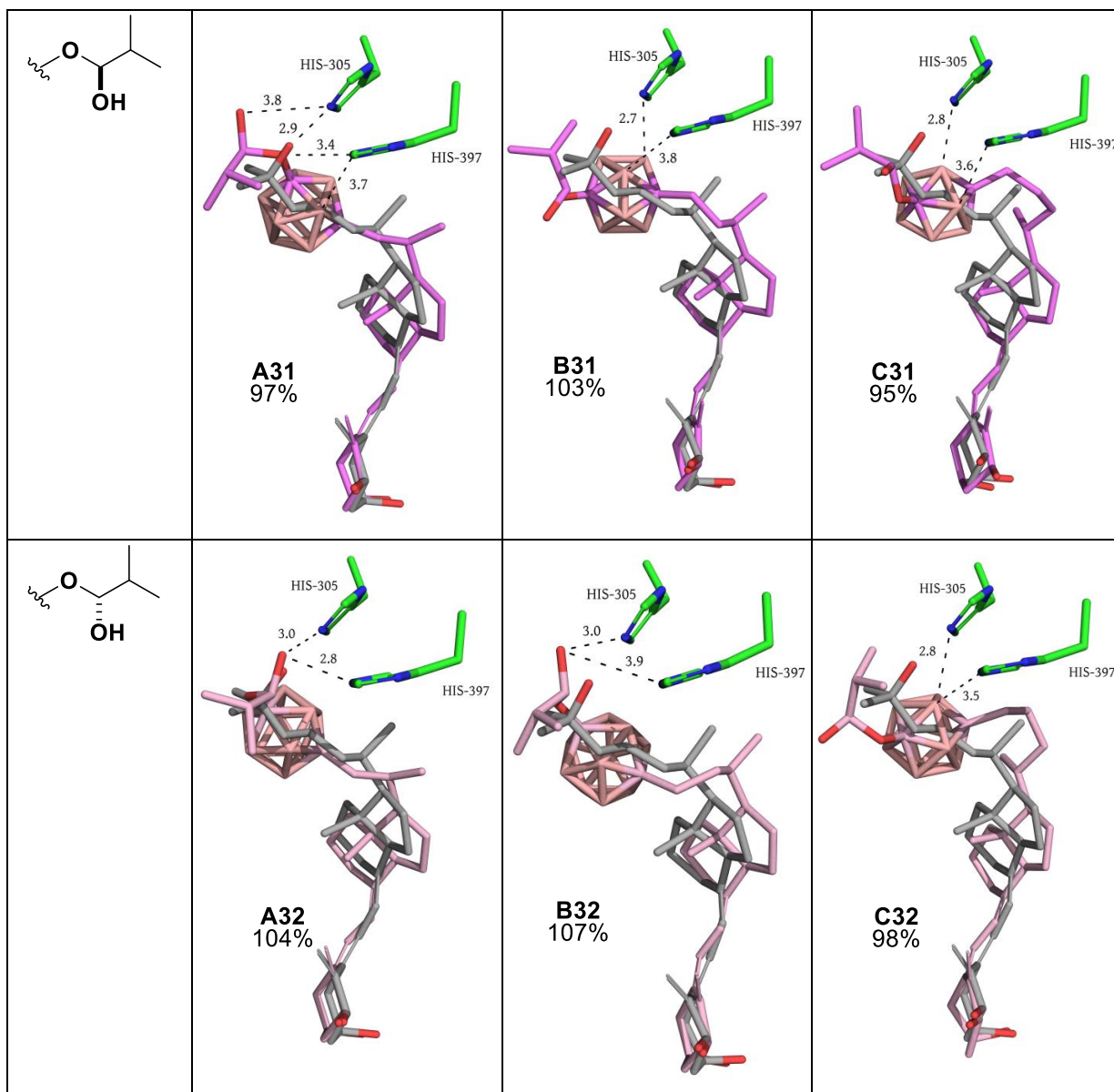




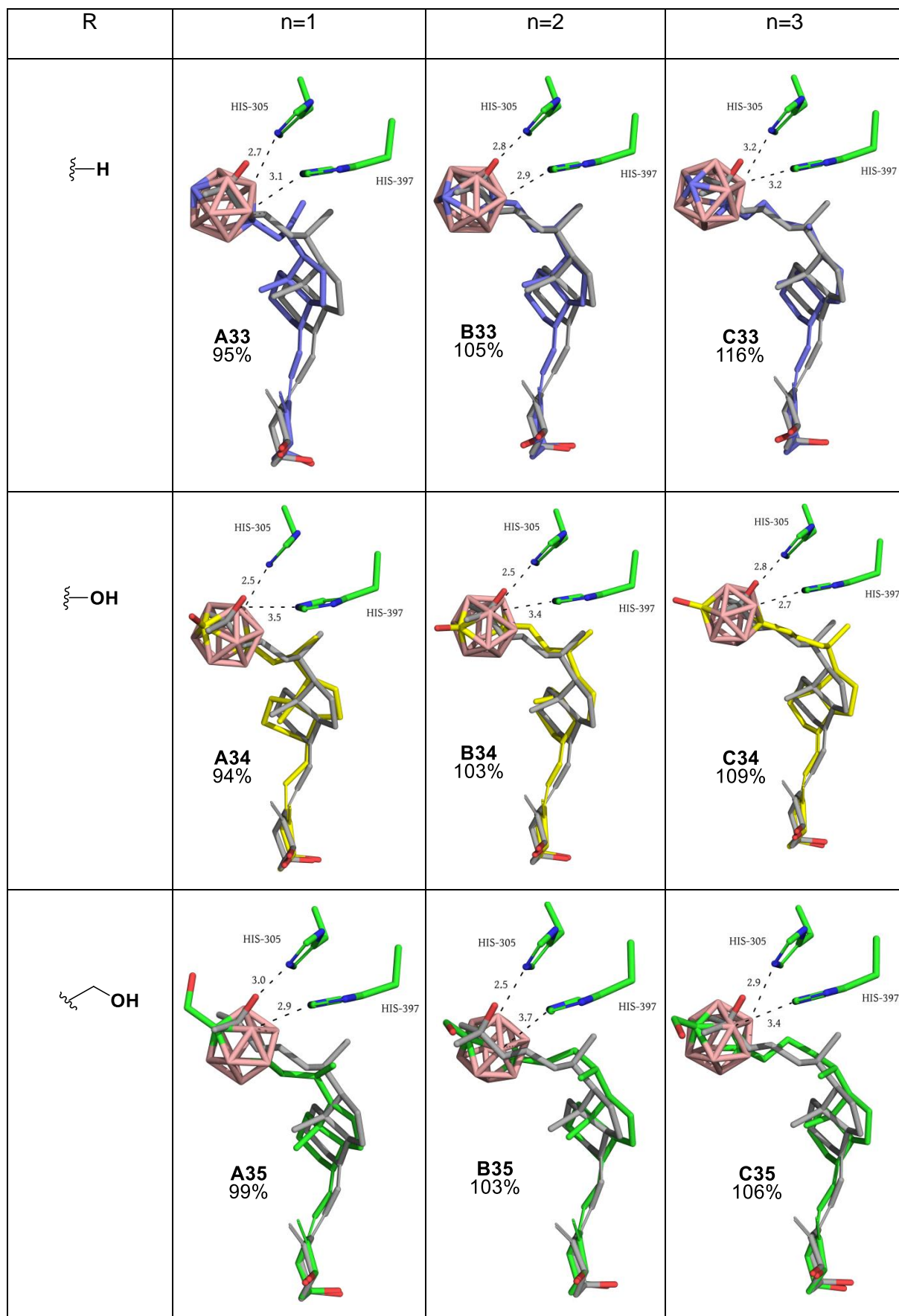


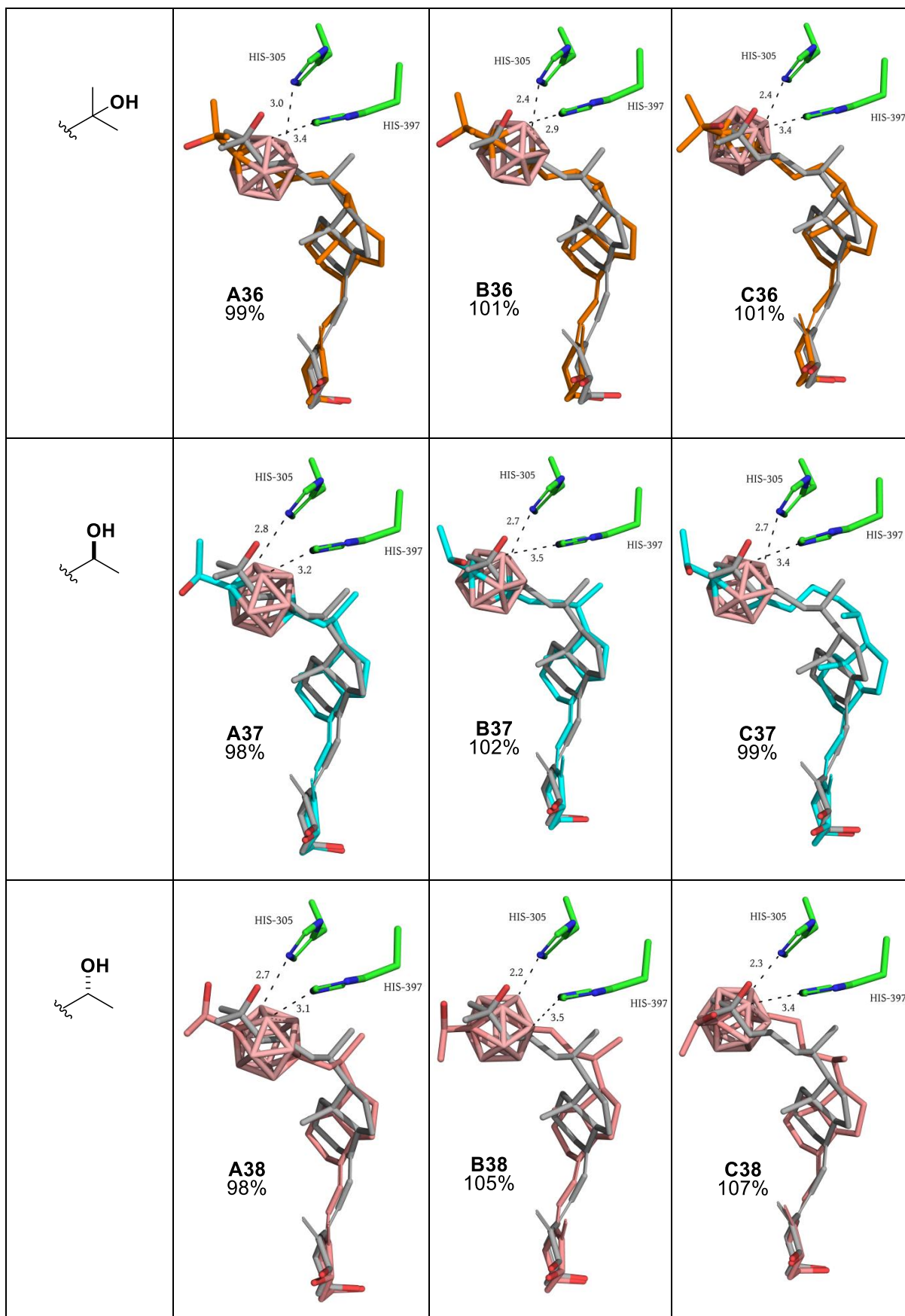


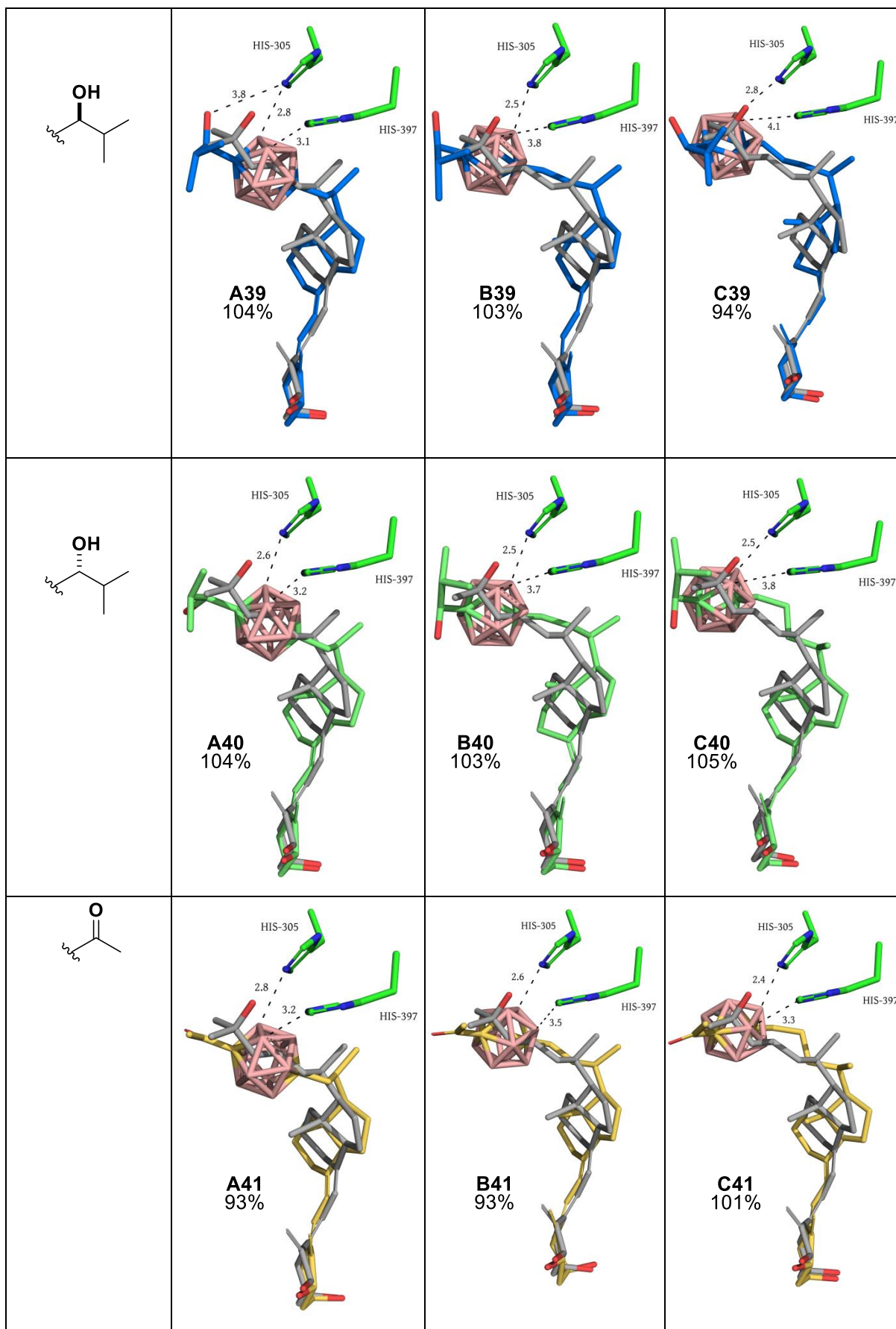


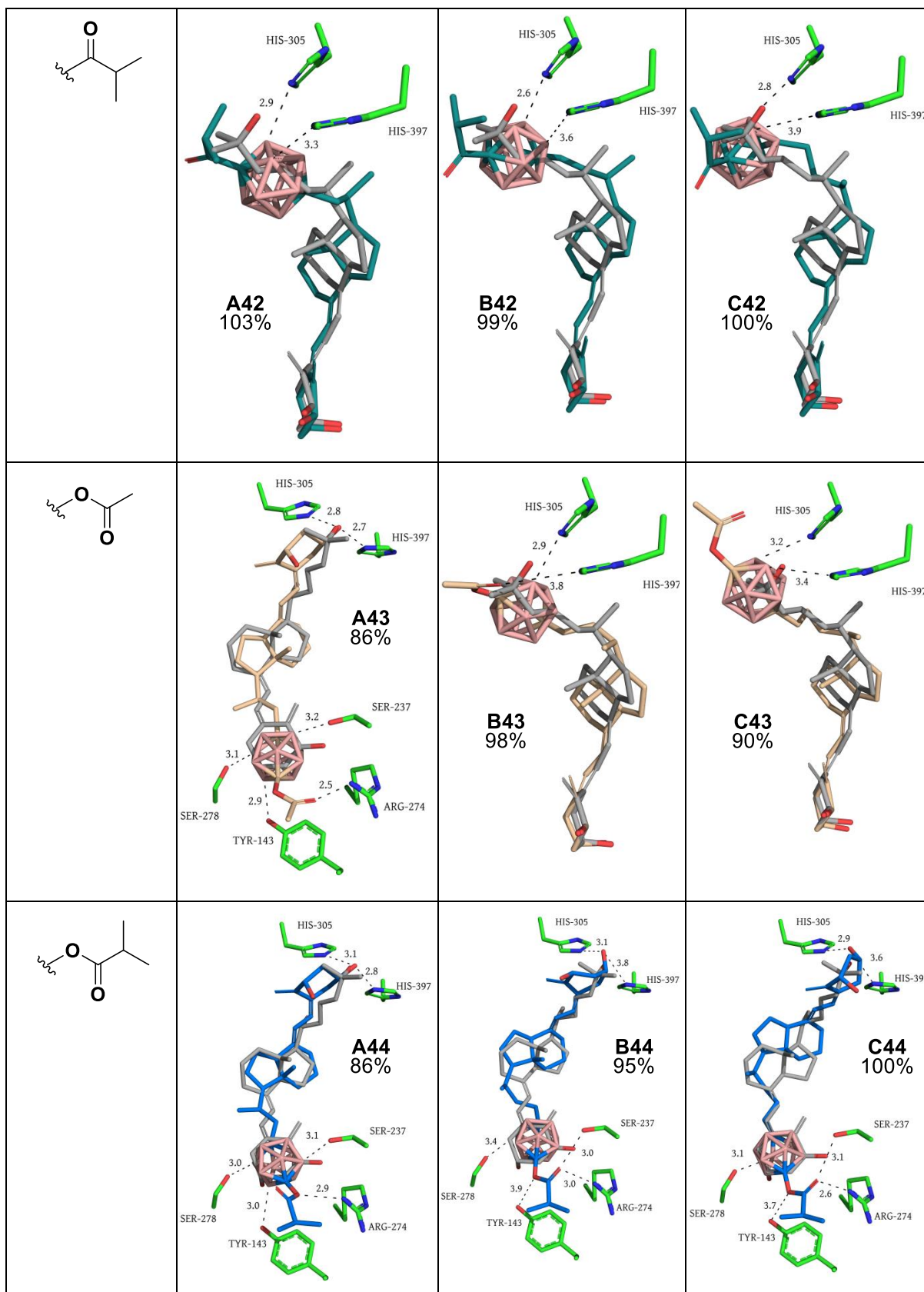


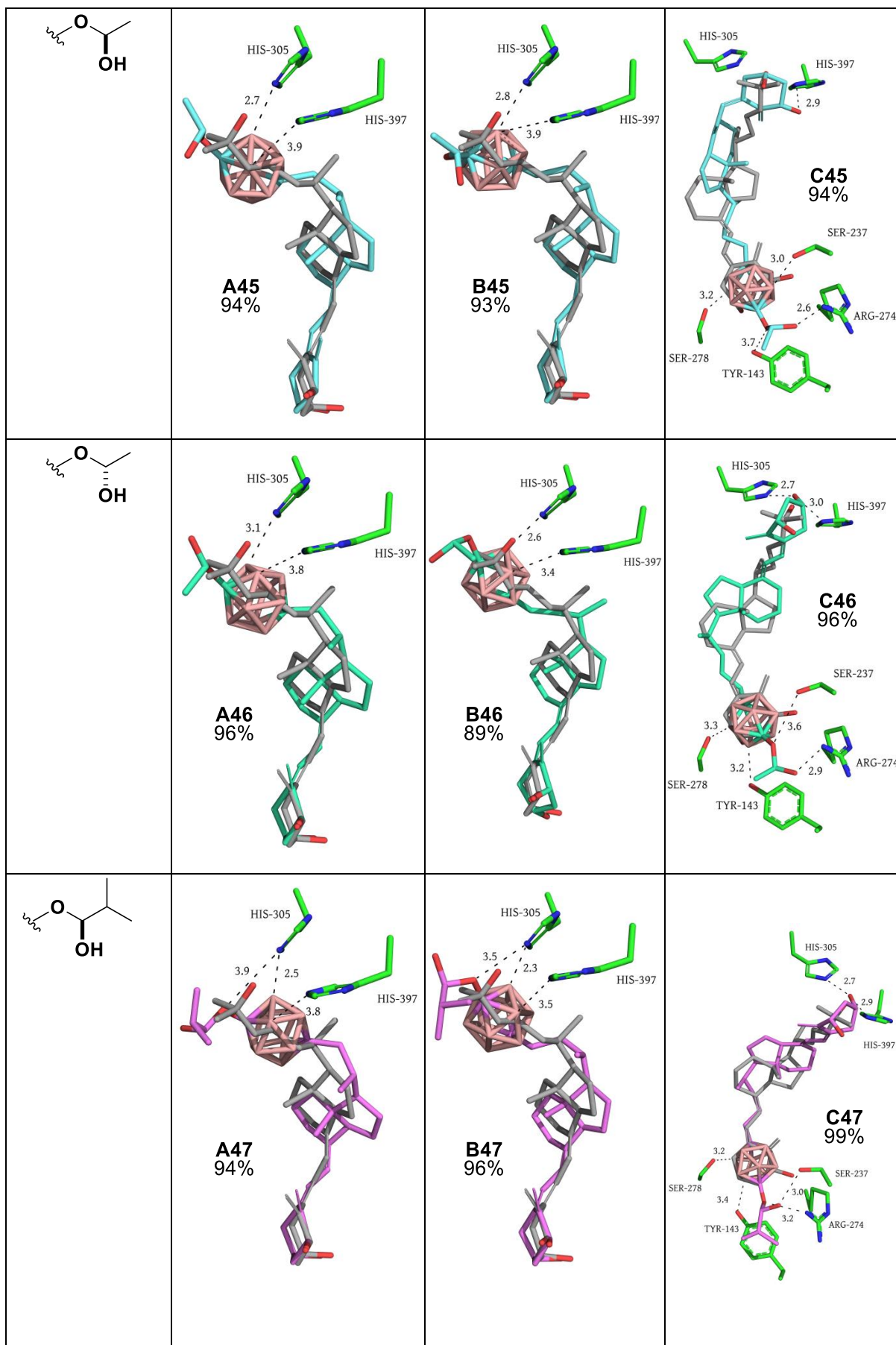
1.3. Para series

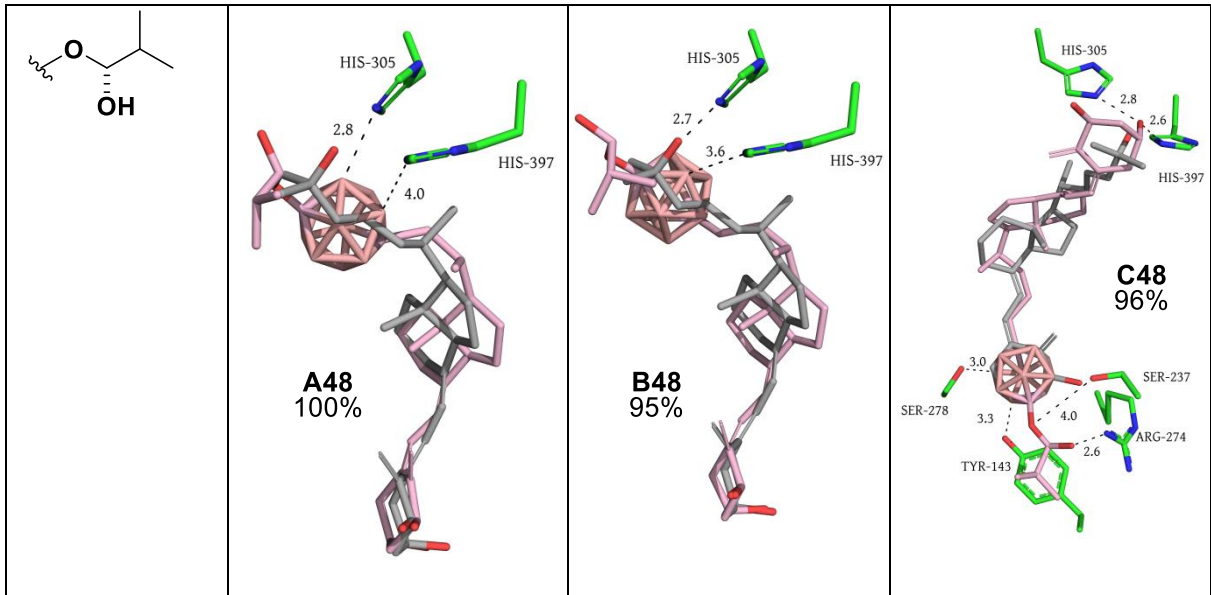






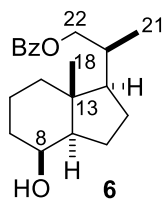




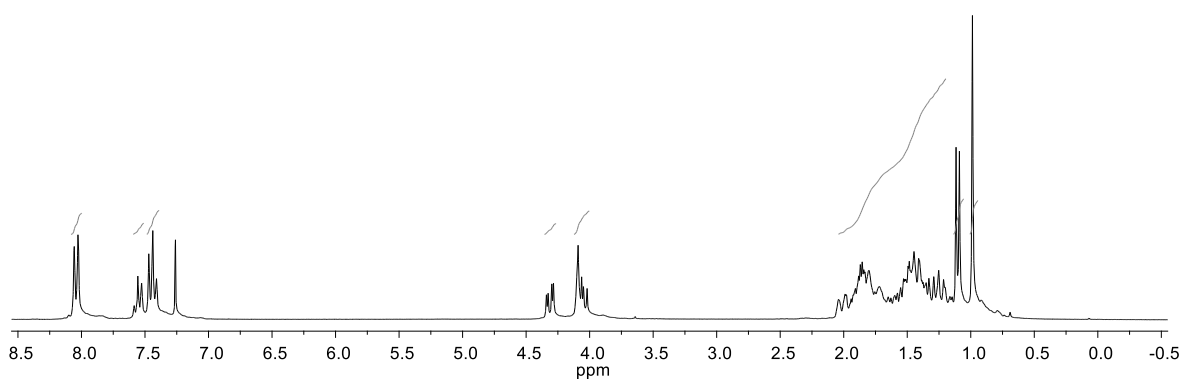


2. NMR SPECTRA

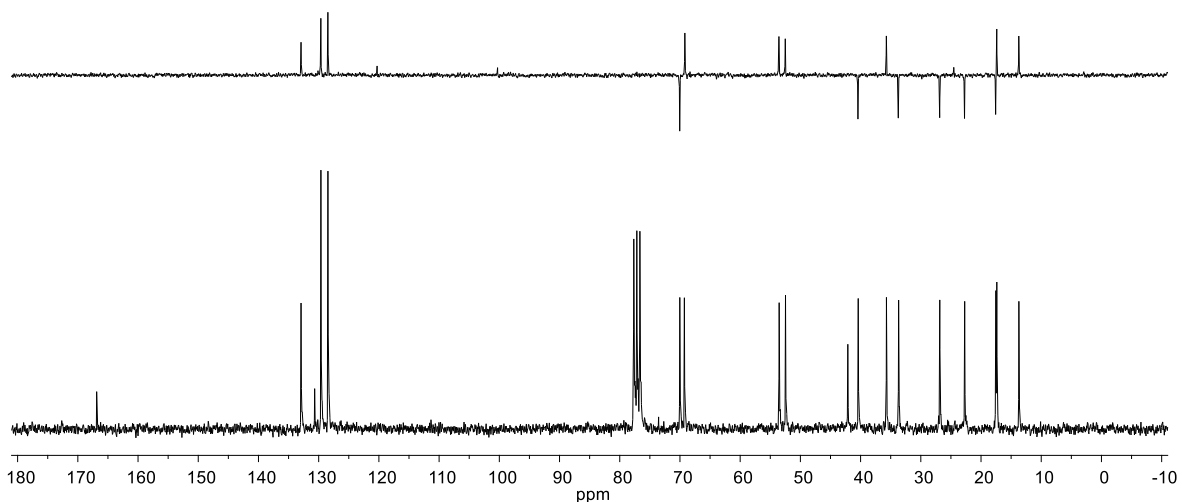
2. NRM Spectra

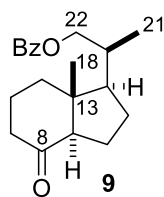


$^1\text{H NMR}$ (250 MHz, CDCl_3): δ 8.04 (d, $J = 7.4$ Hz, 2H, H_{ar}), 7.55 (dd, $J = 8.2$ and 6.4 Hz, 1H, H_{ar}), 7.44 (t, $J = 7.6$ Hz, 2H, H_{ar}), 4.31 (dd, $J = 10.7$ and 3.4 Hz, 1H, H-22), 4.06 (dd, $J = 10.7$ and 7.1 Hz, 2H, H-8 and H-22), 2.04 – 1.20 (m, 14H), 1.10 (d, $J = 6.6$ Hz, 3H, CH_3 -21), 0.99 (s, 3H, CH_3 -18).

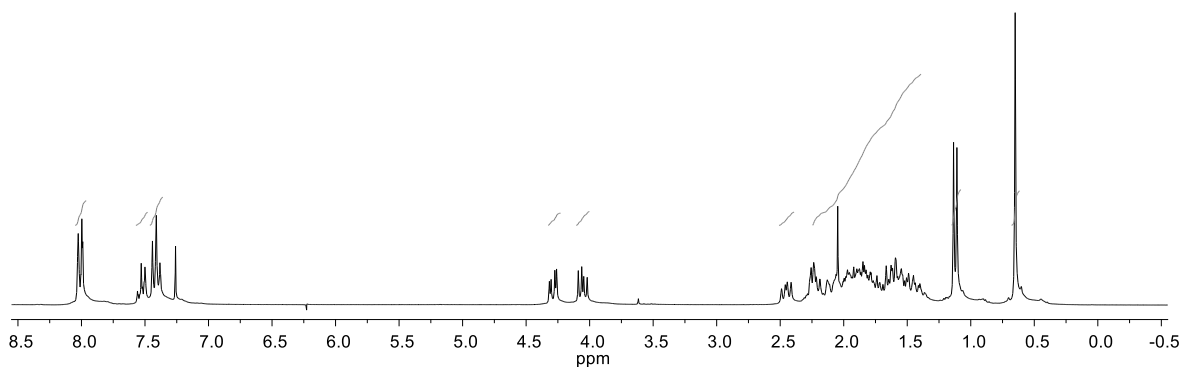


$^{13}\text{C NMR}$ (63 MHz, CDCl_3): δ 166.9 (C, C=O), 132.9 (CH, CH_{ar}), 130.7 (C, C_{ar}), 129.6 (CH, $2\times\text{CH}_{\text{ar}}$), 128.5 (CH, $2\times\text{CH}_{\text{ar}}$), 70.0 (CH_2 , C-22), 69.3 (CH, C-8), 53.5 (CH), 52.5 (CH), 42.1 (C, C-13), 40.4 (CH_2), 35.7 (CH), 33.7 (CH_2), 26.9 (CH_2), 22.71 (CH_2), 17.54 (CH_2), 17.38 (CH_3 , CH_3 -21), 13.71 (CH_3 , CH_3 -18).

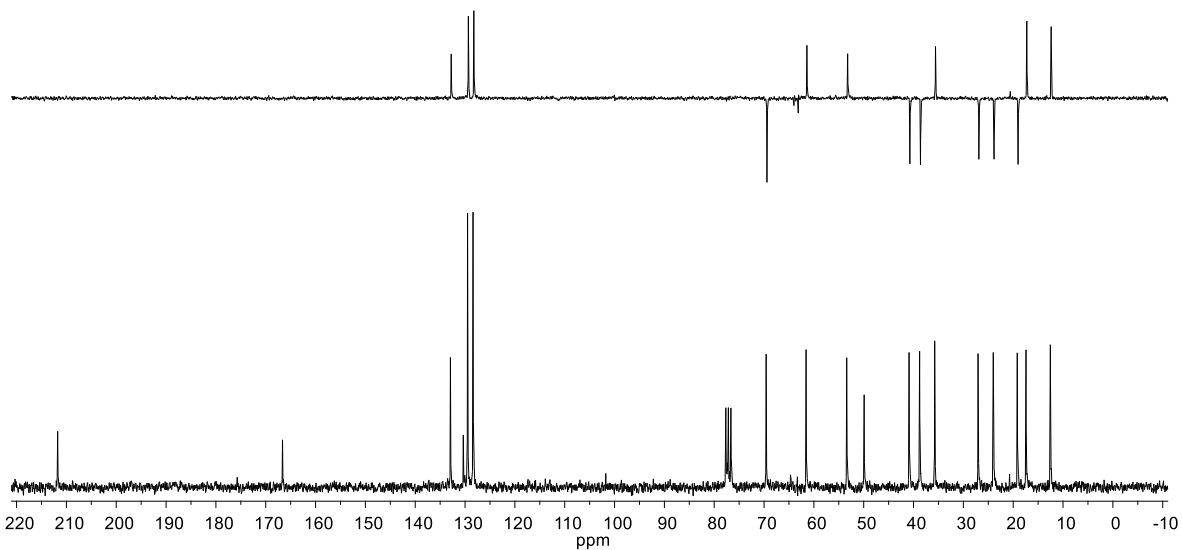


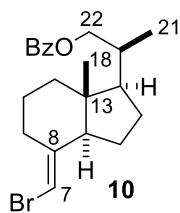


¹H NMR (250 MHz, CDCl₃): δ 8.04 – 7.96 (m, 2H, H_{ar}), 7.57 – 7.48 (m, 1H, H_{ar}), 7.41 (t, *J* = 7.4 Hz, 2H, H_{ar}), 4.29 (dd, *J* = 10.8 and 3.4 Hz, 1H, H-22), 4.05 (dd, *J* = 10.8 and 6.8 Hz, 1H, H-22), 2.45 (dd, *J* = 11.4 and 7.5 Hz, 1H), 2.24 – 1.39 (m, 12H), 1.12 (d, *J* = 6.6 Hz, 3H, CH₃-21), 0.65 (s, 3H, CH₃-18).

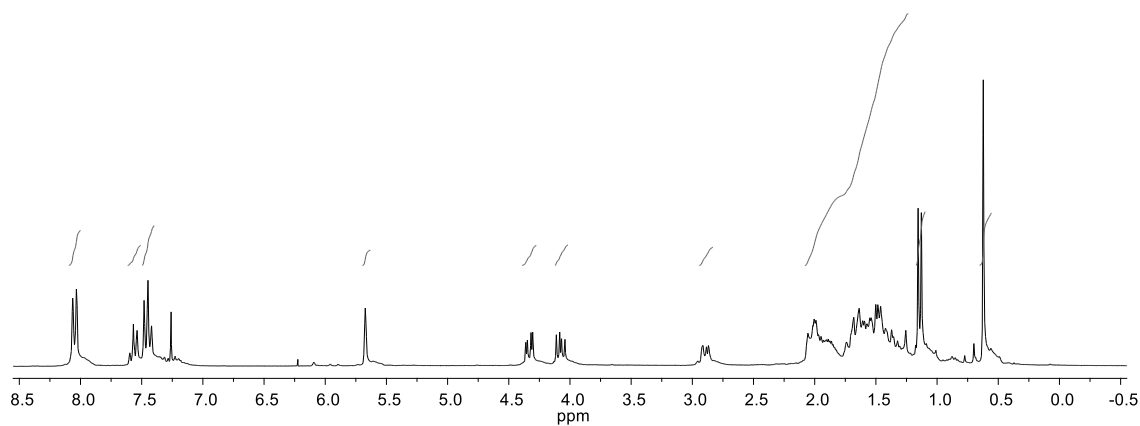


¹³C NMR (63 MHz, CDCl₃): δ 211.7 (C, C=O, C-8), 166.6 (C, C=O), 132.9 (CH, CH_{ar}), 130.4 (C, C_{ar}), 129.5 (CH, 2xCH_{ar}), 128.4 (CH, 2xCH_{ar}), 69.6 (CH₂, C-22), 61.6 (CH), 53.4 (CH), 49.9 (C, C-13), 40.9 (CH₂), 38.8 (CH₂), 35.8 (CH), 27.0 (CH₂), 24.0 (CH₂), 19.2 (CH₂), 17.4 (CH₃, CH₃-21), 12.5 (CH₃, CH₃-18).

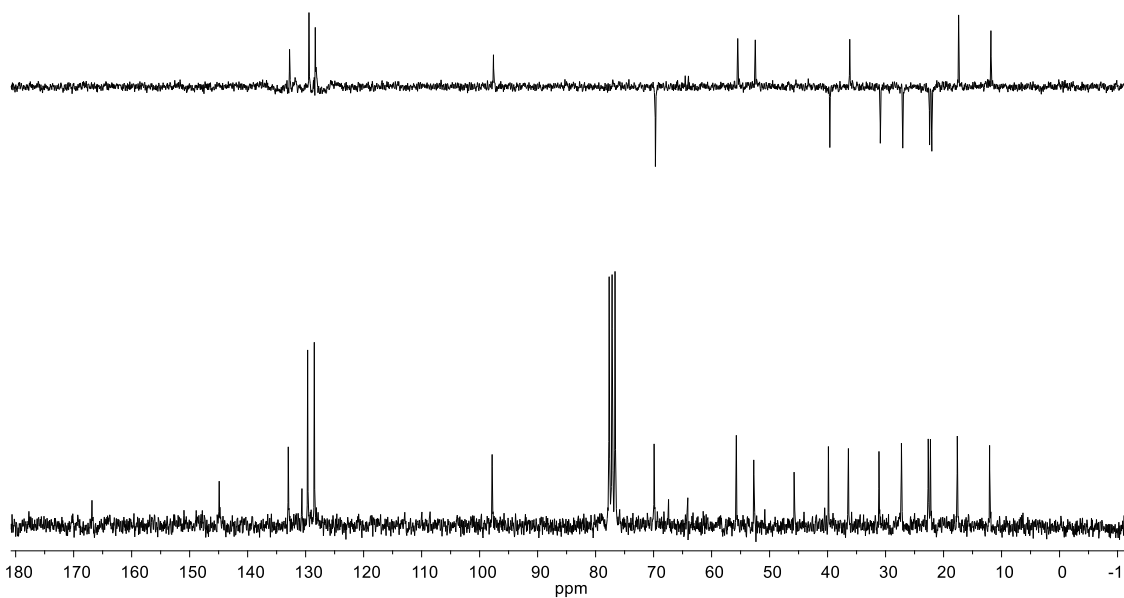


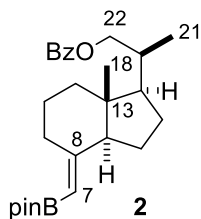


$^1\text{H NMR}$ (250 MHz, CDCl_3): δ 8.10 – 8.00 (m, 2H, H_{ar}), 7.57 (t, $J = 7.3$ Hz, 1H, H_{ar}), 7.45 (t, $J = 7.6$ Hz, 2H, H_{ar}), 5.67 (s, 1H, H-7), 4.33 (dd, $J = 10.8$ and 3.3 Hz, 1H, H-22), 4.08 (dd, $J = 10.7$ and 7.0 Hz, 1H, H-22), 2.90 (dd, $J = 10.2$ and 2.8 Hz, 1H), 2.08 – 1.24 (m, 12H), 1.14 (d, $J = 6.6$ Hz, 3H, CH_3 -21), 0.62 (s, 3H, CH_3 -18).

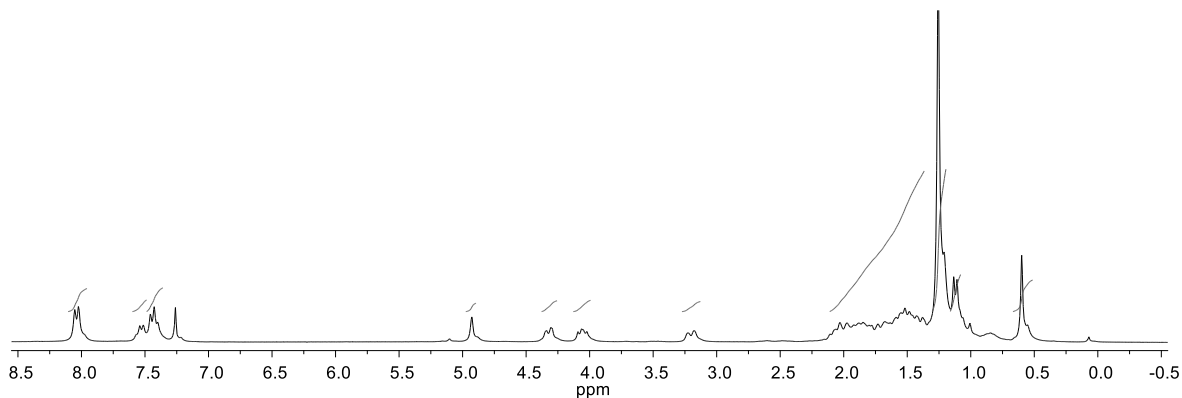


$^{13}\text{C NMR}$ (63 MHz, CDCl_3): δ 166.8 (C, C=O), 144.9 (C, C-8), 133.0 (CH, CH_{ar}), 130.6 (C, C_{ar}), 129.7 (CH, $2\times\text{CH}_{\text{ar}}$), 128.5 (CH, $2\times\text{CH}_{\text{ar}}$), 97.8 (CH, C-7), 69.9 (CH_2 , C-22), 55.7 (CH), 52.7 (CH), 45.8 (C, C-13), 39.9 (CH_2), 36.4 (CH), 31.1 (CH_2), 27.3 (CH_2), 22.6 (CH_2), 22.3 (CH_2), 17.6 (CH_3 , CH_3 -21), 12.1 (CH_3 , CH_3 -18).

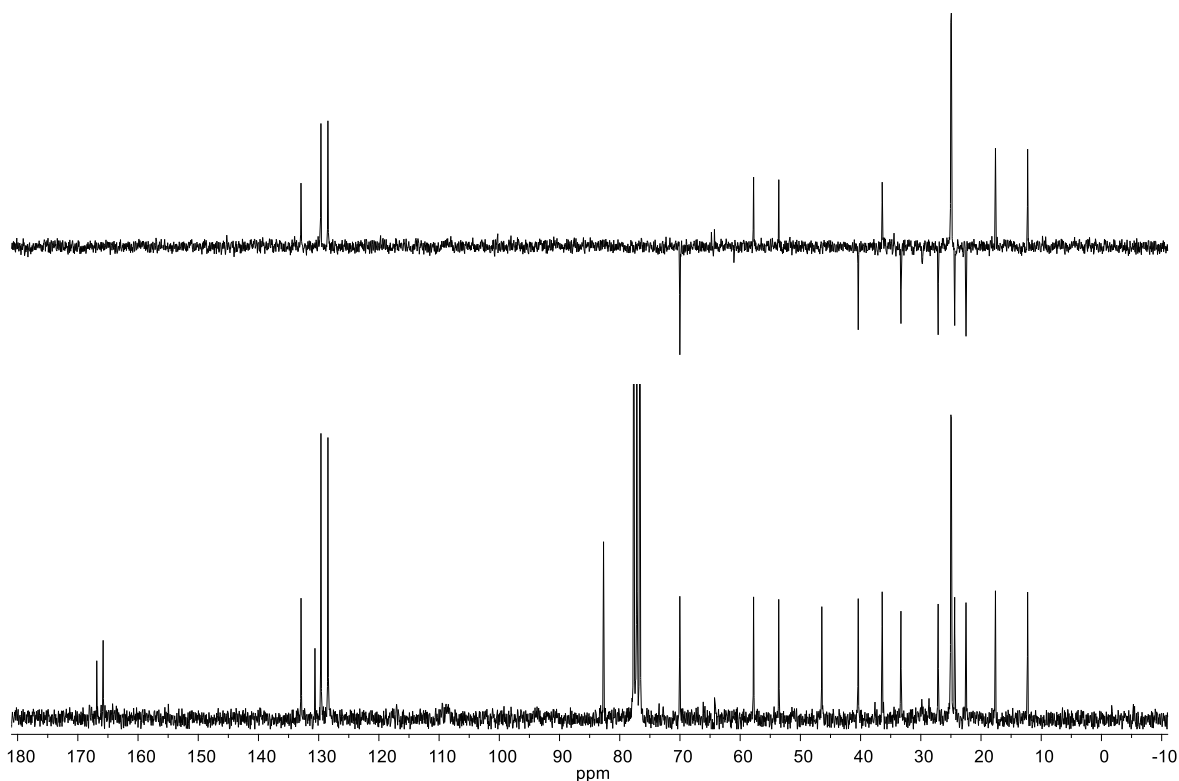


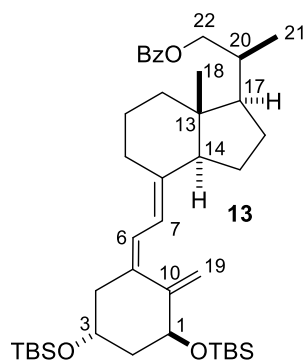


¹H NMR (250 MHz, CDCl₃): δ 8.04 (d, *J* = 7.0 Hz, 2H, H_{ar}), 7.61 – 7.50 (m, 1H, H_{ar}), 7.44 (t, *J* = 7.2 Hz, 2H, H_{ar}), 4.93 (s, 1H, H-7), 4.32 (dd, *J* = 9.9 and 2.0 Hz, 1H, H-22), 4.06 (dd, *J* = 10.4 and 7.0 Hz, 1H, H-22), 3.19 (d, *J* = 12.8 Hz, 1H, H-14), 2.12 – 1.37 (m, 12H), 1.26 (s, 12H, 4xCH₃COB), 1.12 (d, *J* = 6.4 Hz, 3H, CH₃-21), 0.60 (s, 3H, CH₃-18).

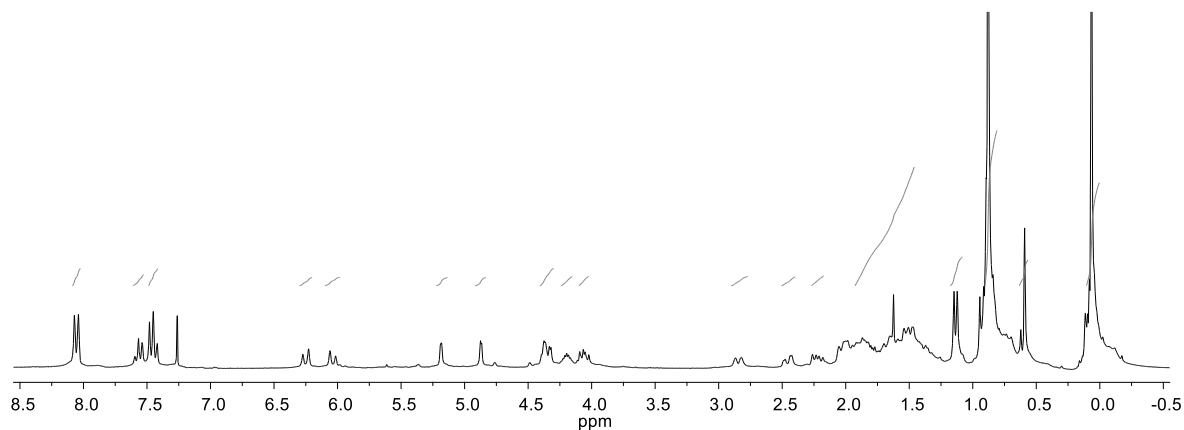


¹³C NMR (63 MHz, CDCl₃): δ 166.9 (C, C-8), 165.8 (C=O, C_{ar}), 132.9 (CH, CH_{ar}), 130.6 (C, C_{ar}), 129.6 (CH, 2xCH_{ar}), 128.5 (CH, 2xCH_{ar}), 82.7 (C, 2xCH₃COB), 70.0 (CH₂, C-22), 57.8 (CH, C-7), 53.6 (CH), 46.4 (C, C-13), 40.4 (CH₂), 36.4 (CH, C-20), 33.3 (CH₂), 27.1 (CH₂), 25.0 (CH₃, 2xCH₃COB), 24.9 (CH₃, 2xCH₃COB), 24.4 (CH₂), 22.5 (CH₂), 17.6 (CH₃, CH₃-21), 12.3 (CH₃, CH₃-18).

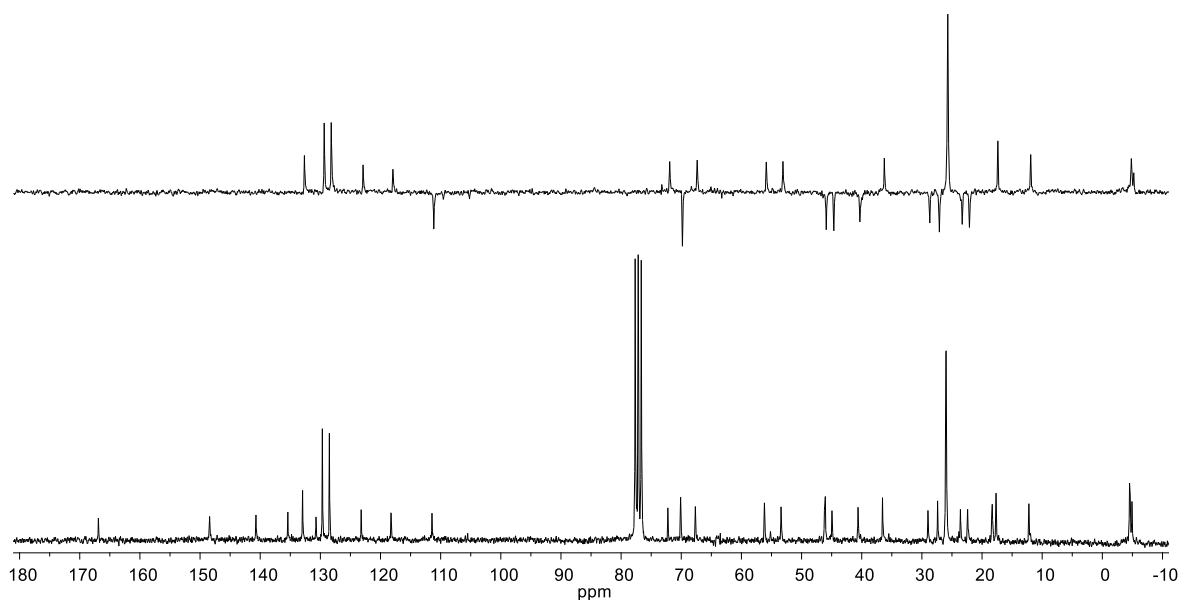


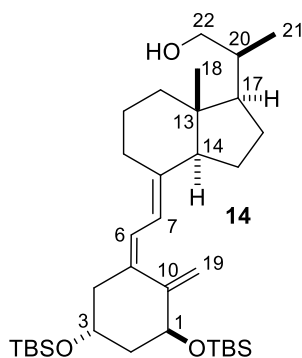


¹H NMR (250 MHz, CDCl₃): δ 8.06 (d, *J* = 8.0 Hz, 2H, H_{ar}), 7.57 (t, *J* = 6.9 Hz, 1H, H_{ar}), 7.45 (t, *J* = 7.7 Hz, 2H, H_{ar}), 6.25 (d, *J* = 11.4 Hz, 1H, H-6), 6.04 (d, *J* = 11.1 Hz, 1H, H-7), 5.22 – 5.14 (s, 1H, H-19), 4.87 (s, 1H, H-19), 4.41 – 4.29 (m, 2H, H-22), 4.25 – 4.14 (m, 1H, H-1), 4.10 – 4.02 (m, 1H, H-3), 2.90 – 2.78 (m, 1H, H-9), 2.46 (dd, *J* = 13.1 and 3.3 Hz, 1H, H-4), 2.22 (dd, *J* = 13.1 and 7.2 Hz, 1H, H-4), 1.92 – 1.45 (m, 14H), 1.14 (d, *J* = 6.4 Hz, 3H, CH₃-21), 0.90 – 0.81 (m, 18H, 2xCH₃CSi), 0.59 (s, 3H, CH₃-18), 0.11 – 0.00 (m, 12H, 4xCH₃Si).

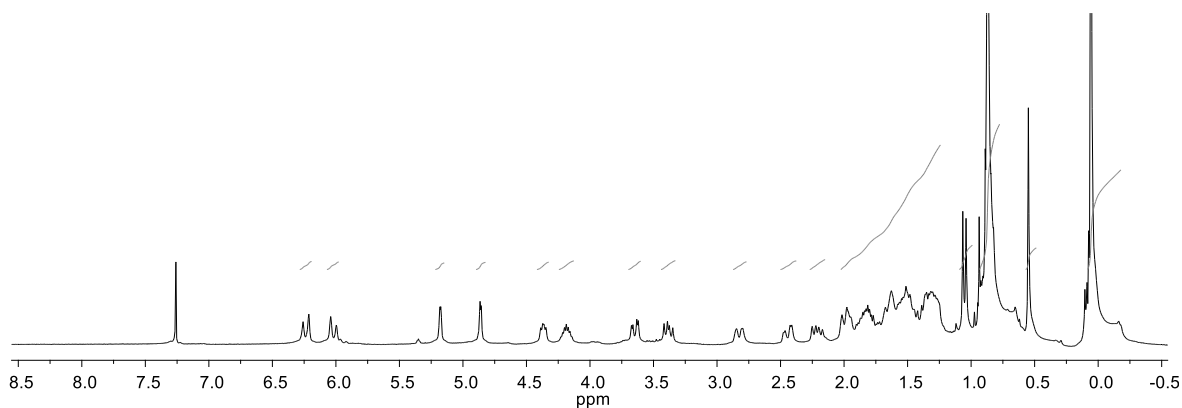


¹³C NMR (63 MHz, CDCl₃): δ 166.9 (C=O, C_{ar}), 148.4 (C, C-10), 140.7 (C, C-8), 135.4 (C, C-5), 133.0 (CH, CH_{ar}), 130.7 (C, C_{ar}), 129.7 (CH, 2xCH_{ar}), 128.5 (CH, 2xCH_{ar}), 123.2 (=CH, C-6), 118.2 (=CH, C-7), 111.4 (CH₂, C-19), 72.2 (CH, C-1), 70.1 (CH₂, C-22), 67.7 (CH, C-3), 56.2 (CH), 53.4 (CH), 46.2 (CH₂), 46.0 (C, C-13), 44.9 (CH₂), 40.6 (CH₂), 36.5 (CH), 29.0 (CH₂), 27.4 (CH₂), 26.0 (CH₃, 3xCH₃CSi), 25.96 (CH₃, 3xCH₃CSi), 23.6 (CH₂), 22.4 (CH₂), 18.4 (C, CH₃CSi), 18.3 (C, CH₃CSi), 17.7 (CH₃, CH₃-21), 12.2 (CH₃, CH₃-18), -4.5 (CH₃, 2xCH₃Si), -4.6 (CH₃, CH₃Si), -4.9 (CH₃, CH₃Si).

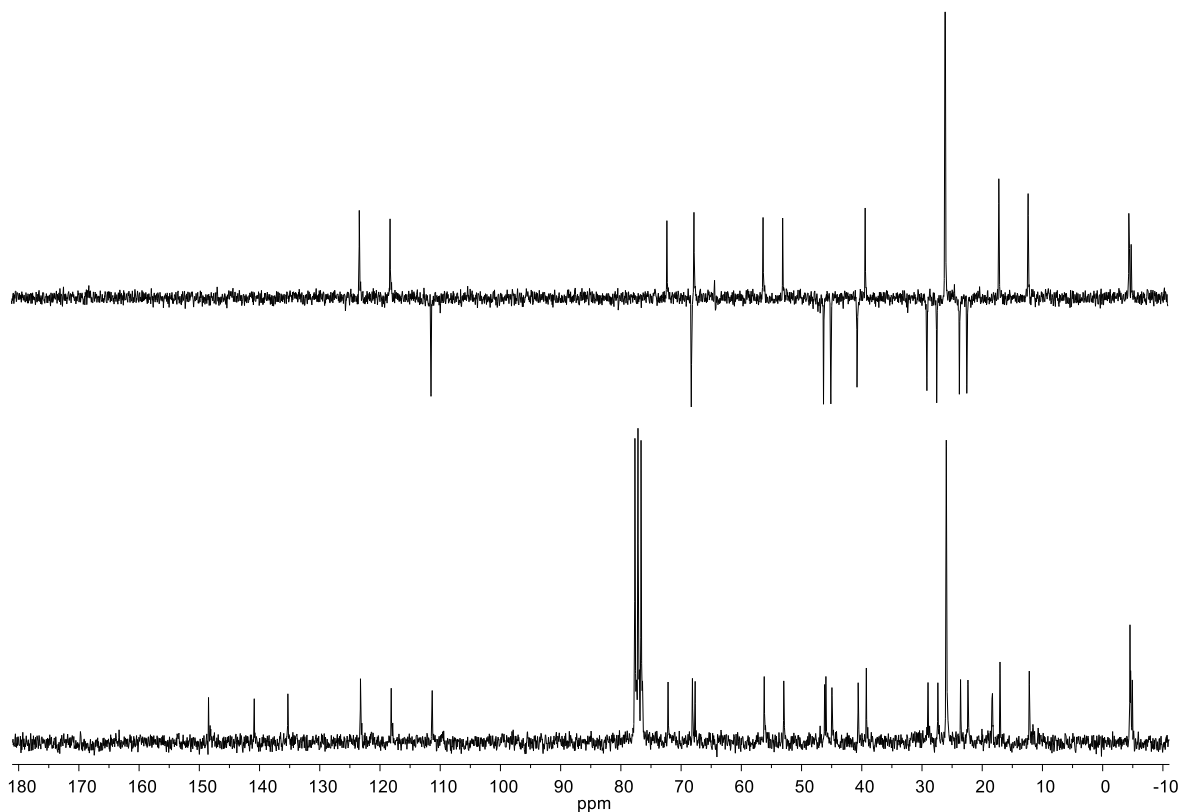


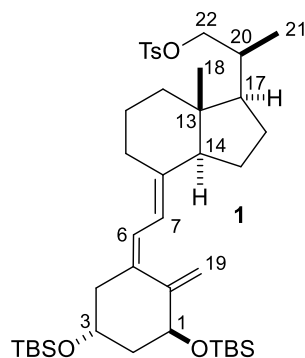


¹H NMR (250 MHz, CDCl₃): δ 6.24 (d, *J* = 11.3 Hz, 1H, H-6), 6.02 (d, *J* = 11.2 Hz, 1H, H-7), 5.18 (s, 1H, H-19), 4.86 (s, 1H, H-19), 4.37 (dd, *J* = 6.3 and 3.8 Hz, 1H, H-1), 4.19 (ddd, *J* = 10.8, 7.2 and 3.8 Hz, 1H, H-3), 3.65 (dd, *J* = 10.5 and 3.0 Hz, 1H, H-22), 3.38 (dd, *J* = 10.5 and 6.7 Hz, 1H, H-22), 2.87 – 2.77 (m, 1H, H-9), 2.44 (dd, *J* = 13.0 and 3.3 Hz, 1H), 2.21 (dd, *J* = 13.0 and 7.1 Hz, 1H, H-4), 2.03 – 1.24 (m, 15H), 1.05 (d, *J* = 6.5 Hz, 3H, CH₃-21), 0.88 (s, 18H, 2x CH₃CSi), 0.55 (s, 3H, CH₃-18), 0.06 (s, 12H, 4x CH₃Si).

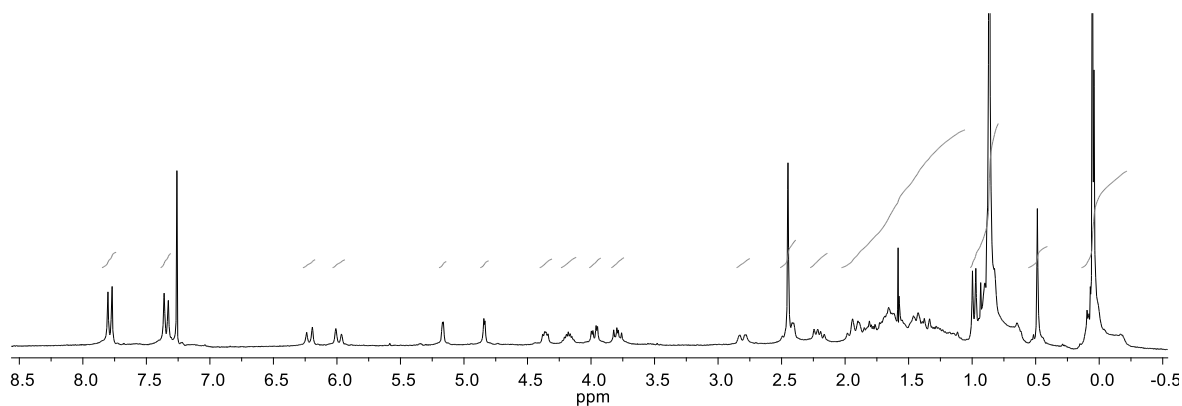


¹³C NMR (63 MHz, CDCl₃): δ 148.5 (C, C-10), 140.9 (C, C-8), 135.3 (C, C-5), 123.2 (=CH, C-6), 118.1 (=CH, C-7), 111.3 (=CH₂, C-19), 72.2 (CH, C-1), 68.1 (CH₂, C-22), 67.7 (CH, C-3), 56.2 (CH), 52.9 (CH), 46.2 (CH₂), 46.0 (C, C-13), 44.9 (CH₂), 40.6 (CH₂), 39.24 (CH), 29.0 (CH₂), 27.4 (CH₂), 26.00 (CH₃, 3xCH₃CSi), 25.96 (CH₃, 3xCH₃CSi), 23.6 (CH₂), 22.4 (CH₂), 18.4 (C, CH₃CSi), 18.3 (C, CH₃CSi), 17.0 (CH₃, CH₃-21), 12.2 (CH₃, CH₃-18), -4.5 (CH₃, 2xCH₃Si), -4.6 (CH₃, CH₃Si), -4.9 (CH₃, CH₃Si).

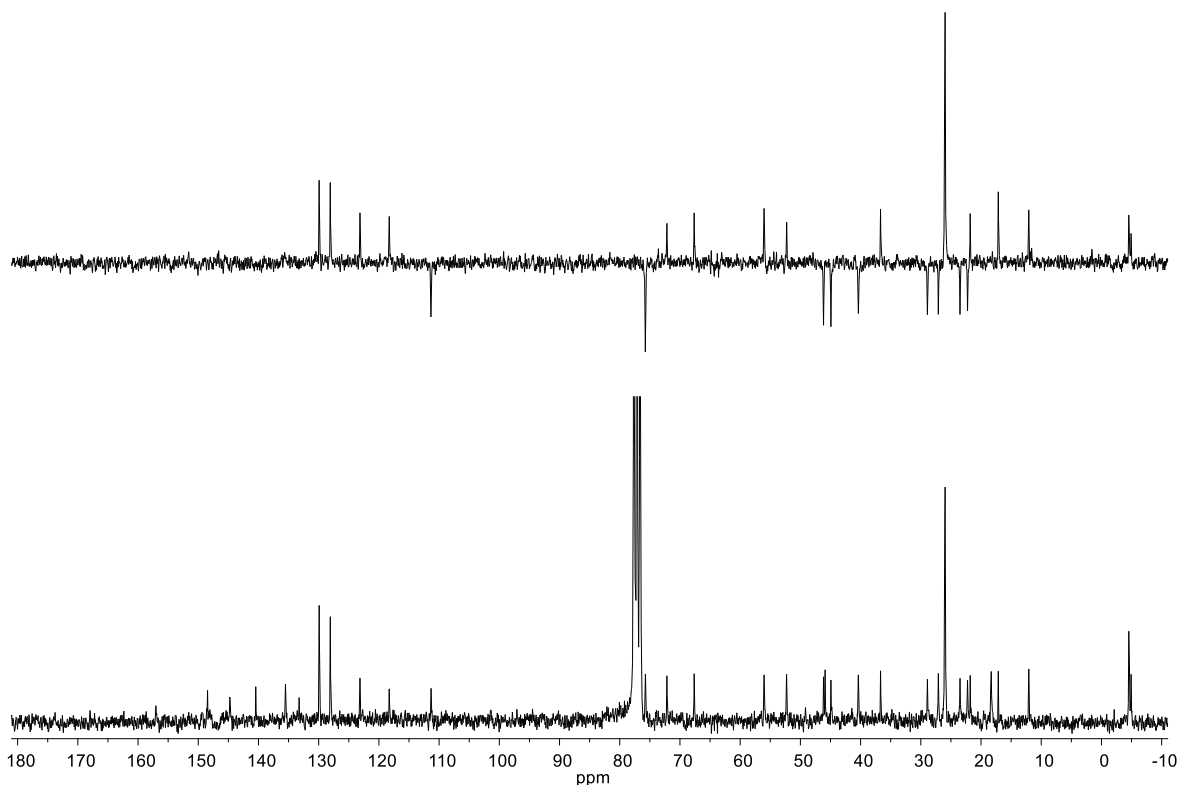


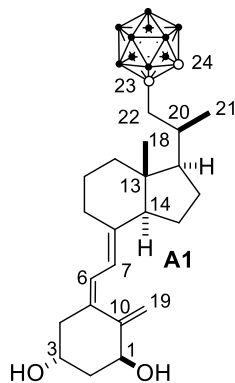


¹H NMR (250 MHz, CDCl₃): δ 7.79 (d, *J* = 8.3 Hz, 2H, H_{ar}), 7.34 (d, *J* = 8.4 Hz, 2H, H_{ar}), 6.22 (d, *J* = 11.3 Hz, 1H, H-6), 5.99 (d, *J* = 11.6 Hz, 1H, H-7), 5.17 (s, 1H, H-19), 4.84 (s, 1H, H-19), 4.36 (dd, *J* = 6.5 and 4.1 Hz, 1H, H-1), 4.24 – 4.12 (m, 1H, H-3), 3.97 (dd, *J* = 9.2 and 2.9 Hz, 1H, H-22), 3.79 (dd, *J* = 9.2 and 6.3 Hz, 1H, H-22), 2.85 – 2.75 (m, 1H), 2.51 – 2.39 (m, 3H), 2.20 (dd, *J* = 13.2 and 6.9 Hz, 2H), 2.03 – 1.06 (m, 17H), 1.01 – 0.79 (m, 18H, 2xCH₃CSi), 0.49 (s, 3H, CH₃-18), 0.05 (s, 12H, 4xCH₃Si).

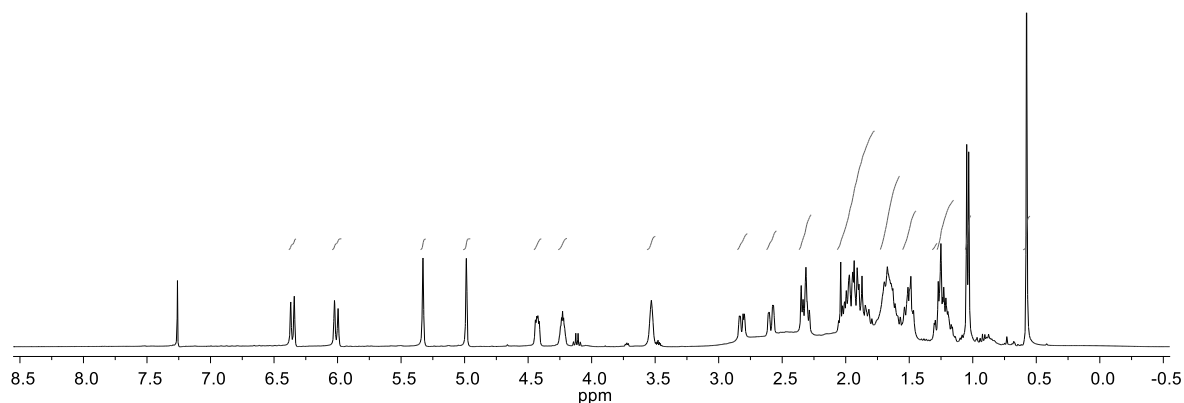


¹³C NMR (63 MHz, CDCl₃): δ 148.5 (C, C-10), 144.7 (C, C_{ar}), 140.4 (C, C-8), 135.5 (C, C-5), 133.2 (C, C_{ar}), 129.9 (2xCH, C_{ar}), 128.1 (2xCH, C_{ar}), 123.1 (=CH, C-6), 118.3 (=CH, C-7), 111.3 (=CH₂, C-19), 75.7 (CH₂, C-22), 72.2 (CH, C-1), 67.6 (CH, C-3), 56.0 (CH), 52.3 (CH), 46.1 (C, C-13), 45.9 (CH₂), 44.9 (CH₂, C-2), 40.4 (CH₂, C-12), 36.7 (CH), 28.9 (CH₂), 27.1 (CH₂), 25.99 (CH₃, 3xCH₃CSi), 25.96 (CH₃, 3xCH₃CSi), 23.5 (CH₂), 22.2 (CH₂), 21.8 (CH₃, CH₃-Ts), 18.37 (C, CH₃CSi), 18.30 (C, CH₃CSi), 17.1 (CH₃, CH₃-21), 12.1 (CH₃, CH₃-18), -4.5 (CH₃, 2xCH₃Si), -4.6 (CH₃, CH₃Si), -4.9 (CH₃, CH₃Si).

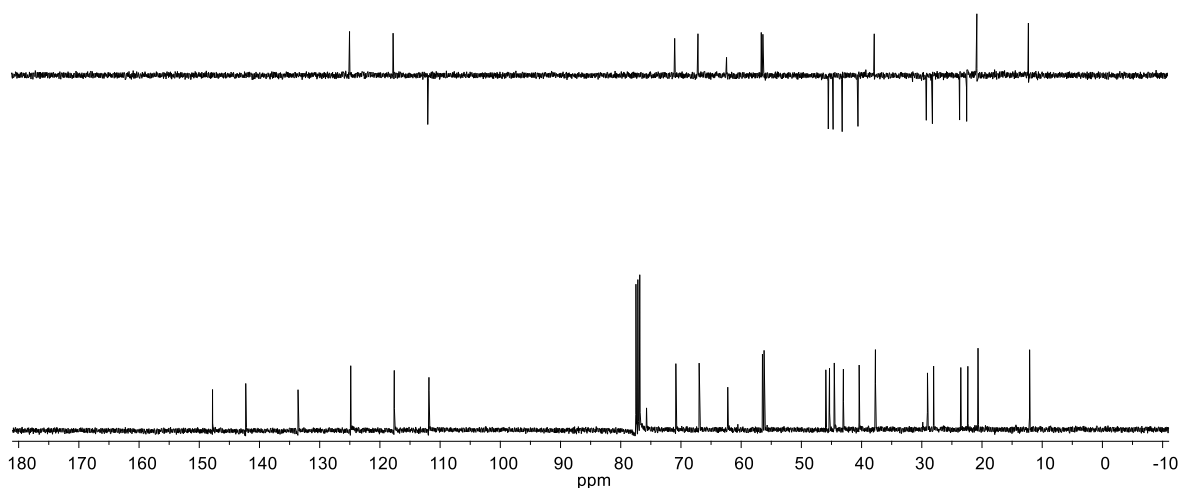


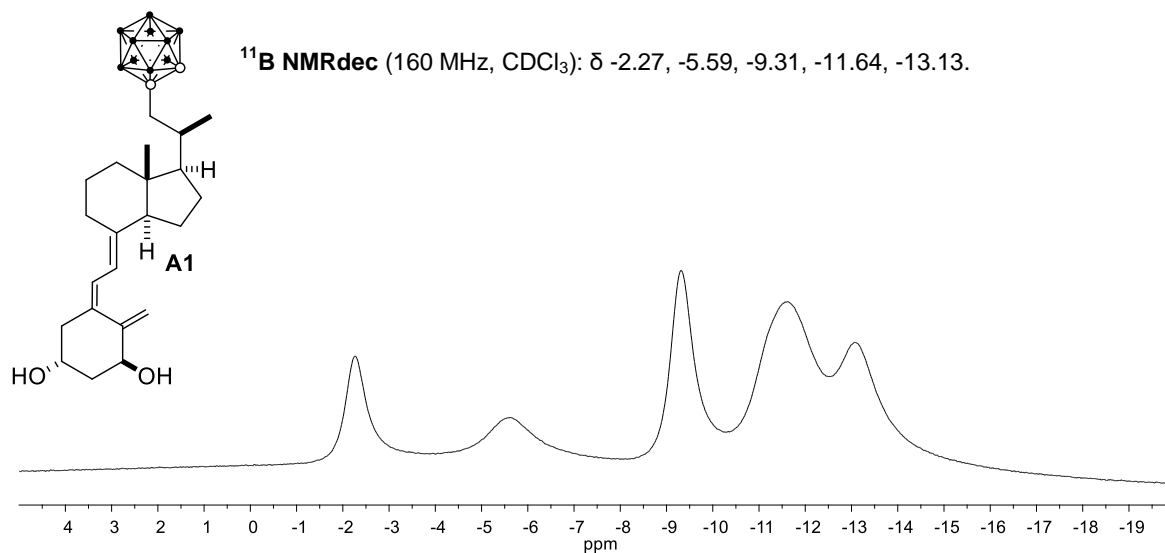


¹H NMR (400 MHz, CDCl₃): δ 6.35 and 6.01 (d, *J* = 11.2 Hz, 2H, H-6 and H-7), 5.33 (s, 1H, H-19), 4.99 (s, 1H, H-19), 4.43 (dd, *J* = 7.7 and 4.2 Hz, 1H, H-1), 4.23 (dq, *J* = 9.5 and 3.3 Hz, 1H, H-3), 3.53 (s, 1H, H-24), 2.82 (dd, *J* = 12.2 and 3.7 Hz, 1H), 2.59 (dd, *J* = 13.4 and 2.8 Hz, 1H), 2.36 – 2.28 (m, 3H), 2.07 – 1.78 (m, 11H), 1.73 – 1.58 (m, 7H), 1.50 (dd, *J* = 18.9 and 9.8 Hz, 3H), 1.31 – 1.16 (m, 5H), 1.04 (d, *J* = 6.3 Hz, 3H, CH₃-21), 0.58 (s, 3H, CH₃-18).

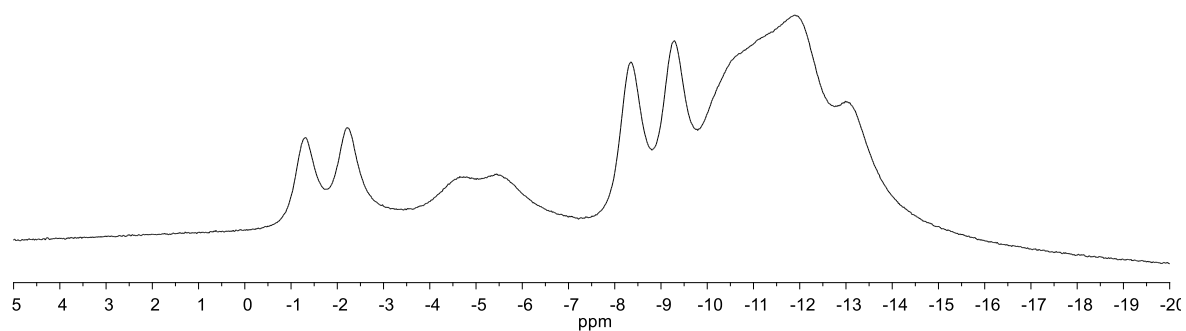


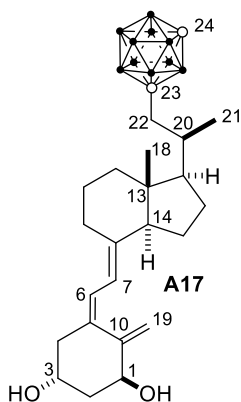
¹³C NMR (63 MHz, CDCl₃): δ 147.8 (C, C-10), 142.3 (C, C-8), 133.6 (C, C-5), 124.9 (=CH, C-6), 117.6 (=CH, C-7), 111.9 (=CH₂, C-19), 75.7 (C, C-23), 70.8 (CH, C-1), 67.0 (CH, C-3), 62.2 (CH, C-24), 56.5 (CH), 56.2 (CH, 45.9 (C, C-13), 45.3 (CH₂, C-4), 44.5 (CH₂), 43.0 (CH₂), 40.4 (CH₂), 37.7 (CH), 29.0 (CH₂), 28.0 (CH₂), 23.5 (CH₂), 22.3 (CH₂), 20.6 (CH₃, CH₃-21), 12.1 (CH₃, CH₃-18).



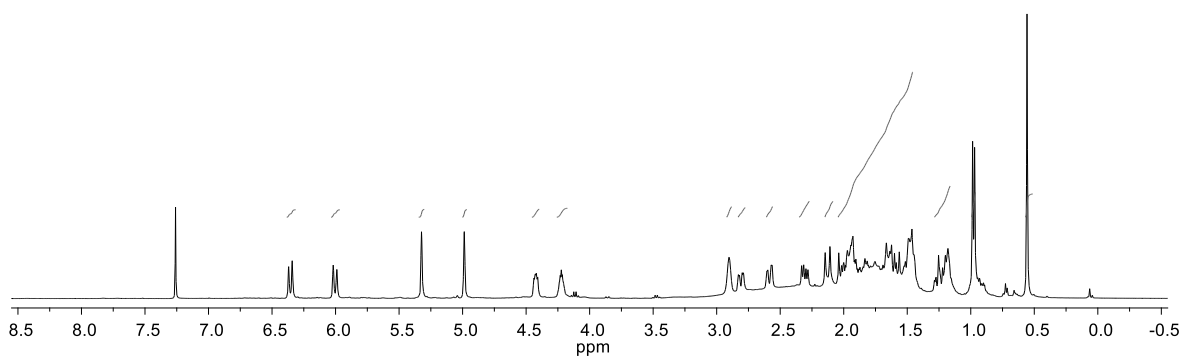


¹¹B NMRac (160 MHz, CDCl₃): δ -1.32, -2.24, -4.68, -5.53, -8.35, -9.29, -11.96, -13.13.

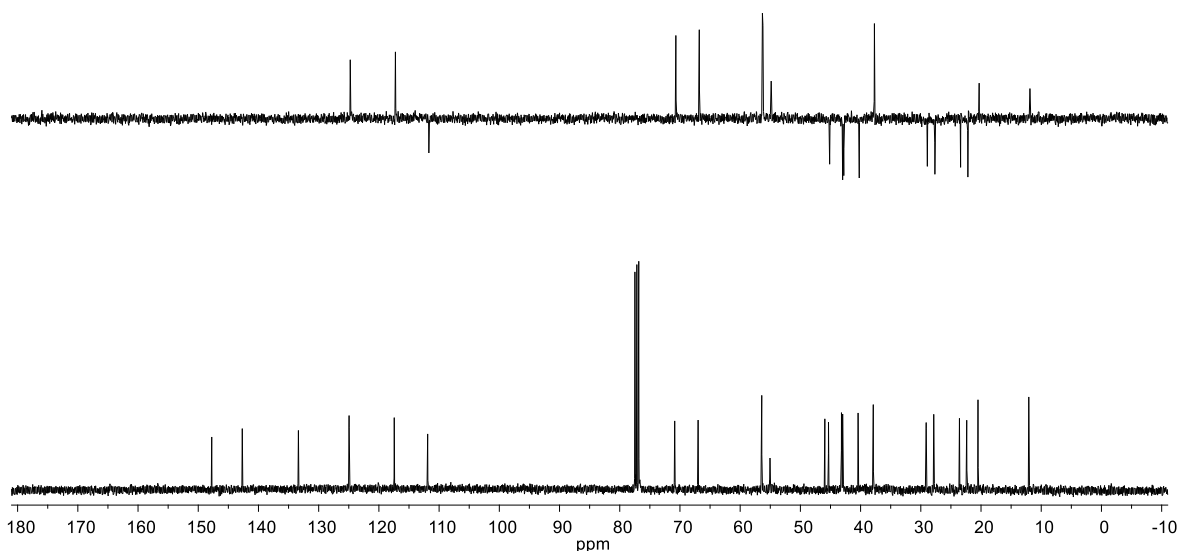


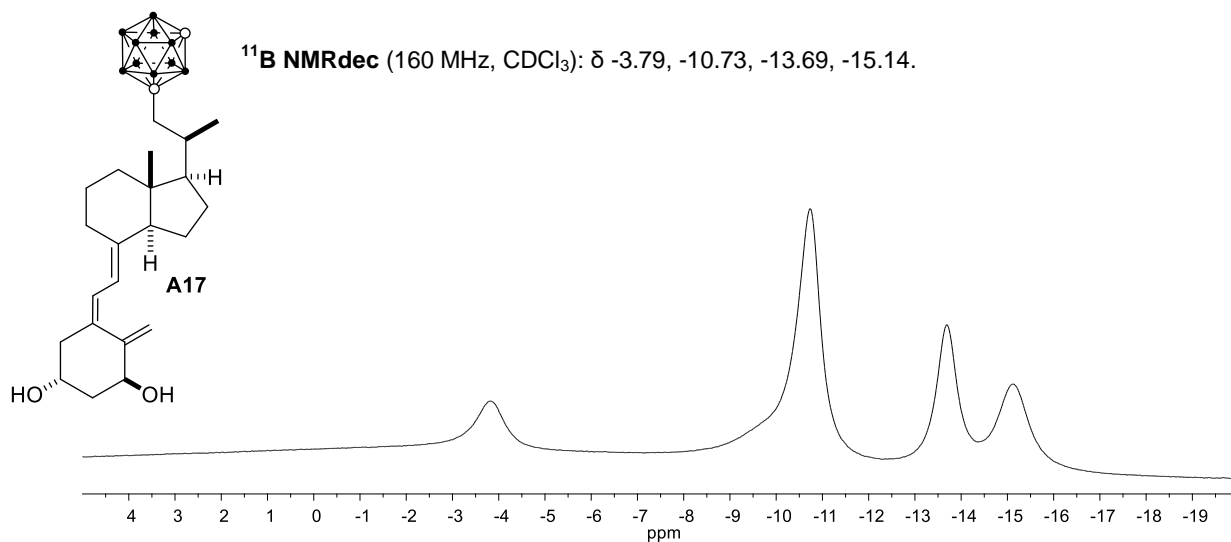


¹H NMR (400 MHz, CDCl₃): δ 6.4 and 6.0 (d, *J* = 11.2 Hz, 2H, H-6 and H-7), 5.32 (s, 1H, H-19), 4.99 (s, 1H, H-19), 4.42 (dd, *J* = 7.5 and 4.2 Hz, 1H, H-1), 4.22 (dq, *J* = 9.5 and 3.3 Hz, 1H, H-3), 2.90 (s, 1H, H-24), 2.81 (dd, *J* = 12.2 and 3.6 Hz, 1H), 2.58 (dd, *J* = 13.3 and 2.7 Hz, 2H), 2.31 (dd, *J* = 13.4 and 6.4 Hz, 2H), 2.13 (d, *J* = 14.8 Hz, 2H), 2.05 – 1.41 (m, 18H), 1.32 – 1.12 (m, 4H), 0.98 (d, *J* = 6.2 Hz, 3H, CH₃-21), 0.56 (s, 3H, CH₃-18).

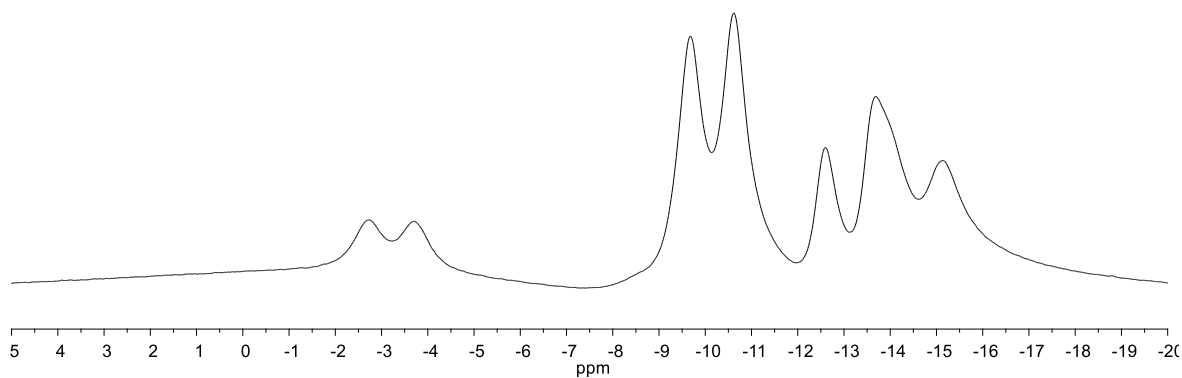


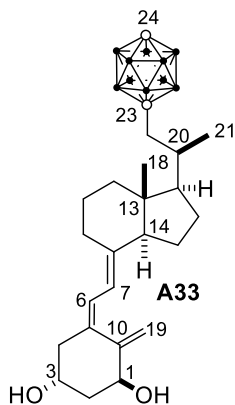
¹³C NMR (101 MHz, CDCl₃): δ 147.8 (C, C-10), 142.7 (C, C-8), 133.4 (C, C-5), 124.9 (=CH, C-6), 117.5 (=CH, C-7), 111.9 (=CH₂, C-19), 77.4 (C, C-23), 70.9 (CH, C-1), 67.0 (CH, C-3), 56.5 (CH), 56.4 (CH), 55.0 (CH, C-24), 45.9 (C, C-13), 45.3 (CH₂), 43.2 (CH₂), 43.0 (CH₂), 40.4 (CH₂), 37.9 (CH), 29.1 (CH₂), 27.8 (CH₂), 23.6 (CH₂), 22.4 (CH₂), 20.5 (CH₃, CH₃-21), 12.1 (CH₃, CH₃-18).



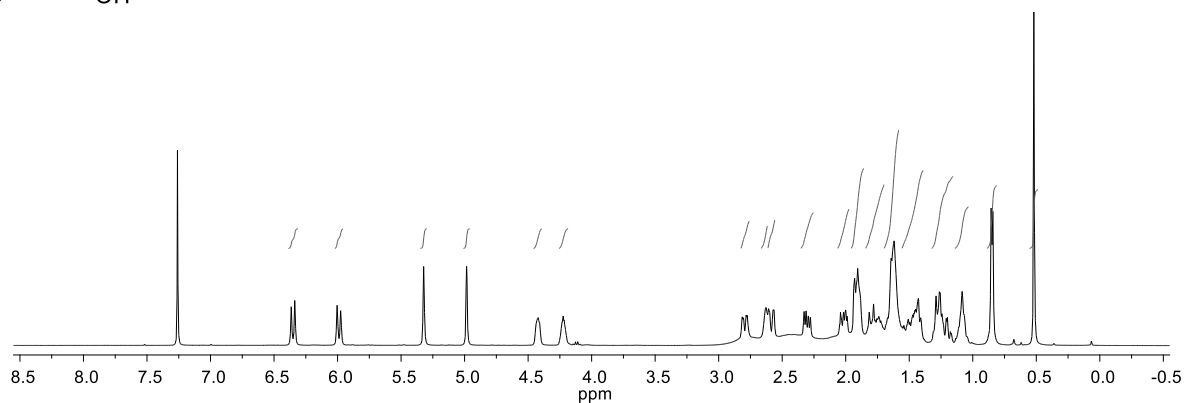


¹¹B NMRac (160 MHz, CDCl₃): δ -2.72, -3.69, -9.68, -10.62, -12.60, -13.69, -15.14.

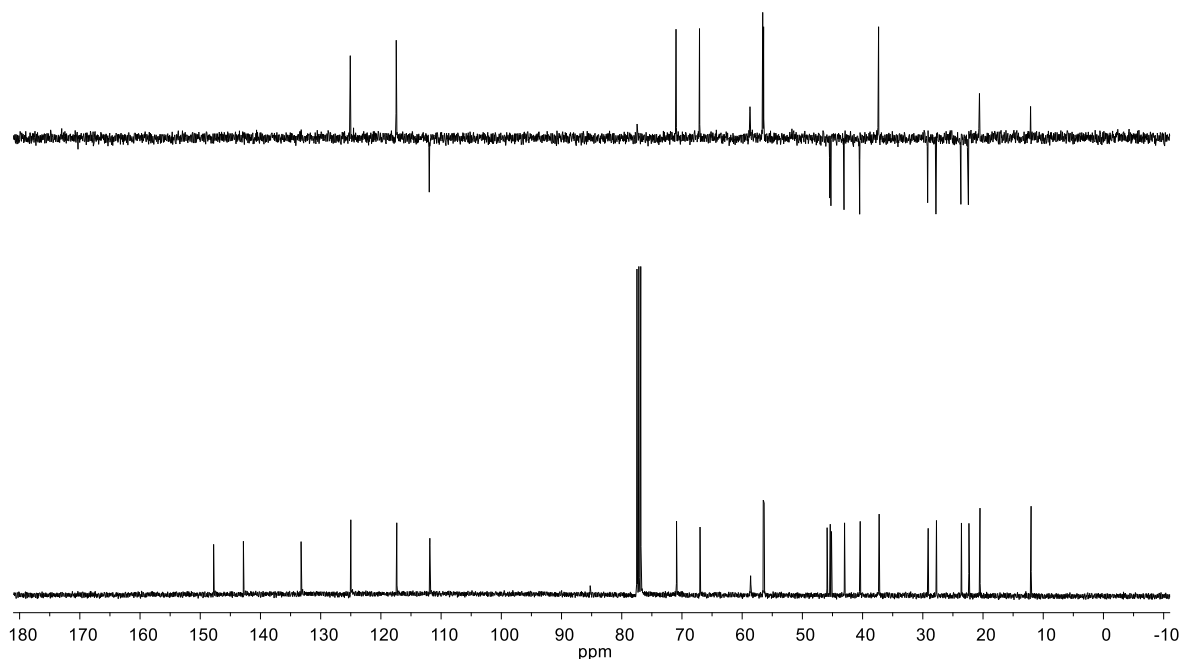


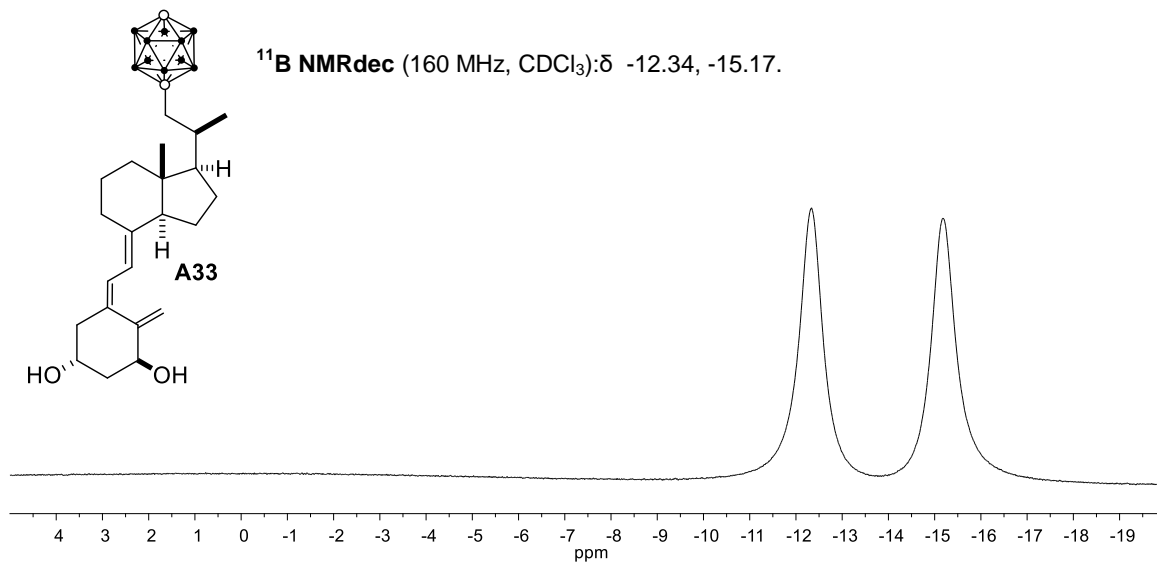


¹H NMR (400 MHz, CDCl₃): δ 6.35 and 5.99 (d, *J* = 11.2 Hz, 2H, H-6 and H-7), 5.32 (s, 1H, H-19), 4.98 (s, 1H, H-19), 4.46 – 4.39 (m, 1H, H-1), 4.26 – 4.19 (m, 1H, H-3), 2.79 (dd, *J* = 12.2 and 3.6 Hz, 1H), 2.63 (s, 1H, H-24), 2.59 (dd, *J* = 14.0 and 2.7 Hz, 1H), 2.30 (dd, *J* = 13.4 and 6.4 Hz, 2H), 2.01 (dd, *J* = 13.6 and 7.3 Hz, 2H), 1.96 – 1.86 (m, 4H), 1.84 – 1.70 (m, 3H), 1.63 (d, *J* = 9.2 Hz, 6H), 1.56 – 1.39 (m, 4H), 1.23 (ddd, *J* = 16.4, 12.7 and 6.8 Hz, 4H), 1.08 (d, *J* = 6.4 Hz, 2H), 0.85 (d, *J* = 5.4 Hz, 3H, CH₃-21), 0.52 (s, 3H, CH₃-18).

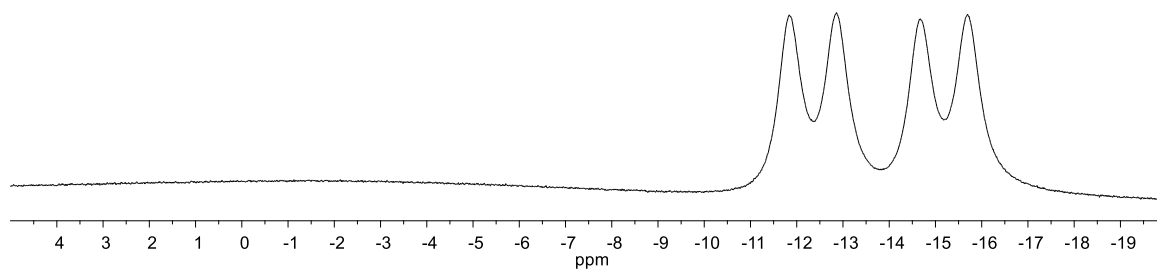


¹³C NMR (101 MHz, CDCl₃): δ 147.8 (C, C-10), 142.8 (C, C-8), 133.2 (C, C-5), 125.0 (=CH, C-6), 117.4 (=CH, C-7), 111.9 (=CH₂, C-19), 85.2 (C, C-23), 70.9 (CH, C-1), 67.0 (CH, C-3), 58.6 (CH, C-24), 56.5 (CH), 56.3 (CH), 45.9 (C, C-13), 45.4 (CH₂), 45.2 (CH₂), 43.0 (CH₂), 40.4 (CH₂), 37.2 (CH), 29.1 (CH₂), 27.7 (CH₂), 23.6 (CH₂), 22.3 (CH₂), 20.5 (CH₃, CH₃-21), 12.0 (CH₃, CH₃-18).



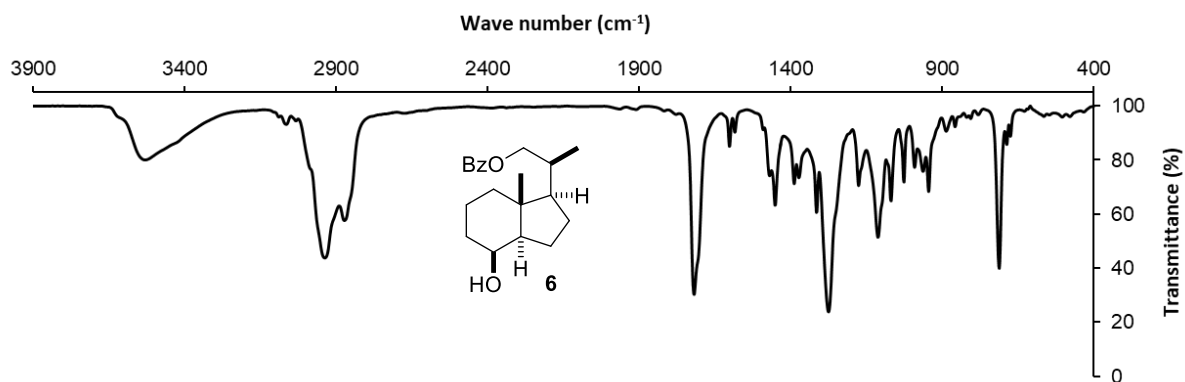


¹¹B NMRac (160 MHz, CDCl₃): δ -11.84, -12.86, -14.66, -15.69.

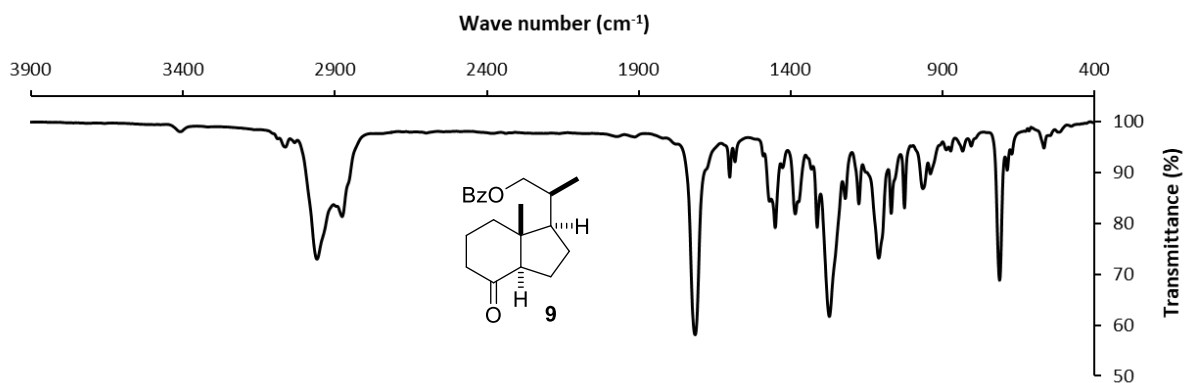


3. IR SPECTRA

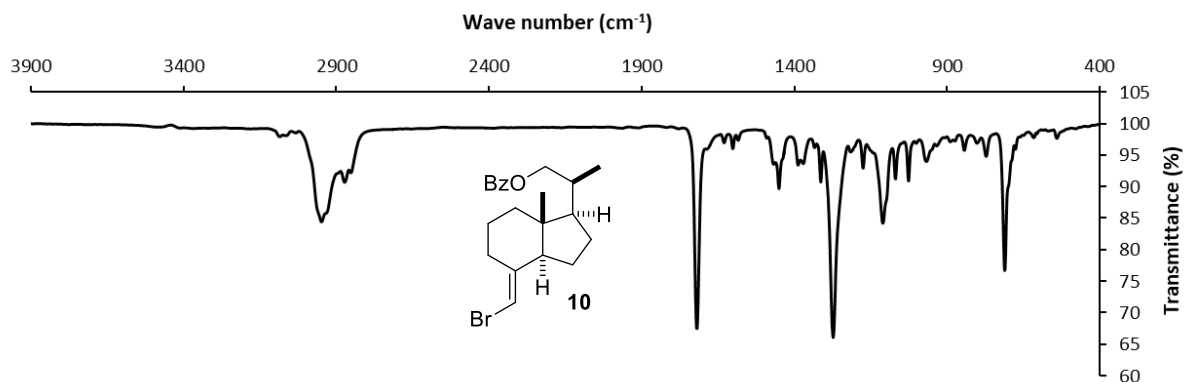
3. IR Spectra



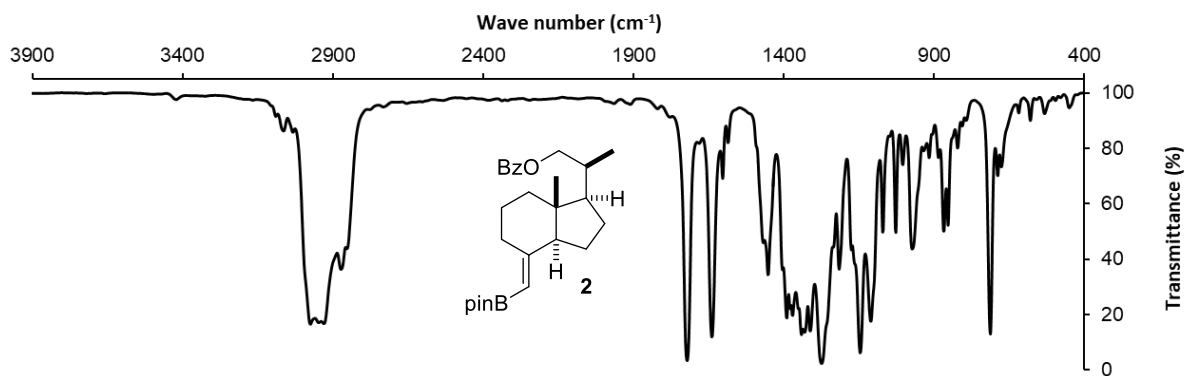
IR (film, cm^{-1}): 3533 ($\nu_{\text{O-H}}$), 2941 ($\nu_{\text{C-Har}}$), 2873 ($\nu_{\text{C-Har}}$), 1718 ($\nu_{\text{C=O}}$), 1450, 1273, 1117, 711



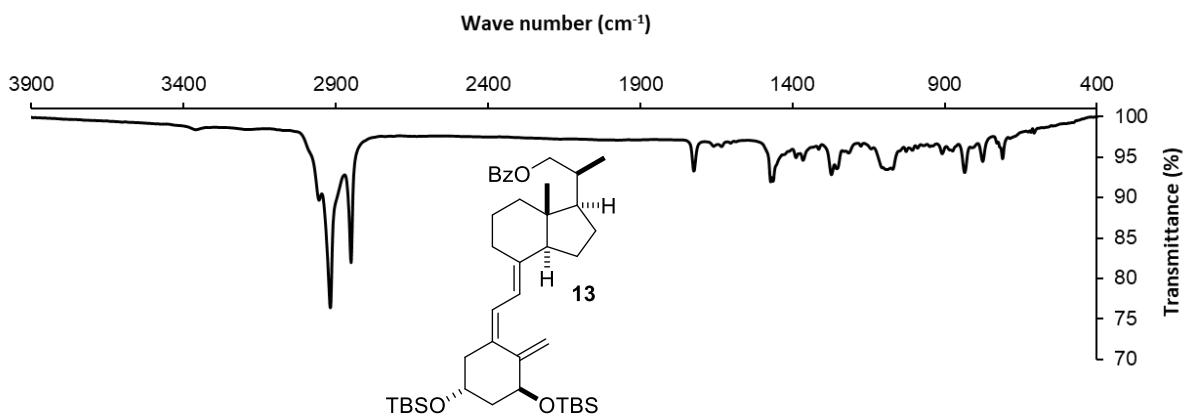
IR (film, cm^{-1}): 2962 (ν), 2873 (ν), 1714 (ν), 1387, 1313, 1273, 1111, 1070, 1026, 714



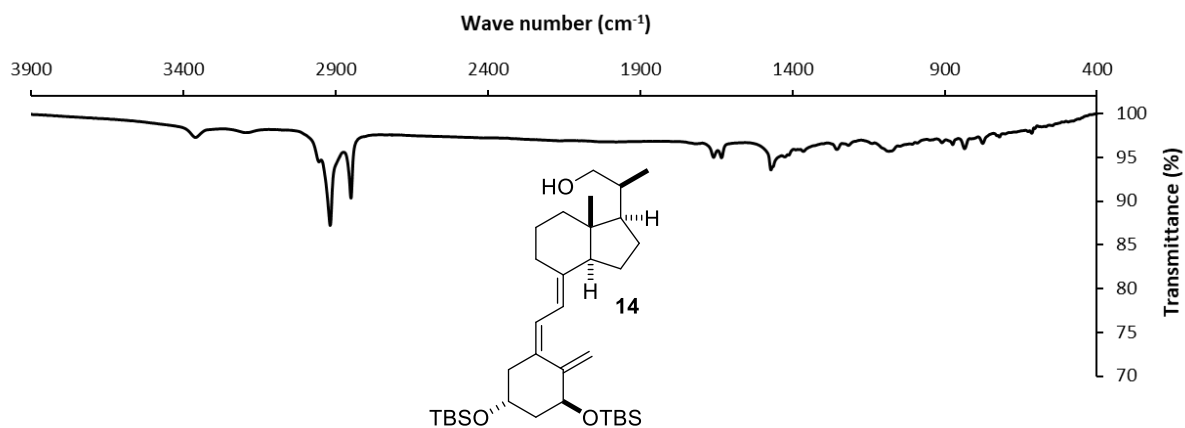
IR (film, cm^{-1}): 2947 (ν), 2870 (ν), 1718 (ν), 1450 (ν), 1273, 1111, 712



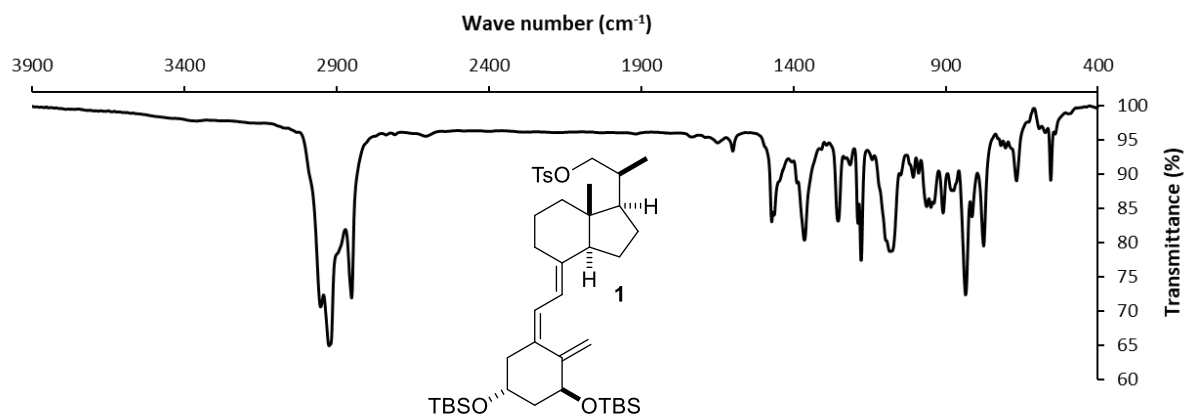
IR (film, cm^{-1}): 2980 ($\nu_{\text{C-H}}$), 2870 ($\nu_{\text{C-H}}$), 1718 (ν), 1639 ($\nu_{\text{C=C}}$), 1452, 1390, 1340, 1271, 1146, 1107, 966, 868, 852, 711



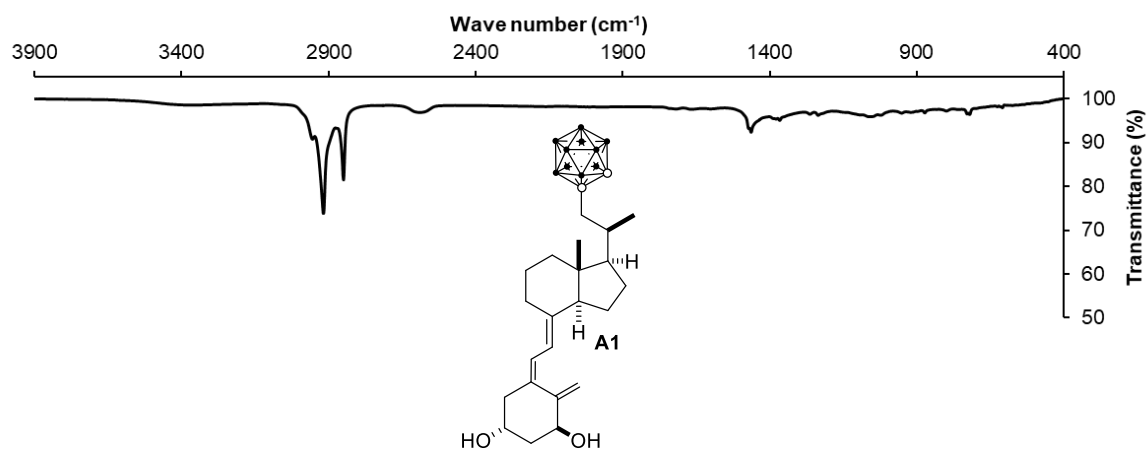
IR (film, cm^{-1}): 2918 ($\nu_{\text{C-H}}$), 2849 ($\nu_{\text{C-H}}$), 1724 (ν), 1472, 1271, 1082, 835, 775, 710



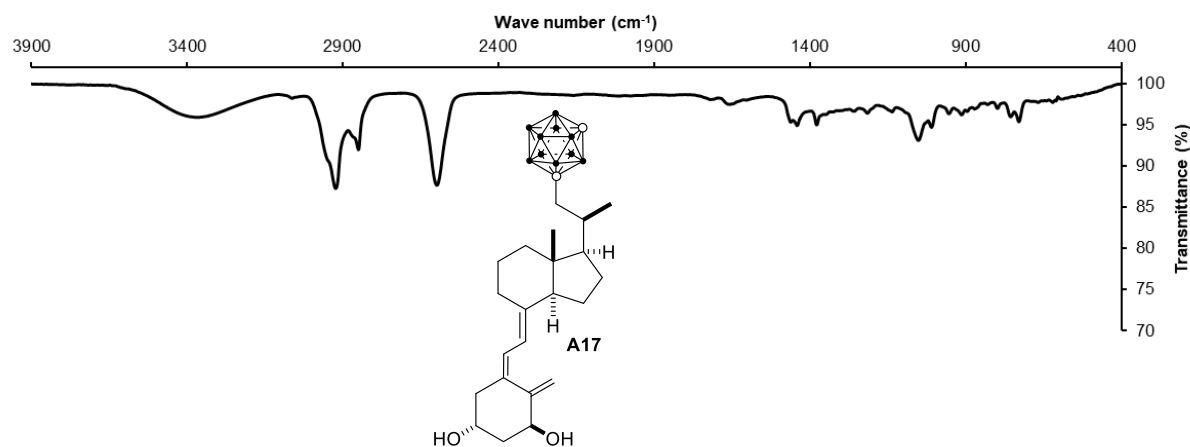
IR (film, cm^{-1}): 3358 ($\nu_{\text{O-H}}$), 2918 ($\nu_{\text{C-H}}$), 2847 ($\nu_{\text{C-H}}$), 1657 (ν), 1634, 1472, 1074, 833, 775



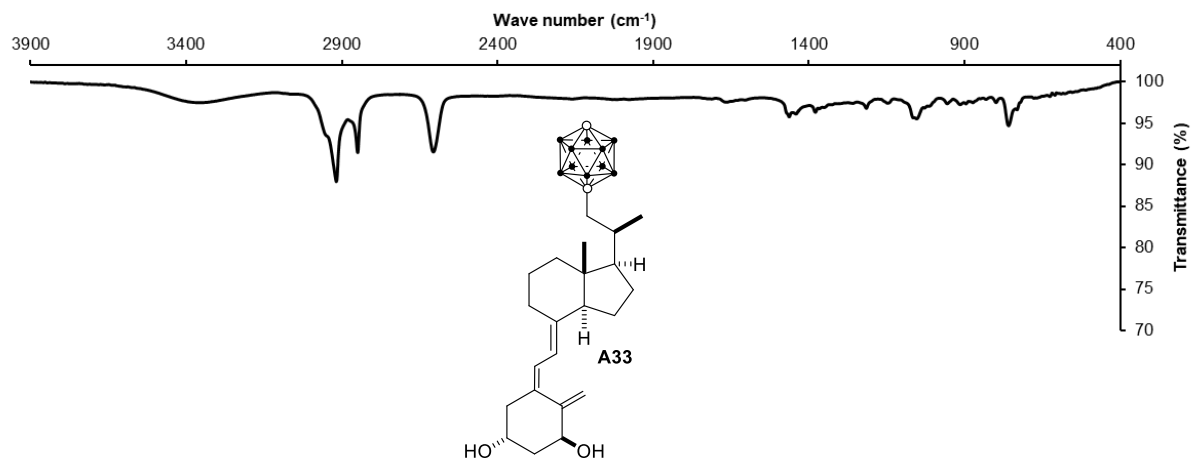
IR (film, cm^{-1}): 2953, 2924 ($\nu_{\text{C-H}}$), 2851 ($\nu_{\text{C-H}}$), 1472, 1364, 1254, 1178, 1074, 962, 908, 835, 775, 667, 557



IR (film, cm^{-1}): 3361 ($\nu_{\text{O-H}}$), 2955, 2918 ($\nu_{\text{C-H}}$), 2849 ($\nu_{\text{C-H}}$), 2594 ($\nu_{\text{B-H}}$), 1462



IR (film, cm^{-1}): 3373 ($\nu_{\text{O-H}}$), 2931, 2851 ($\nu_{\text{C-H}}$), 2600 ($\nu_{\text{B-H}}$)



IR (film, cm^{-1}): 3375 ($\nu_{\text{O-H}}$), 2916, 2851 ($\nu_{\text{C-H}}$), 2607 ($\nu_{\text{B-H}}$)

4. STRUCTURE INDEX

4. Structure Index

